oument Room, DOCUMENT ROOM 36-412
search Laboratory of Electronics
ssachusetts Institute of Technology

ELECTROMAGNETIC WAVE PROPAGATION ON HELICAL CONDUCTORS

SAMUEL SENSIPER

LOAN COPY

TECHNICAL REPORT NO. 194

MAY 16, 1951

RESEARCH LABORATORY OF ELECTRONICS
MASSACHUSETTS INSTITUTE OF TECHNOLOGY
CAMBRIDGE, MASSACHUSETTS

The research reported in this document was made possible through support extended the Massachusetts Institute of Technology, Research Laboratory of Electronics, jointly by the Army Signal Corps, the Navy Department (Office of Naval Research) and the Air Force (Air Materiel Command), under Signal Corps Contract No. DA36-039 sc-100, Project No. 8-102B-0; Department of the Army Project No. 3-99-10-022.

MASSACHUSETTS INSTITUTE OF TECHNOLOGY

RESEARCH LABORATORY OF ELECTRONICS

Technical Report No. 194 May 16, 1951

ELECTROMAGNETIC WAVE PROPAGATION ON HELICAL CONDUCTORS

Samuel Sensiper

This report is based on a doctoral thesis in the Department of Electrical Engineering, Massachusetts Institute of Technology, 1951.

Abstract

The results of a theoretical investigation of the properties of the natural waves or "free modes" which propagate along infinite helical conductors are reported. The sheath model which replaces the helix by an anisotropic cylindrical sheet is considered. The higher modes are investigated, and it is found that several waves per mode can exist. The significance of these waves in terms of inward and outward traveling waves from a source is shown. The manner in which the characteristics of these waves change as the parameters of the system are altered is discussed.

A more physically realistic model of the helix than the sheath model is analyzed. The exact formulation shows the existence of bands where free mode waves are not permitted. The cases of a single wire helix wound with a very narrow tape and a very wide tape for which reasonably valid approximations can be made are analyzed, and solutions are obtained. The usual low frequency behavior predicted by the sheath model and the anomalous behavior of the propagation constant in the region where the circumference of the helix is approximately equal to a wavelength result from these solutions. The problem of multiwire helices is considered, and the manner in which the sheath helix model is obtained as the number of wires becomes infinite is shown.

The integral formulation of the small wire helix problem yields results essentially identical to those obtained by means of the methods and approximations indicated above. This formulation allows a solution for the infinite driven helix to be obtained, and although this is not completely evaluated, the free mode portion is extracted.

CONTENTS

ELECTROMAGNETIC WAVE PROPAGATION ON HELICAL CONDUCTORS

I. The Sheath Helix

Even though several investigators have presented many analyses of an approximate representation of the helix which is called the sheath helix here, there are still properties of this model which should be discussed and clarified.

A determinantal equation for the various free modes characterized by a given angular variation is obtained from the source-free Maxwell equations and the boundary conditions for a sheath helix. Solving this determinantal equation yields the allowed values of the propagation constants for the different modes. It is found that several waves per mode with different propagation characteristics exist in restricted frequency regions. To determine the significance of these waves, the source-present problem is considered, and the resolution of the waves into inward and outward traveling waves is clarified. The incompleteness of the set of free modes is also made evident from the source-present solution since it turns out, as in other open boundary problems, that it is not possible to express the total fields resulting from even a particular source in terms of the free modes alone. In the course of considering the sheath helix, the limiting cases of the sheath ring and the sheath tube are considered, and it is shown how the solutions vary as the sheath helix varies between these extreme limits. Numerical results are not the primary purpose here, although many useful expressions are derived from which such results can be readily obtained.

A. Definitions

The circular cylindrical coordinate system is used and is defined in the usual manner as shown in Fig. 1. $\bar{a}_r$, $\bar{a}_\theta$, and $\bar{a}_z$ are unit vectors in the r, θ, and z directions, respectively. If on a cylinder of radius a, coaxial with the z axis, a helix of pitch p is wound, the configuration appears as in Fig. 2. The helix is assumed to extend to infinity in both directions along the z axis, and the medium is unbounded. The physical helix would, of course, be wound of wire of finite diameter, usually of circular cross section. If the cylinder on which the helix is wound is now cut by a plane of constant θ and unrolled, the resulting development appears, when viewed from the inside, as in Fig. 3. The pitch angle ψ is given by

$$\psi = \cot^{-1} \frac{2\pi a}{p}. \tag{1}$$

The unit vectors $\bar{a}_{\parallel}$ and $\bar{a}_{\perp}$, parallel and perpendicular to the helix wire, are useful and are shown in Fig. 3. These are related to $\bar{a}_r$, $\bar{a}_\theta$, and $\bar{a}_z$ by

$$\bar{a}_r \times \bar{a}_{\parallel} = \bar{a}_{\perp} \tag{2}$$

$$\bar{a}_{\parallel} = \bar{a}_z \sin\psi + \bar{a}_\theta \cos\psi \tag{3}$$

$$\bar{a}_{\perp} = \bar{a}_z \cos\psi - \bar{a}_\theta \sin\psi. \tag{4}$$

Similarly, $\bar{a}_z$ and $\bar{a}_\theta$ can be expressed in terms of $\bar{a}_{\parallel}$ and $\bar{a}_{\perp}$.

Since the time variation of the fields is taken to be harmonic, complex field vectors are used exclusively. Thus, for example, if E_r is the complex component representing the radial electric field, the real component equal to the radial electric field is the real or imaginary part of $E_r e^{j\omega t}$. Similarly, the total real electric field vector is the real or imaginary part of $\bar{E} e^{j\omega t} = (\bar{a}_r E_r + \bar{a}_\theta E_\theta + \bar{a}_z E_z)e^{j\omega t}$.

The rationalized mks system is used throughout this report. The medium in which the helix is immersed is considered homogeneous, isotropic, and linear; it is characterized by ϵ, μ, and σ, the permittivity, permeability, and conductivity, respectively, of the medium. In this case

$$k^2 = (-j\omega\mu)(j\omega\epsilon') = (-j\omega\mu)(\sigma + j\omega\epsilon) = \omega^2\mu\epsilon - j\omega\mu\sigma \tag{5}$$

where ω is the radian frequency. For a lossless medium, $\sigma = 0$

$$k^2 = \omega^2\mu\epsilon = \left(\frac{2\pi}{\lambda}\right)^2 \tag{6}$$

where λ is the wavelength of a uniform plane wave in the medium. Other notations and additional definitions are introduced as they are required.

B. Boundary Conditions

Consider a helix wound of a wire of uniform cross section, say circular, and of infinite conductivity. If Maxwell's equations could be solved in an appropriate coordinate system in which the surface of the wire is a surface described by keeping one of the coordinates constant, the problem could be solved by a procedure identical to that used in simpler waveguide problems. Specifically, the electric field tangential to the wire surface would be expressed in terms of the appropriate coordinate functions and the helix parameters. By requiring this to be zero, the only necessary boundary condition aside from finiteness of the fields if the conductor is perfect, a determinantal equation would be obtained which would then be solved for the unknown propagation constant. This constant, inserted in the appropriate field expressions, would yield a solution to the Maxwell equations which would satisfy the boundary conditions and would therefore be a unique solution. Unfortunately, although it is possible to define coordinate systems which describe the helix in the required manner and to write down the field equations for such systems, it is not possible, or has so far proved impossible, to solve the resulting equations. Consequently, one approach has been to replace the physical helix with a model which seems to retain many of its characteristics and allows a solution to be obtained.

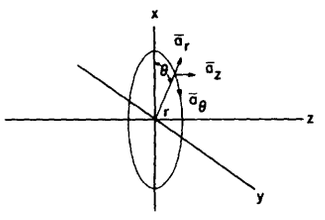

Fig. 1
Circular cylindrical coordinates.

Considering Fig. 2, assume that another wire helix is

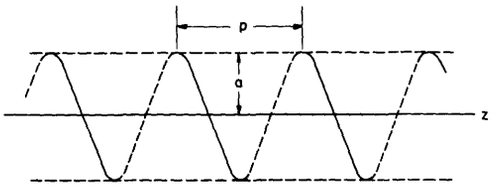

Fig. 2
Helix.

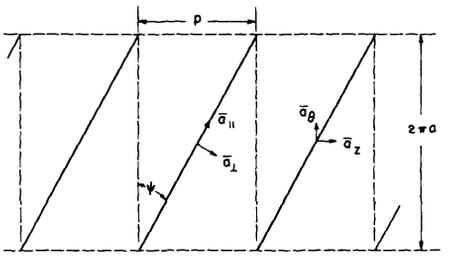

Fig. 3
Developed helix.

wound on the cylinder of radius a, but displaced slightly in the z direction from the first. A third wire is now placed alongside the second, and so on until the entire pitch distance is filled up. In this manner a multiwire helix is obtained. Now assume that the wires are allowed to become of infinitesimal radius so that current can be conducted only in the wire direction. Further, assume that the spacing between the wires becomes infinitesimal and that the number of wires becomes infinitely large. In the limit, the wires may be replaced by a sheath or sheet which can conduct current only in the wire direction; this is the sheath helix. It can be considered to consist of an anisotropic conducting sheet wound on a circular cylinder of radius a. The problem is now to find solutions of Maxwell's equations for the two regions $a \geqslant r \geqslant 0$ and $\infty \geqslant r \geqslant a$ which are connected by the appropriate continuity conditions at r = a. From the limit method by which the above model is derived these are

$$E_{\parallel}^{i} = E_{\parallel}^{e} = 0 \tag{7}$$

$$E_{\perp}^{i} = E_{\perp}^{e} \tag{8}$$

$$H_{\parallel}^{i} = H_{\parallel}^{e} \tag{9}$$

for $r = a$, $2\pi \geqslant \theta \geqslant 0$, and $+\infty > z > -\infty$. The superscripts i and e are used to distinguish the expressions for the internal fields, $a \geqslant r \geqslant 0$, from those for the external fields, $\infty \geqslant r \geqslant a$. The subscripts $\parallel$ and $\perp$ refer to the particular components of the field, parallel and perpendicular to the wires in that order. These equations are essentially expressions of the assumptions that the wires are taken to be perfect conductors and to conduct only in the direction of the windings. In terms of the r, θ, and z components, using Eqs. 3 and 4, the continuity conditions become

$$E_{z}^{i} = E_{z}^{e} \tag{10}$$

$$E_{\theta}^{i} = E_{\theta}^{e} \tag{11}$$

$$E_{z}^{i,e} = -E_{\theta}^{i,e} \cot \psi \tag{12}$$

and

$$H_z^i + H_\theta^i \cot \psi = H_z^e + H_\theta^e \cot \psi \tag{13}$$

for $r = a$, $2\pi \geq \theta \geq 0$, and $+\infty > z > -\infty$. For simplicity, it is assumed that the medium is the same and lossless for $r < a$ as for $r > a$.

Some of the shortcomings of the sheath helix representation are clear immediately. The most serious deficiency is that the periodic structure of the physical helix is completely ignored. This periodic structure gives the actual helix some interesting and unusual properties (see sec. II). Further, the effect of finite wire size is nowhere considered in the sheath model.

Before proceeding with the solution for the sheath helix, it is useful to consider what some of the results may be. Since the configuration being examined has cylindrical symmetry, it is to be expected that solutions exist which have exponential dependence on z. These correspond to waves guided by the helix. Because of the uniformity of the boundary conditions, it is also to be expected that an infinite set of modes characterized by different angular variations exists, although these modes undoubtedly do not constitute a complete set (39). Further, it can be anticipated, in view of the peculiar nature of the boundary conditions, that the solutions consist of a mixture of TE (transverse electric) and TM (transverse magnetic) waves (39).

In solving a problem of the type being considered, there are two related approaches. In one, the homogeneous or source-free field equations are solved subject only to all the boundary conditions. The manner in which the fields are generated is considered immaterial, and the sources are taken to be located at an infinite distance from the point at which a solution is desired. Only the so-called free modes or natural waves and their dependence on the geometry and other parameters of the system are determined by this procedure. In the other approach, the inhomogeneous or source-present field equations are solved subject, of course, to the boundary conditions also. This procedure is perhaps more difficult than the first, but it can yield more information. With it, one can determine which of the free modes are excited by a particular configuration of driving source, and the amplitudes of the free modes can be related to the strength of the source. Both approaches are used here, with the source-free problem considered first.

The Source-Free Problem

C. The Maxwell Equations; The Hertzian Potentials; The Form of the Field Solutions

The fundamental equations which must be solved subject to the boundary conditions are the homogeneous or source-free Maxwell equations, written as

$$\nabla \times \overline{E} = -j\omega\mu\overline{H} \tag{14}$$

$$\nabla \times \bar{H} = j\omega\epsilon\bar{E}. \tag{15}$$

Solutions to these can be obtained in terms of electric and magnetic Hertzian vector potentials (1), $\bar{\Pi}$ and $\bar{\Pi}^*$, respectively, by

$$\bar{E} = \nabla \times \nabla \times \bar{\Pi} - j\omega\mu \nabla \times \bar{\Pi}^* \tag{16}$$

$$\bar{H} = j\omega\epsilon \nabla \times \bar{\Pi} + \nabla \times \nabla \times \bar{\Pi}^* \tag{17}$$

where $\bar{\Pi}$ and $\bar{\Pi}^*$ both satisfy an identical vector wave equation

$$\nabla \times \nabla \times \bar{\Pi} - \nabla\nabla \cdot \bar{\Pi} - k^2\bar{\Pi} = 0 \tag{18}$$

and

$$\nabla \times \nabla \times \bar{\Pi}^* - \nabla\nabla \cdot \bar{\Pi}^* - k^2\bar{\Pi}^* = 0. \tag{19}$$

If $\bar{\Pi}$ and $\bar{\Pi}^*$ are taken to have only z components, Π_z and Π_z^*, respectively, then the electric and magnetic field components in circular cylindrical coordinates can be obtained as follows

$$E_r = \frac{\partial^2 \Pi_z}{\partial z \partial r} - j\frac{\omega\mu}{r}\frac{\partial \Pi_z^*}{\partial \theta} \tag{20}$$

$$E_\theta = \frac{1}{r}\frac{\partial^2 \Pi_z}{\partial z \partial \theta} + j\omega\mu\frac{\partial \Pi_z^*}{\partial r} \tag{21}$$

$$E_z = \frac{\partial^2 \Pi_z}{\partial z^2} + k^2\Pi_z \tag{22}$$

$$H_r = j\omega\epsilon\frac{1}{r}\frac{\partial \Pi_z}{\partial \theta} + \frac{\partial^2 \Pi_z^*}{\partial z \partial r} \tag{23}$$

$$H_\theta = -j\omega\epsilon\frac{\partial \Pi_z}{\partial r} + \frac{1}{r}\frac{\partial^2 \Pi_z^*}{\partial z \partial \theta} \tag{24}$$

$$H_z = \frac{\partial^2 \Pi_z^*}{\partial z^2} + k^2\Pi_z^*. \tag{25}$$

Π_z and Π_z^*, being rectangular components, satisfy the same scalar wave equation

$$\nabla^2\Pi_z + k^2\Pi_z = \frac{1}{r}\frac{\partial}{\partial r}\left(r\frac{\partial \Pi_z}{\partial r}\right) + \frac{1}{r^2}\frac{\partial^2 \Pi_z}{\partial \theta^2} + \frac{\partial^2 \Pi_z}{\partial z^2} + k^2\Pi_z = 0 \tag{26}$$

and

$$\nabla^2\Pi_z^* + k^2\Pi_z^* = \frac{1}{r}\frac{\partial}{\partial r}\left(r\frac{\partial \Pi_z^*}{\partial r}\right) + \frac{1}{r^2}\frac{\partial^2 \Pi_z^*}{\partial \theta^2} + \frac{\partial^2 \Pi_z^*}{\partial z^2} + k^2\Pi_z^* = 0. \tag{27}$$

Equations 26 and 27 are used to simplify the expressions for E_z and H_z obtained from Eqs. 16 and 17. If Π_z^* vanishes but Π_z does not, $H_z = 0$, and a TM wave results; if Π_z vanishes but Π_z^* does not, $E_z = 0$, and a TE wave results. The total electromagnetic field obtained by including both Π_z and Π_z^* is of such generality that a given set of boundary conditions for some constant r can be satisfied.

Applying the usual separation of variables procedure in Eqs. 26 and 27, it is found that the z and θ solutions are expressible in exponential form. Thus, by using in Eqs. 26 and 27 the form

$$\begin{matrix}\Pi_z \\ \Pi_z^*\end{matrix} = f(r)\, e^{-jhz}\, e^{-jn\theta} \tag{28}$$

where n must be integer since the potential and the fields must be single valued, one finds that f(r) must be a solution of

$$r\frac{d}{dr}\left(r\frac{df}{dr}\right) - \left[(h^2 - k^2)r^2 + n^2\right] f = 0. \tag{29}$$

h is the propagation constant whose value must be determined. The independent solutions of Eq. 29 are the modified Bessel functions of order n and argument ζr where ζ is given by

$$\zeta = \sqrt{h^2 - k^2}. \tag{30}$$

Since the fields must be finite, the I_n function is chosen for the solution for $a \geq r \geq 0$ and the K_n function for $\infty \geq r \geq a$. Consequently, for the fundamental solutions

$$\Pi_z^i = A_n^i\, I_n(\zeta r) e^{-jhz}\, e^{-jn\theta}, \quad a \geq r \geq 0 \tag{31}$$

$$\Pi_z^e = A_n^e\, K_n(\zeta r) e^{-jhz}\, e^{-jn\theta}, \quad \infty \geq r \geq a \tag{32}$$

$$\Pi_z^{*i} = B_n^i\, I_n(\zeta r) e^{-jhz}\, e^{-jn\theta}, \quad a \geq r \geq 0 \tag{33}$$

$$\Pi_z^{*e} = B_n^e\, K_n(\zeta r) e^{-jhz}\, e^{-jn\theta}, \quad \infty \geq r \geq a. \tag{34}$$

$A_n^{i,e}$ and $B_n^{i,e}$ are coefficients related by the boundary conditions and are functions of n, ω, and the character of the exciting sources, but not of the coordinates. It is clear that E_z and H_z rather than Π_z and Π_z^* can be used as the scalar quantities from which the other field components can be derived.

D. Application of the Boundary Conditions; The Determinantal Equation; The Sheath Helix Fields

Generally, in constructing a complete solution from the fundamental solutions, Eqs. 31 through 34, one has to sum over all values of n. However, since the boundary

conditions for the sheath helix are the same for all θ and z, the orthogonality in θ of the fundamental solutions allows the possibility of the boundary conditions being satisfied for each n separately.

Using the expressions for the Hertzian potentials, Eqs. 31 through 34, in Eqs. 21, 22, 24, and 25 to determine the tangential fields, and then using these in the boundary condition Eqs. 10 through 13, one obtains from Eq. 10

$$I_n A_n^i - K_n A_n^e = 0 \tag{35}$$

from Eq. 11

$$-\frac{hn}{a} I_n A_n^i + \frac{hn}{a} K_n A_n^e + j\omega\mu\zeta\, I_n' B_n^i - j\omega\mu\zeta\, K_n' B_n^e = 0 \tag{36}$$

from Eq. 12

$$\left(\zeta^2 + \frac{hn}{a}\cot\psi\right) I_n A_n^i - j\omega\mu\zeta\cot\psi\, I_n' B_n^i = 0 \tag{37}$$

and from Eq. 13

$$-j\omega\epsilon\zeta\cot\psi\, I_n' A_n^i + j\omega\epsilon\zeta\cot\psi\, K_n' A_n^e$$

$$-\left(\zeta^2 + \frac{hn}{a}\cot\psi\right) I_n B_n^i + \left(\zeta^2 + \frac{hn}{a}\cot\psi\right) K_n B_n^e = 0. \tag{38}$$

Here, the argument of all the modified Bessel functions is ζa, and the prime means differentiation with respect to the argument. Equations 35 through 38 are a homogeneous system of linear equations relating $A_n^{i,e}$ and $B_n^{i,e}$. A nontrivial solution exists only if the determinant of the system is zero, and the propagation constant h is determined from the equation resulting from the requirement that the determinant vanish. Solving directly, it is found that

$$A_n^e = \frac{I_n}{K_n} A_n^i \tag{39}$$

$$B_n^i = \frac{\left(\zeta^2 + \frac{hn}{a}\cot\psi\right) I_n}{j\omega\mu\zeta\cot\psi\, I_n'} A_n^i \tag{40}$$

$$B_n^e = \frac{I_n'}{K_n'} B_n^i = \frac{\left(\zeta^2 + \frac{hn}{a}\cot\psi\right) I_n}{j\omega\mu\zeta\cot\psi\, K_n'} A_n^i \tag{41}$$

and, finally

$$\frac{I_n'(\zeta a) K_n'(\zeta a)}{I_n(\zeta a) K_n(\zeta a)} = -\frac{(\zeta^2 a^2 + nha\cot\psi)^2}{k^2 a^2 \zeta^2 a^2 \cot^2\psi} \tag{42}$$

as the determinantal equation.

Using Eqs. 31 through 34 in Eqs. 20 through 25, and then using Eqs. 39 through 41, it is possible to express all the field components in terms of A_n^i alone. It is more convenient, however, to express the fields in terms of the surface current density. This

is readily done since the surface current density vector $\bar{K}$, where

$$\bar{K} = \bar{a}_\theta K_\theta + \bar{a}_z K_z \tag{43}$$

is related to the discontinuity in the tangential magnetic field by

$$\bar{a}_r \times (\bar{H}^e - \bar{H}^i)_{r=a} = \bar{K}. \tag{44}$$

Expanding Eq. 44 results in

$$K_\theta = (H_z^i - H_z^e)_{r=a} \tag{45}$$

and

$$K_z = (H_\theta^e - H_\theta^i)_{r=a}. \tag{46}$$

Further, since

$$K_{\parallel} = K_z \sin\psi + K_\theta \cos\psi \tag{47}$$

and

$$K_{\perp} = K_z \cos\psi - K_\theta \sin\psi \tag{48}$$

(see Eqs. 3 and 4) it is found that $K_{\perp}$ vanishes, as would be expected from the boundary conditions, while Eq. 47 yields a relationship between A_n^i and $K_{\parallel}$. In the course of carrying through these calculations, it is necessary to use the Wronskian identity and the determinantal equation 42. There finally results for the field expressions

$$E_\theta^e = j\omega\mu a \left[nha \frac{a}{r} \frac{(\zeta^2 a^2 + nha \cot\psi)}{k^2 a^2 \zeta^2 a^2} I_n(\zeta a) K_n(\zeta r) \right.$$

$$\left. + \cot\psi\, I_n'(\zeta a) K_n'(\zeta r) \right] \sin\psi |K_{\parallel}| e^{-jhz} e^{-jn\theta} \tag{49}$$

$$E_r^e = -\frac{\omega\mu a}{\zeta a} \left[ha \frac{(\zeta^2 a^2 + nha \cot\psi)}{k^2 a^2} I_n(\zeta a) K_n'(\zeta r) \right.$$

$$\left. + n \frac{a}{r} \cot\psi\, I_n'(\zeta a) K_n(\zeta r) \right] \sin\psi |K_{\parallel}| e^{-jhz} e^{-jn\theta} \tag{50}$$

$$E_z^e = j\omega\mu a \frac{(\zeta^2 a^2 + nha \cot\psi)}{k^2 a^2} I_n(\zeta a) K_n(\zeta r) \sin\psi |K_{\parallel}| e^{-jhz} e^{-jn\theta} \tag{51}$$

$$H_\theta^e = -\frac{1}{\zeta a} \left[(\zeta^2 a^2 + nha \cot\psi) I_n(\zeta a) K_n'(\zeta r) \right.$$

$$\left. + nha \frac{a}{r} \cot\psi\, I_n'(\zeta a) K_n(\zeta r) \right] \sin\psi |K_{\parallel}| e^{-jhz} e^{-jn\theta} \tag{52}$$

$$H_r^e = -j \left[n \frac{a}{r} \frac{(\zeta^2 a^2 + nha \cot \psi)}{\zeta^2 a^2} I_n(\zeta a) K_n(\zeta r) \right.$$

$$\left. + ha \cot \psi \, I_n'(\zeta a) K_n'(\zeta r) \right] \sin \psi \, |K_{\parallel}| e^{-jhz} e^{-jn\theta} \tag{53}$$

$$H_z^e = -\zeta a \, I_n'(\zeta a) K_n(\zeta r) \cos \psi \, |K_{\parallel}| e^{-jhz} e^{-jn\theta} \tag{54}$$

where $|K_{\parallel}|$ is the magnitude of the surface current density in the direction of the wires. Only the external field expressions are given since the internal field expressions are identical, except that the I_n and K_n functions are interchanged everywhere. $|K_{\parallel}|$ is the usual undetermined constant which remains in free mode solutions and can only be evaluated if the power flow associated with the mode or the character of the exciting sources is known.

The continuity condition

$$\nabla_s \cdot \bar{K} + j\omega q_s = \nabla_s \cdot \bar{K} + j\omega\epsilon \, (E_r^e - E_r^i) = 0, \quad r = a \tag{55}$$

where $\nabla_s \cdot \bar{K}$ is the surface divergence of the surface current density and q_s is the surface charge density, is satisfied for all n as well as for n = 0. The fulfillment of the continuity condition for n = 0 alone for the sheath model considered here had previously been noted (13).

Equations 49 through 54 constitute the proper fields for the free modes on a sheath helix if values of h and ζ are used which satisfy the determinantal equation 42. To complete the solution these values must be determined.

E. Solutions of the Determinantal Equation

Although these solutions have been considered elsewhere (refs. 9, 10, 11, 19, 65, etc.), it is thought that the following discussion is more complete than any which has appeared so far.

For purposes of brevity only the results which are derived from Eq. 42 are given. The details are shown in reference 68. It should be emphasized that, in general, it has been the intent to determine the existence and general character of the solutions rather than specific numerical results.

It can be shown (68) that the propagation constant h is required in general to be real and in magnitude larger than k if free mode solutions are to exist when the medium is lossless. This limitation has also been noted (39) in other open-boundary problems and immediately reduces the magnitude of the task of looking for solutions of the determinantal equation, since one need only investigate this equation for ζa real and $\zeta a > 0$.

In addition to the general case of the sheath helix for $\psi \neq 0°$ or $90°$, there are the two special cases of $\psi = 0°$, called the sheath ring, and $\psi = 90°$, called the sheath tube.

For $\psi = 0°$ there are solutions for $|h| > k$, and these turn out to have considerable interest not only for themselves but also for their rather close connection with the solutions for $\psi \neq 0°$. Further, a knowledge of the solutions for $\psi = 0°$ is exceedingly useful in investigating the cases for $\psi \neq 0°$. For $\psi = 90°$, free mode solutions exist for values of $|n| \geq 1$ and $h = \pm k$. It turns out that these solutions are the limiting ones for a set of the sheath helix modes and are therefore of considerable interest. Ordinary waveguide modes also exist for $\psi = 0°$ and $90°$.

1. The Sheath Ring, $\psi = 0°$

For $\psi = 0°$ the determinantal equation is

$$\frac{I_n'(\zeta a)K_n'(\zeta a)}{I_n(\zeta a)K_n(\zeta a)} = -\frac{n^2h^2a^2}{k^2a^2\zeta^2a^2}. \tag{56}$$

This results if the Maxwell equations are solved subject to the boundary conditions

$$E_{\parallel}^i = E_{\parallel}^e = E_{\theta}^i = E_{\theta}^e = 0 \tag{57}$$

$$E_{\perp}^i = E_{\perp}^e = E_z^i = E_z^e \tag{58}$$

$$H_{\parallel}^i = H_{\parallel}^e = H_{\theta}^i = H_{\theta}^e \tag{59}$$

for $r = a$, $2\pi \geq \theta \geq 0$, and $+\infty > z > -\infty$. These correspond to Eqs. 7 through 13 for the special case of $\psi = 0°$. The sheath ring system may be considered the limiting one which results from an infinite series of equally spaced perfectly conducting circular rings coaxial with the z axis as the wire of which the rings are made becomes infinitesimally small and the spacing between the rings becomes likewise small. Equation 56 also results if in Eq. 42 ψ is allowed to approach zero and the limit taken in the usual manner. The field expressions in this case may likewise be obtained from Eqs. 49 through 54 if, there, ψ is allowed to approach and finally equal zero. Therefore they are not written out explicitly. As might be expected from the symmetry of the boundary conditions, for this case the determinantal equation 56 is an even function of h and n. Consequently, there exist field solutions whose angular dependence is sin $n\theta$ or cos $n\theta$ as well as $e^{-jn\theta}$, and whose z dependence is sin hz and cos hz as well as e^{-jhz}. Such solutions are obtained by a proper linear combination of the expressions given by Eqs. 49 through 54 with $\psi = 0°$, of course, and correspond to solutions which are standing waves in z or θ or both. Such solutions would fit the boundary conditions imposed if perfectly conducting infinite planes were placed perpendicular to the z axis or along planes of constant θ (at intervals of $\pi/|n|$) or both. In the following only the unbounded system is considered.

In solving Eq. 56 it is most convenient to find those values of ζa, for a given n as ka varies, for which Eq. 56 is satisfied. However, it is the propagation constant h and the ratio ka/ha which are of greatest interest, and it is these quantities which are considered below. For $\psi = 0°$ for $n = 0$ there are no free mode solutions of the type

which are of most interest here, whereas for $|n| \geq 1$ the solutions can be shown as in Fig. 4. In $|h_{n,m}|a$ the n subscript refers to the mode number, and the m subscript refers to the branch of the solution. The reason for distinguishing between the different parts of a solution for a given n by using m and by showing the different portions of the curves as solid and dotted lines is considered below. Quite similar curves occur for $-|h_{n,m}|a$ which can be obtained by reflection about the ka axis in Fig. 4 if care is taken to account for a complication which is also discussed below. Another form of presentation is shown in Fig. 5, where the corresponding parts of the curves are related to those of Fig. 4 in an obvious manner. Because Eq. 56 is an even function of n and h, it is evident that $|h_{|n|,m}| = |h_{-|n|,m}|$. The nth mode exists only in the range

$$|n| + \Delta_n \geq ka > \sqrt{n^2 - 1}$$

where Δ_n is a very small positive number. $\Delta_1 \approx 0.015$, $\Delta_2 \approx 0.01$, and Δ_n becomes increasingly small as $|n|$ increases. The curves of Figs. 4 and 5 are only approximately to scale, and the effect of Δ_n is exaggerated very much.

Since the sheath ring may be considered as the limit of an infinite series of circular rings when the rings have become infinitesimally wide and similarly spaced, one might expect from an approximate lumped circuit analogy for such a transmission system that it would support a free mode at or near the frequency for which each individual element, i.e. each ring, is separately resonant. This would occur when the circumference of the rings is an integral number of wavelengths, or for $2\pi a/\lambda = ka = |n|$. This is essentially the performance of the sheath ring, and the spread in frequency over which each free mode solution exists can be considered the result of the coupling between the elements (the rings) of this system. A physical explanation for the absence of the $n = 0$ mode of the type considered here is simply that no ring resonance can exist which produces such a mode. The persistence of the $|n| = 1$ mode down to low frequencies distinguishes it somewhat from the others. This is a property which the sheath ring has in common with the open dielectric rod (refs. 2, 39, 49). An explanation for this action would seem to be that for ka small, and thus ζa exceedingly small, the solution appears as essentially a perturbed uniform plane wave which is linearly or circularly polarized depending on whether the trigonometric or exponential dependence on θ is chosen. This may be shown from the field expressions by taking ka very small so that $|h_{\pm 1,1}|a$ is near ka with ζa exceedingly small, and by considering the region where ζr is small but r is not necessarily small. In this case the $E_z^{i,e}$ and $H_z^{i,e}$ components are substantially ka times as large as the $E_{r,\theta}^{i,e}$ and $H_{r,\theta}^{i,e}$ components, the latter are essentially independent of r, and the ratios

$$\frac{E_\theta^{i,e}}{H_\theta^{i,e}} \text{ and } \frac{E_r^{i,e}}{H_r^{i,e}}$$

are given by $\pm j(\mu/\epsilon)^{1/2}$.

In Figs. 4 and 5 portions of the curves are dotted. The reason is that the solutions corresponding to the dotted and solid lines are really different branches of the curves, so that for $|n| + \Delta_n \gtrsim ka > |n|$ there are two waves per mode. Assuming $z > 0$ for the moment, one of these has z dependence like $e^{-j|h_{n,1}|z}$; whereas the other has z dependence like $e^{+j|h_{n,2}|z}$. The absolute bars are used to avoid any confusion of sign, the sign of the exponential being given explicitly. The procedure used to obtain the above is explained best by considering the inhomogeneous or source-present problem (see sec. I-G). Here, only the results and their physical significance are discussed.

The phenomenon can be interpreted by considering a curve for both positive and negative $|h_{n,m}|a$ for a particular n as shown in Fig. 6. Assume that a finite source is placed at $z = 0$ which can excite only the nth mode. The z axis is, of course, taken to coincide with the axis of the sheath ring, and the radius of the sheath ring, a, is assumed to remain constant while the frequency is varied in the following. Now assume that one stations himself on the positive z axis so the source is very far away. The sheath ring system continues on towards $z = +\infty$. As the frequency of the source or ka is increased, no field is observed (it is assumed that the source is sufficiently far away so that the radiation field is negligible) until $ka = (n^2 - 1)^{1/2}$ after which a free mode wave traveling towards $z = +\infty$ appears with a propagation constant $|h_{n,1}|$. Here, traveling refers to the axial phase velocity and its direction or sign. As ka increases, the propagation constant of this wave increases, varying along the solid $|h_{n,1}|a$ curve in Fig. 6 in the direction indicated there. For ka larger than |n| by any small amount, another free mode wave appears which travels towards the source with a propagation constant of magnitude $|h_{n,2}|$. This varies with increasing ka along the solid $-|h_{n,2}|a$ curve in Fig. 6 in the manner shown there. Both waves continue to exist until $ka = |n| + \Delta_n$. At this point they become waves traveling in both directions with propagation constants of equal magnitude and, it turns out, field components of equal amplitude, so that a pure standing wave exists on the system. For $ka > |n| + \Delta_n$, nothing is observed again, the free mode waves disappearing. If one stations himself on the negative z axis so that the source is very far away, the system continuing on towards $z = -\infty$, a situation similar to the above results, except that the dotted curves in Fig. 6 are traced. It should be remembered that solutions whose z and t behavior is like $e^{-jhz}\, e^{j\omega t}$ are being used.

A physical interpretation of the inward traveling wave, the wave traveling towards the source, is that it is the total result of the backward scattering which occurs when the frequency is such that the rings are slightly beyond resonance, or for $ka > |n|$. It should be emphasized that for $|n| + \Delta_n \gtrsim ka > |n|$ the total free mode consists of the sum of both inward and outward traveling waves. The inward traveling wave does not come from any source at infinity, and if the medium is taken to be slightly lossy, it has a z dependence for $z > 0$ like $e^{j|h_{n,2}|z}\, e^{-|\alpha_{n,2}|z}$, the outward traveling wave having

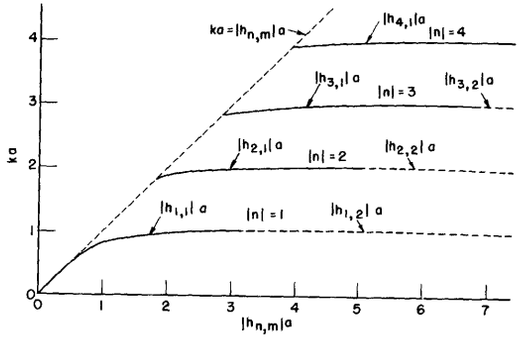

Fig. 4

The sheath ring; $|n| \geq 1$, ka vs $|h_{n,m}|a$, $\psi = 0°$. Curves continue in a similar manner for $|n| \geq 5$.

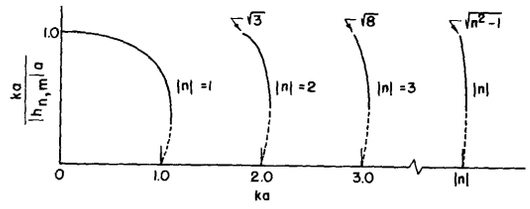

Fig. 5

The sheath ring; $ka/|h_{n,m}|a$ vs ka, $\psi = 0°$.

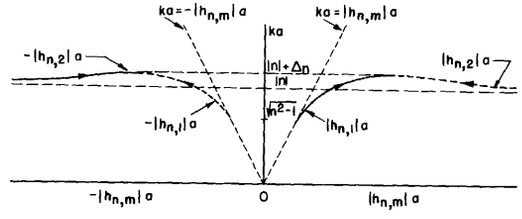

Fig. 6

The sheath ring; $|n| \geq 1$, ka vs $\pm |h_{n,m}|a$, $\psi = 0°$.

a z dependence like $e^{-j|h_{n,1}|z}\, e^{-|a_{n,1}|z}$. The action here is somewhat reminiscent of the performance of structures which are periodic in the z direction (5, 37). There, however, a multiplicity of pass and attenuation bands usually exists even for a particular mode as characterized by the transverse field structure, and the inward traveling wave which occurs is interpreted as the total result of scattering from the periodically located elements. Here, only one passband exists for a particular mode (the mode does not even exist outside this band), the system is continuous in z, and the inward traveling wave occurs only when the elements of the system themselves, or the rings, are slightly beyond resonance.

The ratio of the phase velocity of a free mode wave along the axis of a transmission system v_p to the phase velocity of a uniform plane wave in the medium v_o is given by

$$\frac{v_p}{v_o} = \frac{ka}{ha}. \tag{60}$$

If the medium is free space, $v_o = c$ where c is the velocity of light in free space. Also

$$\frac{\lambda_g}{\lambda} = \left| \frac{v_p}{v_o} \right| = \left| \frac{ka}{ha} \right| \tag{61}$$

where λ_g is the wavelength of the free mode waves on the system. Phase velocity is the velocity with which a constant phase front or point of a steady-state wave may be considered to travel. In the previous discussion the inward and outward traveling waves were distinguished by the direction of phase change in the axial direction. With $e^{j\omega t}$ as the time variable, outward traveling waves are those with z variation like $e^{-j|h|z}$, $z > 0$, or $e^{j|h|z}$, $z < 0$, that is, with increasing phase retardation away from the source. On the other hand, inward traveling waves are those with z variation like $e^{j|h|z}$, $z > 0$, or $e^{-j|h|z}$, $z < 0$, that is, with increasing phase advance away from the source. Group velocity is generally considered as the envelope velocity of a narrow spectrum of waves, or as the velocity with which energy is propagated along the system (refs. 1, 5, 39). In either case, with v_g as the group velocity and v_o as before

$$\frac{v_g}{v_o} = \frac{d(ka)}{d(ha)}. \tag{62}$$

(See also sec. I-F.)

In Figs. 4 and 6 the slope of a straight line from the origin to some point on a curve equals v_p/v_o, whereas the slope of a tangent line at the point is the value of v_g/v_o, both for a particular ka and $|n|$. It is evident that v_p/v_o and v_g/v_o may be positive or negative. Further, it should be noted that it is the phase and group velocities in the z direction which are defined above. Only these are considered throughout this section.

For the purposes of the following discussion, which is quite similar to the previous one except that the remarks refer to the phase and group velocities, it is convenient to

consider z very large and positive and to confine attention to the solid curves in Fig. 6. However, similar remarks can be made if one takes $z < 0$ and regards only the dotted curves in Fig. 6. For $|n| \geq ka > (n^2 - 1)^{1/2}$ only an outward traveling wave exists. For all modes the initial value of v_p/v_o for this wave is unity and decreases as ka increases. The initial value of v_g/v_o is unity only for $|n| = 1, 2$ and can be shown to be given by

$$\frac{v_g}{v_o} = \frac{1}{1 + \frac{2(n^2 - 4)n^2}{5n^2 - 2}} \tag{63}$$

for $|n| \geq 3$. These values are limiting values which result if ka is allowed to approach $(n^2 - 1)^{1/2}$ from above. Note that the group velocity of the outward traveling wave is positive as would be expected since the total average flow of power must be outward. For $|n| + \Delta_n \geq ka > |n|$ outward and inward traveling waves exist, and the phase velocity of the latter is, of course, negative for $z > 0$. The magnitude of the phase velocity of the inward traveling wave is at first zero and increases rapidly as ka increases, so that at $ka = |n| + \Delta_n$ it equals the magnitude of the phase velocity of the outward traveling wave. It can be seen that the group velocity of the inward traveling wave is at first zero, increases to a small positive value, and then decreases to zero again for $ka = |n| + \Delta_n$. Even though the phase velocity of the inward traveling wave is negative, its group velocity is positive or zero. Since both waves have positive group velocities, the total average flow of power is outward for $|n| + \Delta_n > ka > |n|$, as well as for $|n| \geq ka > (n^2 - 1)^{1/2}$ where only an outward traveling wave exists. As already noted, for $ka = |n| + \Delta_n$ the magnitude of the phase velocity of both the outward and inward traveling waves is the same, and the amplitudes of their field components are likewise equal. Consequently, a pure standing wave in z exists, and there is no net average power flow in either direction. This is indicated by the zero slope of the ka versus $|h_{n,m}|$ curves in Figs. 4 and 6 for $ka = |n| + \Delta_n$. The problem of power flow is considered in greater detail in section I-F.

2. The Sheath Tube, $\psi = 90°$

For $\psi = 90°$ the boundary conditions (Eqs. 7-13) become

$$E_{\parallel}^i = E_{\parallel}^e = E_z^i = E_z^e = 0 \tag{64}$$

$$E_{\perp}^i = E_{\perp}^e = E_{\theta}^i = E_{\theta}^e \tag{65}$$

$$H_{\parallel}^i = H_{\parallel}^e = H_z^i = H_z^e \tag{66}$$

for $r = a$, $2\pi \geq \theta \geq 0$, and $\infty > z > -\infty$. The sheath tube system may be considered as the limiting one which results from several perfectly conducting infinitely long z directed wires spaced uniformly on the circumference of a circle of radius a, when the diameter of the wires and their spacing become infinitesimally small, while the number

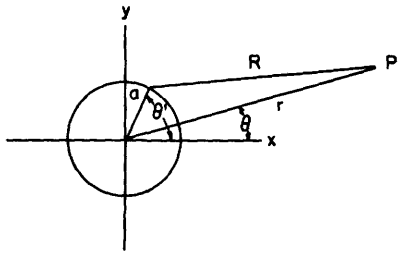

Fig. 7
The sheath tube.

of wires becomes infinitely large. For $h = \pm k$ free mode solutions can exist, and in this case the solutions are TEM waves, $E_z = H_z = 0$. The field expressions may therefore be readily derived from static considerations since for TEM waves the distribution of the fields in the transverse plane, the xy plane here, is a static one. Although this section is concerned primarily with a discussion of the determinantal equation, we shall digress briefly and derive the fields for $\psi = 90°$ in a simple manner.

For $n = 0$, although a solution to the Maxwell equations exists for $r > a$ for these boundary conditions, it is not a free mode in the sense used here since it can never be excited by a finite source. For $|n| \geq 1$, however, free mode fields exist which can be simply derived in the following manner. Assume that current flows only in the z direction on the surface of a cylinder of radius a, and that the current density distribution K_z is given by

$$K_z = |K_{11}| \cos|n|\theta \, e^{-jkz} \tag{67}$$

with $|n| \geq 1$. A cross sectional view of such an arrangement is shown in Fig. 7 and is, of course, the sheath tube. The mediums for $r > a$ and $r < a$ are assumed, as before, to be the same and lossless. The continuity condition (Eq. 55) gives for the surface charge density

$$q_s = -\frac{\nabla_s \cdot \bar{K}}{j\omega} = \frac{k}{\omega} |K_{11}| \cos|n|\theta \, e^{-jkz}. \tag{68}$$

The potential V at point P resulting from this surface charge is given by

$$V = \frac{a}{2\pi\epsilon} \int_0^{2\pi} q_s \ln\frac{1}{R} \, d\theta' + C \tag{69}$$

where R and θ' are defined as shown in Fig. 7, and C is some arbitrary constant. By using the expansions

$$\ln\frac{1}{R} = \sum_{m=1}^{\infty} \frac{1}{m}\left(\frac{a}{r}\right)^m (\cos m\theta' \cos m\theta + \sin m\theta' \sin m\theta) - \ln r, \quad r > a \tag{70a}$$

and

$$\ln\frac{1}{R} = \sum_{m=1}^{\infty} \frac{1}{m}\left(\frac{r}{a}\right)^m (\cos m\theta' \cos m\theta + \sin m\theta' \sin m\theta) - \ln a, \quad r < a \tag{70b}$$

(see reference 50, page 252) in Eq. 69, there results

$$V^e = \frac{a}{2}\sqrt{\frac{\mu}{\epsilon}}\,|K_{11}|\,\cos|n|\theta\,\frac{1}{|n|}\left(\frac{a}{r}\right)^{|n|}\,e^{-jkz} + C, \quad r \geq a \tag{71a}$$

and

$$V^i = \frac{a}{2}\sqrt{\frac{\mu}{\epsilon}}\,|K_{11}|\,\cos|n|\theta\,\frac{1}{|n|}\left(\frac{r}{a}\right)^{|n|}\,e^{-jkz} + C, \quad r \leq a. \tag{71b}$$

The electric field components are given by

$$E_r = -\frac{\partial V}{\partial r} \tag{72}$$

$$E_\theta = -\frac{1}{r}\frac{\partial V}{\partial \theta} \tag{73}$$

with $E_z = 0$, and the magnetic field components can be obtained from Eqs. 72 and 73 by using the Maxwell equation 14. Proceeding in this manner, one finds the field components to be

$$E_r^i = -\frac{1}{2}\sqrt{\frac{\mu}{\epsilon}}\,|K_{11}|\,\cos|n|\theta\left(\frac{r}{a}\right)^{|n|-1}\,e^{-jkz} \tag{74a}$$

$$E_r^e = \frac{1}{2}\sqrt{\frac{\mu}{\epsilon}}\,|K_{11}|\,\cos|n|\theta\left(\frac{a}{r}\right)^{|n|+1}\,e^{-jkz} \tag{74b}$$

$$E_\theta^i = \frac{1}{2}\sqrt{\frac{\mu}{\epsilon}}\,|K_{11}|\,\sin|n|\theta\left(\frac{r}{a}\right)^{|n|-1}\,e^{-jkz} \tag{75a}$$

$$E_\theta^e = \frac{1}{2}\sqrt{\frac{\mu}{\epsilon}}\,|K_{11}|\,\sin|n|\theta\left(\frac{a}{r}\right)^{|n|+1}\,e^{-jkz} \tag{75b}$$

and

$$H_r^i = -\frac{1}{2}\,|K_{11}|\,\sin|n|\theta\left(\frac{r}{a}\right)^{|n|-1}\,e^{-jkz} \tag{76a}$$

$$H_r^e = -\frac{1}{2}\,|K_{11}|\,\sin|n|\theta\left(\frac{a}{r}\right)^{|n|+1}\,e^{-jkz} \tag{76b}$$

$$H_\theta^i = -\frac{1}{2}\,|K_{11}|\,\cos|n|\theta\left(\frac{r}{a}\right)^{|n|-1}\,e^{-jkz} \tag{77a}$$

$$H_\theta^e = \frac{1}{2}\,|K_{11}|\,\cos|n|\theta\left(\frac{a}{r}\right)^{|n|+1}\,e^{-jkz}. \tag{77b}$$

It can be shown that the above constitute permissible free mode solutions for $|n| \geq 1$, since for each n they satisfy the Maxwell equations and the boundary conditions, and can be excited by a finite source.

If it is now assumed that a surface current density of the form

$$K_z = j\,|K_{11}|\,\sin|n|\theta\,e^{-jkz} \tag{78}$$

exists, the resulting field expressions derived by the above procedure are quite similar

in form to Eqs. 74 through 77; the component E_θ^e, for example, is given in this case by

$$E_\theta^e = - j \frac{1}{2}\sqrt{\frac{\mu}{\epsilon}} |K_{||}| \cos |n| \theta \left(\frac{a}{r}\right)^{|n|+1} e^{-jkz}. \tag{79}$$

Since the field equations are linear, Eqs. 67 and 78 can be added to obtain a total current density like

$$K_z = |K_{||}| e^{j|n|\theta} e^{-jkz} \tag{80}$$

the resulting field components being obtained by adding Eqs. 74 through 77 to their counterparts obtained from Eq. 78. Thus, for example, with a current density like Eq. 80, the E_θ^e component becomes

$$E_\theta^e = - j \frac{1}{2}\sqrt{\frac{\mu}{\epsilon}} |K_{||}| \left(\frac{a}{r}\right)^{|n|+1} e^{j|n|\theta} e^{-jkz}. \tag{81}$$

As might be expected from physical considerations, a set of solutions for the sheath helix approaches the type of waves considered here as ψ approaches 90°. In fact, for these it is found that as ψ approaches 90°, some of the h approach k in magnitude and the corresponding ζ approach zero. Using this in the field expressions 49 through 54 and similar ones for the internal fields, it can be shown that in the limit of $\psi = 90°$ one obtains precisely the current density given by Eq. 80 and its associated field components. Of course, one may obtain solutions whose θ dependence is like $e^{-j|n|\theta}$ by finding the fields resulting from a current density distribution like

$$K_z = - j |K_{||}| \sin |n| \theta \, e^{-jkz} \tag{82}$$

and adding these to the fields obtained using Eq. 67; or again, with some precautions these may be obtained from the limiting values of the sheath helix solution. The limit of the sheath helix solution always gives fields whose θ dependence is like $e^{-jn\theta}$, since, indeed, for $\psi \neq 0°$ or 90° only this form of θ dependence is allowed by the boundary conditions. However, as seen above and as would be expected from the symmetry of the boundary conditions, for $\psi = 90°$ linearly as well as circularly polarized fields are possible. It should be noted (see also sec. I-E-3) that only those sheath helix modes for which the product nh is negative go over into the TEM waves discussed in the foregoing as ψ approaches the limit of 90°.

The solutions with e^{-jkz} dependence correspond to waves whose phase retardation increases in the positive z direction. Solutions whose phase retardation increases in the negative z direction, that is, with z dependence like e^{jkz}, can also exist on a sheath tube and can be readily found in the above manner. Thus, solutions with z dependence like sin kz or cos kz, as well as with θ dependence like sin $|n|\theta$ and cos $|n|\theta$ can occur; and, of course, these correspond to standing waves in θ or z or both. Here, as for $\psi = 0°$, such solutions would fit the boundary conditions imposed if perfectly conducting infinite planes were placed perpendicular to the z axis or along planes

of constant θ (at intervals of $\pi/|n|$) or both. However, contrary to the sheath ring case, only outward traveling waves can occur on an unbounded sheath tube as the result of excitation by a single finite source. Further, the magnitude of the ratios v_p/v_o and v_g/v_o for these waves is always unity for all values of ka as would be expected for TEM waves. The solutions discussed here correspond to the various symmetrical component waves or modes which can exist on a multiwire circular "cage" transmission line as the number of wires and, consequently, the number of component waves becomes infinitely large. The positive and negative sequence waves correspond to the $e^{\pm j|n|\theta}$ solutions, and the zero sequence solution, $n = 0$, may be said not to be possible since there is no "ground return."

3. The Sheath Helix, the General Case

For the sheath ring, $\psi = 0°$, and the sheath tube, $\psi = 90°$, solutions whose θ dependence is like $\sin|n|\theta$ or $\cos|n|\theta$ are possible. In the general sheath helix case, $\psi \neq 0°$ or $90°$, it can be shown that such solutions are not possible, and the θ dependence must be like $e^{-jn\theta}$ if the boundary conditions are to be satisfied. Of course, for $n = 0$ the sheath helix solutions are independent of θ, but the effect of the boundary conditions is still evident as noted below. In Figs. 2 and 3 the single wire helix from which the sheath helix is developed by the multiple winding and limit process is shown as positively wound. Such a helix is one in which motion of a point along the wire axis, which increases the z coordinate of the point positively, increases its θ coordinate in a positive direction, and for this $\cot\psi$ and ψ are positive. A negatively wound helix is one in which motion of a point along the wire axis, which increases its z coordinate positively, decreases θ, and for this $\cot\psi$ and ψ are negative. The same definition applies in an obvious manner to the sheath helix. It is clear that either a positively or negatively wound helix may be considered without altering the really fundamental characteristics of the possible solutions. In other words, if field component solutions exist for a positively wound sheath helix with a functional form like $f_n(r)e^{-jhz}\,e^{-jn\theta}$, then solutions of the form $f_{-n}(r)e^{-jhz}\,e^{jn\theta}$ also exist for the negatively wound sheath helix, both for a given positive or negative n and both with identical characteristics. This is also proved by determinantal equation 42, where the product $n\cot\psi$ occurs and where the other functions of ψ and n are even. The choice of positive or negative ψ fixes the boundary conditions, that is, the direction of skewness with respect to the coordinates, and once having taken either sign of ψ, this must be retained throughout as the condition to which the solutions apply. Here, it is assumed that the helix is positively wound so that $90° > \psi > 0°$ or $0 < \cot\psi < \infty$.

Because of the skewness of the boundary conditions, it seems evident from physical considerations that if outward traveling wave solutions exist for the sheath helix with θ dependence like $e^{-j|n|\theta}$ and $e^{+j|n|\theta}$ for a given $|n|$, then these must have different propagation characteristics. Roughly speaking, one of these solutions represents waves traveling along the wires, whereas the other represents waves traveling across the wires. It would be expected that the properties of these solutions must be different. A

similar remark can clearly be made about inward traveling wave solutions. The determinantal equation indicates this since in the numerator of the right side of Eq. 42 the product nh occurs. Consequently, with h positive or negative, this numerator is different for n positive than for n negative, the other factors in the determinantal equation being unchanged since they are even functions of n and h. Note, however, that if solutions are obtained for h positive for both positive and negative n, then the same solutions exist for h negative but with the n numbering reversed. This is to be expected from the required z and θ dependence of the field solutions, $e^{-jhz}\, e^{-jn\theta}$, and from the physically evident requirement that if solutions exist for increasing or decreasing phase retardation in the positive z direction with positive and negative angular phase retardation, then there must exist identical solutions with increasing or decreasing phase retardation in the negative z direction with negative and positive angular phase retardation, respectively.

For n = 0 the sheath helix determinantal equation becomes

$$\frac{I_1(\zeta a)K_1(\zeta a)}{I_o(\zeta a)K_o(\zeta a)} = \frac{\zeta^2 a^2}{k^2 a^2 \cot^2 \psi}. \tag{83}$$

Figure 8 shows some exact results obtained from Eq. 83 for particular values of ψ, where $ka/|h_o|a$ is plotted versus ka (ref. 10). The m subscript on $h_{n,m}$ for n = 0 is unnecessary and is omitted. This sheath helix mode has been rather thoroughly considered by other investigators, since for ka between about 0.1 and 0.5 its characteristics closely approximate those of the single wire helix which has been extensively used in traveling-wave tubes (9, 10, 11). If ka is plotted versus $|h_o|a$ for this mode, for a given ψ the result appears as in Fig. 9. Since Eq. 83 is even in h, an identical curve exists for negative $|h_o|a$ which can be obtained by reflection about the ka axis in Fig. 9. The initial magnitude of $ka/|h_o|a = |v_p/v_o|$ is unity and decreases as ka increases, approaching the asymptotic value of $\sin \psi$ from above. The magnitude of the initial slope of the ka versus $|h_o|a$ curve, $|v_g/v_o|$, is also unity and decreases as ka increases, also approaching the asymptotic value of $\sin \psi$. This asymptotic value is the result one might expect from simple considerations since, if a wave traveled along the sheath wires with the velocity v_o, it would be anticipated that the axial velocity, or velocity in the z direction, would be $v_o \sin \psi$ (9, 10).

For a given ka, the magnitude of the phase velocity decreases as ψ becomes smaller. For any small but finite ψ a solution exists, although for ψ exceedingly small, the phase and group velocities have correspondingly small magnitudes. For $\psi = 0°$, that is, for the sheath ring, there is no free mode solution for n = 0 with finite fields for r > a and r < a together. As ψ approaches 90°, the magnitudes of the phase and group velocities differ by only a small amount from v_o, and ζa becomes small for all ka. In fact, for ψ near but not equal to 90°, for the region where ζr is small but r is not small, it can be shown from the field expressions 49 through 54, with n = 0, that all the external field components except E_r^e and H_θ^e are of small order, that these

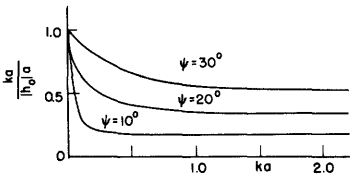

Fig. 8

The sheath helix;
$ka/|h_o|a$ vs ka, n = 0.

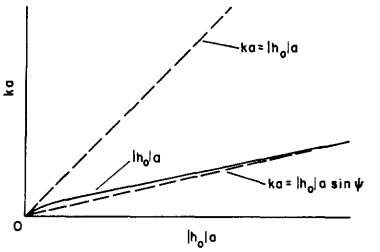

Fig. 9

The sheath helix;
ka vs $|h_o|a$, n = 0,
$90° > \psi > 0°$.

two are proportional to $1/r$, that the magnitude of their ratio is given by $\sqrt{\mu/\epsilon}$, and that $\oint rH_\theta^e \, d\theta$ equals the total enclosed conduction current. Thus, for ψ close to 90°, the external fields of the n = 0 mode resemble those of the TEM wave surrounding a straight infinite perfectly conducting wire. However, as noted previously, for r > a the n = 0 mode for the sheath tube, $\psi = 90°$, is a nonphysical solution since it requires that an infinite amount of power be supplied to the system.

Since the determinantal equation for n = 0 is even in h, similar solutions are obtained for positive and negative h, that is, $h = \pm|h_o|$. These are interpreted in the usual manner as similar waves traveling in the positive and negative z direction. However, despite this symmetry, it must not be thought that the wave traveling in the negative z direction can be obtained from the wave traveling in the positive z direction simply by reflection from an infinite perfectly conducting plane placed perpendicular to the z axis. Even for the n = 0 mode, "a wave reflected at a plane boundary tends to spiral in the wrong direction" (22). Another way of viewing this is to note that from the field expressions 49 through 54 it is not possible to choose positive and negative traveling waves which result in a pure standing wave in z for which both E_r and E_θ are simultaneously zero over a plane of constant z. Some field plots for this mode are shown in references 19 and 22.

For $n \neq 0$ the propagation characteristics of the sheath helix modes are somewhat more complicated than for the various special cases discussed so far. In the curves which are presented now for these propagation characteristics, portions of the lines are shown solid and dotted in different ways. As in the sheath ring case these different parts correspond to different branches of the curves. The procedure whereby this is deduced is explained best by considering the inhomogeneous or source-present problem; this is done in section I-G. Here, only the results and their physical significance are discussed. The modes for which $nh'_{n,m} > 0$ are considered first. The single prime is used here to distinguish these solutions for $\psi \neq 0°$ from another set for $\psi \neq 0°$ considered shortly, and from those for $\psi = 0°$. The m values here are related to the ones used for $\psi = 0°$, although now, for $\psi \neq 0°$, an additional solution may occur. Graphs of $ka/|h'_{n,m}|a$ versus ka for $|n| = 1$ and $|n| = 2$ are shown in Fig. 10. For $|n| \geq 2$ the

characteristics of the modes are essentially identical. As in the sheath ring case the $|n| = 1$ mode is somewhat exceptional in that a solution persists to arbitrarily small values of ka. Plots of ka versus $|h'_{n,m}|a$ are shown in Fig. 11 for $|n| = 1$ and $|n| = 2$. In Figs. 10 and 11 the $\psi = 0°$ curve is included for reference and to indicate how the transition occurs. As ψ approaches and becomes equal to 0°, $|h'_{n,1}|$ becomes $|h_{n,1}|$, $|h'_{n,2}|$ becomes $|h_{n,2}|$, and $|h'_{n,3}|$ vanishes. Note that for ka slightly larger than $|n|$ and $\psi > 0°$ three solutions or waves occur. This happens only for exceedingly small values of ψ and over a narrow range of ka for ka slightly larger than $|n|$. For example, by calculation using the determinantal equation 42, it has been found that for $|n| = 1$ the propagation characteristics are given by a curve like the one labeled ${}_1\psi_1$ for $0.191° \geqslant \psi > 0°$, whereas for $\psi \geqslant 0.286°$ the curve becomes like the one labeled ${}_1\psi_2$. The transition occurs for $0.286° > \psi > 0.191°$ and for ka approximately equal to 1.026. It has not been possible to find a simple expression which gives the largest ψ, say ${}_{|n|}\psi_{max}$, for which curves like those labeled ${}_1\psi_1$ for $|n| = 1$, ${}_2\psi_1$ for $|n| = 2$, etc. just barely occur, that is, the $|h'_{n,2}|$ and $|h'_{n,3}|$ branches just barely occur, although a straightforward but lengthy calculative procedure for finding ${}_{|n|}\psi_{max}$ is available. Since the specific value of ${}_{|n|}\psi_{max}$ seems to be of minor interest, it should be sufficient to note that ${}_{|n|}\psi_{max}$ is less that 0.286° for $|n| = 1$, and that it becomes increasingly smaller as $|n|$ increases. Further, as $|n|$ increases, the transition occurs for values of ka which approach $|n|$ more closely. It can be realized from the above that the transition effect has been very much exaggerated in Figs. 10 and 11 in order to show it in detail.

As in the $n = 0$ case for ka becoming larger, for all $|n|$ the value of $ka/|h'_{n,m}|a$ decreases from its initial value and approaches the asymptotic value of $\sin\psi$ from above for both the $|h'_{n,1}|$ and $|h'_{n,3}|$ branches. However, the values for different $|n|$ are still slightly different, the magnitudes being such that

$$\left[\frac{ka}{|h_o|a}\right]_{n=0} < \left[\frac{ka}{|h'_{n,m}|a}\right]_{|n|=1} < \left[\frac{ka}{|h'_{n,m}|a}\right]_{|n|=2} \quad \ldots \text{ etc.} \tag{84}$$

for a fixed value of ψ for large values of ka. Actually, Eq. 84 holds for any value of ka, as well as for ka large, for a fixed value of ψ where $90° > \psi > 0°$ (see Figs. 8 and 10).

In the sheath ring case the $|n|^{th}$ mode solutions occur only for $|n| + \Delta_n \geqslant ka > (n^2 - 1)^{1/2}$. In other words, for $\psi = 0°$ there is both an upper and lower cut-off or divergence frequency (39), and outside the band they define the $|n|^{th}$ mode does not exist. For $\psi \neq 0°$ an upper frequency limit no longer exists, and for $|n| \geqslant 2$ the low frequency limit is modified. It can be shown (68) that if $ka < {}_nk_da$ for a given ψ, where

$${}_nk_da = \frac{(n^2 - 1) + \sqrt{(n^2 - 1)^2 + (n^2 - 1)n^2\cot^2\psi}}{|n|\cot\psi} \tag{85}$$

or if $\cot\psi < \cot {}_n\psi_{min}$ for a given ka, where

$$\cot_n\psi_{min} = \frac{2ka}{|n|\left(\frac{k^2a^2}{n^2 - 1} - 1\right)} \tag{86}$$

then there is no solution for the $|n|^{th}$ mode. It should be recalled that the modes for which $nh'_{n,m} > 0$ are being considered. As ψ becomes increasingly large, the minimum value of ka for which the $|n| \geq 2$ modes can occur, ${}_nk_da$, also becomes increasingly large, such that in the limit of $\psi = 90°$ these modes vanish. For ψ very close to 90° and for the $|n| = 1$ mode the solution appears as essentially a perturbed uniform plane wave which is circularly polarized. This can be shown from the field expressions by taking $\cot\psi$ very small so that $|h'_{\pm 1,1}|a$ is close to ka with ζa exceedingly small and by considering the region where ζr is small but r is not necessarily small. In this case the $E_z^{i,e}$ and $H_z^{i,e}$ components are substantially $\cot\psi$ times as large as the $E_{r,\theta}^{i,e}$ and $H_{r,\theta}^{i,e}$ components, the latter are essentially independent of r, and the ratios

$$\frac{E_r^{i,e}}{H_r^{i,e}} \quad \text{and} \quad \frac{E_\theta^{i,e}}{H_\theta^{i,e}}$$

are given by $-j\sqrt{\mu/\epsilon}$. Since the magnitudes of both $H_\theta^{i,e}$ and $H_r^{i,e}$ are equal to $|K_{||}|$ for $\cot\psi$ very small, if this mode existed in the limiting case of $\psi = 90°$ with finite $|K_{||}|$, it would transmit infinite energy. Consequently, such a free mode must be excited to only a very small amplitude by any finite source for ψ near 90°, and $|K_{||}|$ must approach and finally equal zero as ψ approaches and finally equals 90°. Therefore, for all $|n|$ and $nh'_{n,m} > 0$ for any ka, with ψ increasing, the solutions vanish in the manner indicated above as the sheath helix becomes the sheath tube.

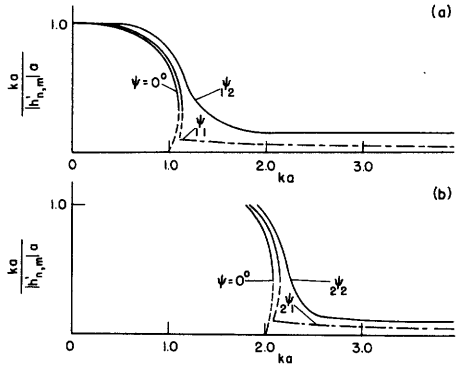

Fig. 10
The sheath helix. (a) $ka/|h'_{n,m}|a$ vs ka, $|n| = 1$ and $nh'_{n,m} > 0$, ${}_1\psi_2 > {}_1\psi_1 > 0°$. (b) $ka/|h'_{n,m}|a$ vs ka, $|n| = 2$ and $nh'_{n,m} > 0$ (similar for $|n| \geq 3$), ${}_2\psi_2 > {}_2\psi_1 > 0°$.

For $nh''_{n,m} < 0$, graphs of $ka/|h''_{n,m}|a$ versus ka for $|n| = 1, 2$, and 3 are shown in Fig. 12. For identical values of $|n|$, Fig. 13 shows curves of ka versus $-|h''_{n,m}|a$. The double prime is used in these to distinguish them from the previous solutions for $\psi \neq 0°$ but where $nh'_{n,m} > 0$, and from the solutions for $\psi = 0°$. Here again, the m values correspond to those for $\psi = 0°$, although an additional solution occurs for $\psi \neq 0°$ also. As in many previous graphs of the propagation constants, the curves in Figs. 12 and 13 are essentially qualitative only and are considerably distorted for convenience in plotting; nevertheless, their relative positions for different ψ and the signs of their slopes are quite correct. The propagation characteristics of the various modes

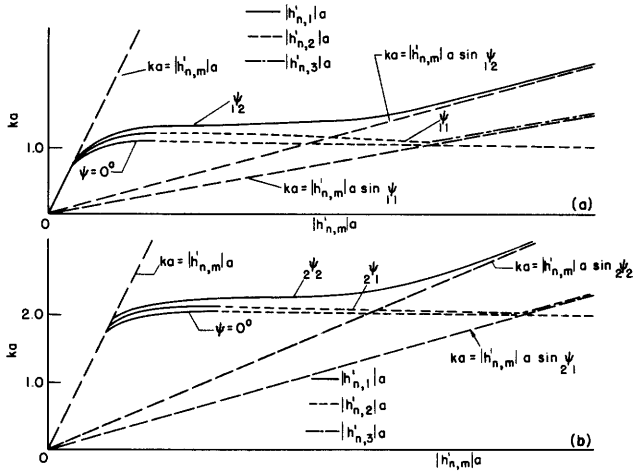

Fig. 11

The sheath helix. (a) ka vs $|h'_{n,m}|a$, $|n| = 1$ and $nh'_{n,m} > 0$, ${}_1\psi_2 > {}_1\psi_1 > 0°$.
(b) ka vs $|h'_{n,m}|a$, $|n| = 2$ and $nh'_{n,m} > 0$ (similar for $|n| \geq 3$), ${}_2\psi_2 > {}_2\psi_1 > 0°$.

are similar, particularly for $|n| \geq 3$. The solutions are shown in Fig. 13 for negative $|h''_{n,m}|$ for convenience in a later discussion. The $\psi = 0°$ curve is included in Figs. 12 and 13 for reference and to indicate how the transition occurs. As ψ approaches and becomes equal to 0°, $|h''_{n,1}|$ becomes $|h_{n,1}|$, $|h''_{n,2}|$ becomes $|h_{n,2}|$, and $|h''_{n,4}|$ vanishes. The fact that for $\psi = 0°$ the $-|h''_{n,1}|a$ and $-|h''_{n,2}|a$ branches as a function of $-|h''_{n,m}|a$ are shown as solid and dotted curves, respectively, in Fig. 13 and in an opposite manner in Fig. 6 is unimportant and should lead to no confusion. The prime on the various ${}_n\psi'_m$ in Figs. 12 and 13 is used merely to distinguish them from those in Figs. 10 and 11 since, in general, they need not be equal. Also, in both cases the n,m subscript numbering of ψ is used only to aid in labeling the curves and to indicate what happens as ψ increases and has no other significance.

For $|n| = 1$ with $nh''_{n,m} < 0$ for $90° > \psi > 0°$, three solutions or waves occur for $ka > 0$ but not too large. As ka increases for a given ψ, two of these, the $|h''_{n,1}|$ and $|h''_{n,2}|$ branches, come together, and for ka still larger only the $|h''_{n,4}|$ branch remains. The $|h''_{n,1}|$ and $|h''_{n,2}|$ branches for $|n| = 1$ always exist over some range of ka for $90° > \psi > 0°$. However, they vanish for smaller values of ka as ψ approaches 90°. It can be shown (68) that for $|n| = 2$ with $nh''_{n,m} < 0$ for a given ψ, if

$$ka < \frac{(n^2 - 1)}{|n| \cot\psi} \left(\sqrt{1 + \frac{n^2 \cot^2\psi}{n^2 - 1}} - 1 \right) \tag{87}$$

then only two solutions, the $|h''_{n,2}|$ and $|h''_{n,4}|$ branches, occur. For ka larger than the limit given by Eq. 87 the $|h''_{n,1}|$ branch also occurs, but only over a small range of ka.

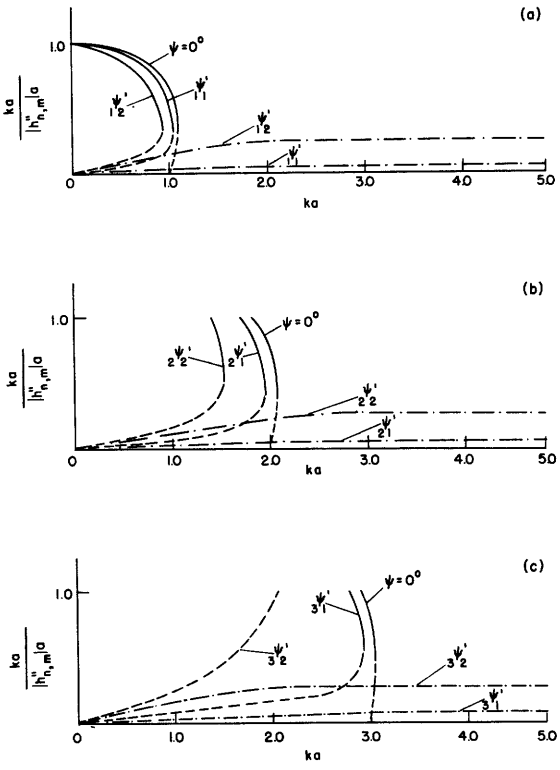

Fig. 12

The sheath helix. (a) $ka/|h''_{n,m}|a$ vs ka, $|n| = 1$ and $nh''_{n,m} < 0$, ${}_1\psi'_2 > {}_1\psi'_1 > 0°$. (b) $ka/|h''_{n,m}|a$ vs ka, $|n| = 2$ and $nh''_{n,m} < 0$, ${}_2\psi'_2 > {}_2\psi'_1 > 0°$. (c) $ka/|h''_{n,m}|a$ vs ka, $|n| = 3$ and $nh''_{n,m} < 0$ (similar for $|n| \geq 4$), ${}_3\psi'_2 > {}_3\psi'_1 > 0°$.

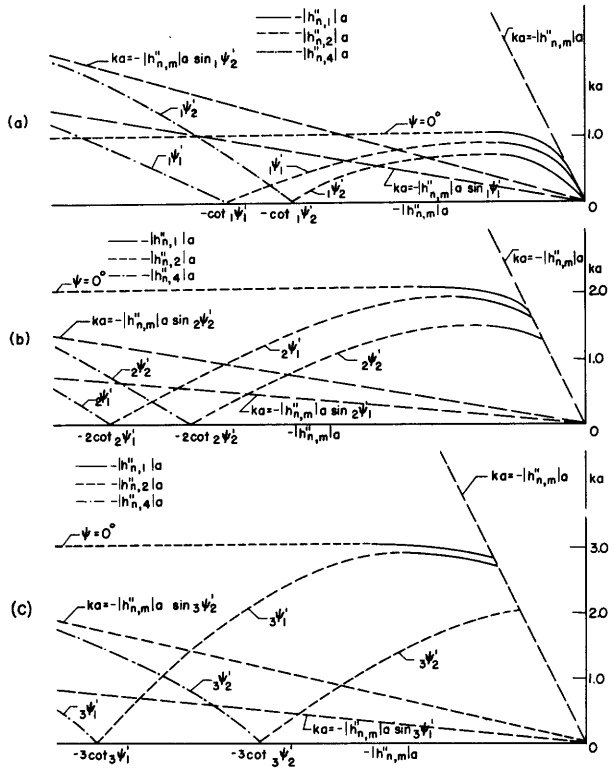

Fig. 13

The sheath helix. (a) ka vs $-|h''_{n,m}|a$, $|n| = 1$ and $nh''_{n,m} < 0$, ${}_1\psi'_2 > {}_1\psi'_1 > 0°$. (b) ka vs $-|h''_{n,m}|a$, $|n| = 2$ and $nh''_{n,m} < 0$, ${}_2\psi'_2 > {}_2\psi'_1 > 0°$. (c) ka vs $-|h''_{n,m}|a$, $|n| = 3$ and $nh''_{n,m} < 0$ (similar for $|n| \geq 4$), ${}_3\psi'_2 > {}_3\psi'_1 > 0°$.

As ka increases, the $|h''_{n,1}|$ and $|h''_{n,2}|$ branches come together, and for ka still larger only the $|h''_{n,4}|$ branch remains. For $|n| = 2$ as for $|n| = 1$ for any $\psi < 90°$, the $|h''_{n,1}|$ and $|h''_{n,2}|$ branches always occur. However, for $|n| \geq 3$, although the limitation given by Eq. 87 still exists, if ψ is larger than a minimum value for a particular n, the $|h''_{n,2}|$ and $|h''_{n,4}|$ branches become the only solutions. In this case the propagation characteristic curve becomes like the one labeled ${}_3\psi'_2$ in Fig. 13c. It has not been possible to find a simple expression which gives the value of ka for a given ψ and n for which the $|h''_{n,1}|$ and $|h''_{n,2}|$ branches come together when both such branches exist. However, this occurs for ka greater than the value given by Eq. 87 satisfied with an equality sign, and it is believed to be within Δ_n of this value.

As ka becomes larger for all $|n|$, the value of $ka/|h''_{n,4}|a$ increases from its initial value and approaches the asymptotic value of $\sin\psi$ from below. However, the values for different $|n|$ are still slightly different, the magnitudes being such that

$$\left[\frac{ka}{|h_o|a}\right]_{n=0} > \left[\frac{ka}{|h''_{n,4}|a}\right]_{|n|=1} > \left[\frac{ka}{|h''_{n,4}|a}\right]_{|n|=2} \quad \ldots \text{ etc.} \tag{88}$$

for a fixed value of ψ for large ka. For ka approaching zero both $|h''_{n,2}|a$ and $|h''_{n,4}|a$ approach $|n|\cot\psi$. It should now be clear how the propagation characteristics of the modes for which $nh''_{n,m} < 0$ change as ψ varies from 0° to 90°. As ψ approaches 90°, the $|h''_{n,1}|$ branch (if it exists at all) and the $|h''_{n,2}|$ branch exist over a smaller range of ka, whereas the $|h''_{n,4}|$ branch approaches its asymptotic value more closely over a larger range of ka. Thus, in the limit of $\psi = 90°$ for all $|n|$, the $|h''_{n,1}|$ and $|h''_{n,2}|$ branches disappear leaving only the $|h''_{n,4}|$ branch for which $ka/|h''_{n,4}|a = 1$ for all ka. These are TEM waves and are, in fact, the symmetrical component waves of the sheath tube discussed in section I-E-2.

The curves of Figs. 11 and 13 are best understood by considering what happens when the sheath helix is driven by a finite source placed at z = 0 which can excite only the nth mode. With no loss of generality as far as this description is concerned, it is assumed that the θ dependence of the source and the resulting waves are of the form $e^{-jn\theta}$ with $n > 0$. The z axis coincides with the axis of the sheath helix, and the radius of the sheath helix, a, as well as the pitch angle, ψ, are considered to remain constant while the frequency is varied in the following. It is now assumed that one stations oneself on the positive or negative z axis at such large distances from the source that the radiation field from the source is negligible. If one is on the positive z axis, depending on the value of ψ, one observes waves whose propagation constants and corresponding phase and group velocities vary along the $|h'_{n,1}|$, $|h'_{n,3}|$, and $-|h''_{n,2}|$ branches as ka is varied; these waves have a z dependence like

$$e^{-j|h'_{n,1}|z}, \quad e^{-j|h'_{n,3}|z}, \quad \text{and} \quad e^{+j|h''_{n,2}|z},$$

respectively. Conversely, if one is on the negative z axis, again depending on the value of ψ, one observes waves whose propagation constants and corresponding phase and group velocities vary along the $|h'_{n,2}|$, $-|h''_{n,1}|$, and $-|h''_{n,4}|$ branches as ka is varied; these waves have a z dependence like

$$e^{-j|h'_{n,2}|z}, \quad e^{+j|h''_{n,1}|z}, \quad \text{and} \quad e^{+j|h''_{n,4}|z},$$

respectively. The $|h'_{n,2}|$ and $|h'_{n,3}|$ waves may not exist if ψ is larger than a quite small maximum value, and also the $|h''_{n,1}|$ wave might not occur for $|n| \geq 3$ for ψ still relatively small. Note that all the waves which exist for positive z have positive group velocities, whereas all the waves which exist for negative z have negative group velocities. Thus, the total power flow is always outward from the source, irrespective of the number of waves which occur for a particular ψ and ka or their phase velocities. Further, if the medium is considered slightly lossy, all the waves become exponentially attenuated in the direction of energy propagation, again irrespective

of their phase velocities.

A few other points are of interest. It would appear that the waves for a given mode or n are inseparable. If the sheath helix is excited by a finite source having a θ dependence like $e^{-jn\theta}$, and if ka and ψ are of such value that more than one wave can exist, then this multiplicity of waves seems to occur always. Although the source may possibly be arranged so that one wave is more strongly excited than another, it does not appear possible that any of the waves can be completely eliminated in general. In the discussion of Figs. 11 and 13 it was assumed that the source and the resulting waves have θ dependence like $e^{-jn\theta}$ with $n > 0$. It should be clear that if a source with θ dependence like $e^{-jn\theta}$ with $n < 0$ is assumed, the waves which now appear for $z > 0$ and $z < 0$ are exactly those which appeared for $z < 0$ and $z > 0$, respectively, with $n > 0$. In the case of $n < 0$, the propagation constants may be considered as obtained by a reflection about the ka axis of Figs. 11 and 13 but with a change in the sign of n. This point may be made clearer by noting again that the determinantal equation is unchanged if the sign of nh is unchanged. Thus

$$|n|h'_{|n|,m} = -|n|h'_{-|n|,m} \tag{89a}$$

$$h'_{|n|,m} = -h'_{-|n|,m} \tag{89b}$$

and

$$|h'_{|n|,m}| = |h'_{-|n|,m}|. \tag{89c}$$

Also

$$|n|h''_{|n|,m} = -|n|h''_{-|n|,m} \tag{90a}$$

$$h''_{|n|,m} = -h''_{-|n|,m} \tag{90b}$$

and

$$|h''_{|n|,m}| = |h''_{-|n|,m}|. \tag{90c}$$

Note that

$$|h'_{|n|,m}| = |h'_{-|n|,m}| \neq |h''_{|n|,m}| = |h''_{-|n|,m}| \tag{91}$$

except for $\psi = 0°$, so that

$$|h'_{\pm|n|,m}|_{\psi=0°} = |h''_{\pm|n|,m}|_{\psi=0°} = |h_{\pm|n|,m}| \tag{92}$$

with the $\pm$ chosen in any order in Eq. 92. If the source has θ dependence like sin $n\theta$ or cos $n\theta$, an identical mixture of all the waves occurs for $z > 0$ and $z < 0$. The final point here is concerned with noting a somewhat anomalous situation which occurs for ψ near and equal to 90°. As previously mentioned, for ψ approaching 90° the modes for which $nh''_{n,m} < 0$, in particular the $h''_{n,4}$ waves, approach the symmetrical component waves of the sheath tube, whereas the modes for which $nh'_{n,m} > 0$ occur only for increasingly large values of ka or become of increasingly small amplitude. Thus, if the limit of $\psi = 90°$ is approached in this manner, only waves with θ and z dependence like

$e^{-jkz}\, e^{+j|n|\theta}$ with $z > 0$ or $e^{+jkz}\, e^{-j|n|\theta}$ with $z < 0$ seem possible. However, it is evident from symmetry and the discussion of section I-E-2 that for $\psi = 90°$ the θ and z dependence of the waves may be of the form $e^{-jkz}\, e^{\pm j|n|\theta}$ with $z > 0$ and $e^{+jkz}\, e^{\pm j|n|\theta}$ with $z < 0$. Consequently, it is evident that waves whose coordinate dependence is like $e^{-jkz}\, e^{-j|n|\theta}$ with $z > 0$ and $e^{+jkz}\, e^{+j|n|\theta}$ with $z < 0$ are not stable on the sheath system considered here. For ψ any small amount less than 90° and ka finite, such waves vanish for $|n| \geq 2$, although for $|n| = 1$ a wave with exceedingly small amplitude can exist.

F. Power Flow.

Since the field expressions of the free modes are available, the real power flow associated with these modes can be readily determined. In the following only the real power is considered. The real part of the complex Poynting vector gives the average intensity of the energy flow, and integrating this quantity over the appropriate cross section yields the desired power (1). Thus, with

$$\bar{S}^* = \frac{1}{2}(\bar{E} \times \tilde{\bar{H}}) \tag{93}$$

where $\bar{S}^*$ is the complex Poynting vector and the tilde means complex conjugate, the total average flow in the z direction is

$$P_z = \mathrm{Re}\left[\int_A \bar{S}_z^*\, dA\right] = \mathrm{Re}\left[\frac{1}{2}\int_A \bar{a}_z \cdot (\bar{E} \times \tilde{\bar{H}})dA\right]$$

$$= \mathrm{Re}\left[\frac{1}{2}\int_0^{\infty}\int_0^{2\pi} \bar{a}_z \cdot (\bar{E} \times \tilde{\bar{H}})r\,dr\,d\theta\right]. \tag{94}$$

Since the field expressions for $r < a$ and $r > a$ are different, the integration on r must be performed in two steps so that

$$P_z^{i,e} = \mathrm{Re}\left[\frac{1}{2}\int_0^{2\pi}\int_{0,a}^{a,\infty} (E_r^{i,e}\, \tilde{H}_\theta^{i,e} - E_\theta^{i,e}\, \tilde{H}_r^{i,e})r\,dr\,d\theta\right] \tag{95}$$

and the total average power P_z is obviously the sum of P_z^i and P_z^e. It is necessary, of course, that the values of ζa and ha which satisfy the determinantal equation 42 for particular values of ka, n, and ψ be used in the power expression. It can be assumed that only one wave occurs on the system, but this imposes no undue restriction on the final results as noted later.

Using the appropriate field expressions of Eqs. 49 through 54 in Eq. 95, one finds after considerable manipulation (68) that

$$P_z = -\pi |K_{\parallel}|^2 \omega\mu a^3 \frac{I_n'(\zeta a) K_n'(\zeta a)}{\zeta^2 a^2} \cos^2\psi \left\{ \frac{ha}{2} \left[4 + f_n^o(\zeta a) \right] \right.$$

$$\left. - n \cot\psi \frac{(k^2a^2 + h^2a^2)}{(\zeta^2 a^2 + nha \cot\psi)} \right\} \qquad (96)$$

where $f_n^o(\zeta a)$ is given by

$$f_n^o(\zeta a) = \zeta a \left[\frac{I_n'(\zeta a)}{I_n(\zeta a)} + \frac{K_n'(\zeta a)}{K_n(\zeta a)} - \frac{I_n(\zeta a)}{I_n'(\zeta a)} - \frac{K_n(\zeta a)}{K_n'(\zeta a)} \right] - \frac{n^2}{\zeta a} \left[\frac{I_n(\zeta a)}{I_n'(\zeta a)} + \frac{K_n(\zeta a)}{K_n'(\zeta a)} \right]. \qquad (97)$$

It can be readily shown that Eq. 96 agrees with the expression given in reference 9 for the power flow on the sheath helix for the n = 0 mode alone. Further, Eq. 96 is valid for $\psi = 0°$ although in this case the second term in the braces becomes $-(k^2a^2 + h^2a^2)/ha$.

In this case if the parallel current density, which is K_θ only for $\psi = 0°$, is given by $|K_{\parallel}| \sin n\theta e^{-jhz}$ or $|K_{\parallel}| \cos n\theta e^{-jhz}$ instead of $|K_{\parallel}| e^{-jn\theta} e^{-jhz}$, π on the right side of Eq. 96 must be replaced by $\pi/2$. Reference 68 shows graphs of $f_n^o(\zeta a)$ for $3 \geqslant n \geqslant 0$, for $10 \geqslant \zeta a \geqslant 0.1$ and simple expressions for $f_n^o(\zeta a)$ valid for large and small ζa.

It can be shown that Eq. 96 also gives the proper expression for the power flow for the sheath tube modes in the limit of $\psi = 90°$. In evaluating the limiting expression the fact that it is the sheath helix modes for which $nh''_{n,m} < 0$, specifically the $h''_{n,4}$ waves, which go over into the TEM waves on the sheath tube must be used. The power can also be evaluated by using Eqs. 94 and 95 and the field expressions given in section I-E-2. In either case there results for $\psi = 90°$ the simple expression

$$P_z = \frac{\pi}{2|n|} \sqrt{\frac{\mu}{\epsilon}} |K_{\parallel}|^2 a^2, \quad |n| \geqslant 1 \qquad (98)$$

if the parallel current density, which is K_z only for $\psi = 90°$, is given by $|K_{\parallel}| e^{-jn\theta} e^{-jkz}$. If the current density is given by $|K_{\parallel}| \cos|n|\theta e^{-jkz}$ or $|K_{\parallel}| \sin|n|\theta e^{-jkz}$, $\pi/2$ on the right side of Eq. 98 must be replaced by $\pi/4$.

In calculating the total average power flow given by Eq. 96 it is assumed that only one wave is present for a particular mode or n. If more than one wave is present, Eq. 96 is used for each wave separately, and the total average power flow is then given by the sum of the powers contributed by each wave alone. To prove this it is first necessary to show that the total average axial power flow is independent of z irrespective of the number of waves present. This in turn is readily proved by applying Poynting's theorem to the lossless source-free volume enclosed by two planes placed perpendicular to the z axis an arbitrary distance apart and a cylindrical surface at r = R, where R approaches infinity (1). The average radial power flow across the cylindrical surface approaches zero since the fields become exponentially or otherwise sufficiently small as R approaches infinity. Consequently, the total average power flow across the two

planes must be equal, and, further, since they are an arbitrary distance apart, it follows that under all circumstances the total average axial power flow for free mode propagation is not a function of z. If P_z is calculated from Eqs. 94 or 95 for the situation where several waves for a given n are present, some consideration shows that the resulting expression is a sum of terms resulting from each wave separately, plus cross terms resulting from the $\bar{E} \times \tilde{\bar{H}}$ product of the different waves, these latter being functions of z. Since the total fields are proper solutions of the Maxwell equations, and Poynting's theorem certainly applies, it is clear from the above that these cross terms must vanish. In this manner the validity of the procedure whereby the entire total average power is obtained by adding the power in each wave alone is established. In order to complete the calculation for the power flow it is necessary to know the $|K_{11}|$ associated with each wave, and this can only be determined by solving the source-present problem as in the next section. It is evident that the power flow resulting from waves in different modes, that is, different n, can be calculated separately since in this case the field representations are orthogonal in θ.

In the previous section it was stated without proof that the group velocity is the velocity of energy propagation, so that the direction or algebraic sign of total average power flow is the same as that of the group velocity. Although this property has been proved for transmission systems with various assumed boundary conditions, it appears not to have been proved for such sheath systems as are discussed here (1, 5, 39). The proof is given below where the procedure used in section 4.2 of reference 39 for a similar proof for different boundary conditions is followed rather closely. In the following it is necessary to split off the z dependence of the field vectors. Since this is the same for all components, one writes $\bar{E} = \underline{E}\, e^{-jhz}$ and $\bar{H} = \underline{H}\, e^{-jhz}$, where $\underline{E}$ and $\underline{H}$ are now complex field vectors independent of z. Note that the product of a vector by a complex conjugate vector is the same whether one uses $\bar{E}$, $\bar{H}$, or $\underline{E}$, $\underline{H}$. The basis for the proof is the energy theorem for lossless systems which states that (39)

$$\nabla \cdot \left(\tilde{\bar{E}} \times \frac{\partial \bar{H}}{\partial \omega} + \frac{\partial \bar{E}}{\partial \omega} \times \tilde{\bar{H}} \right) = - j \left(\epsilon \bar{E}\, \tilde{\bar{E}} + \mu \bar{H}\, \tilde{\bar{H}} \right). \tag{99}$$

This may be readily shown by expanding the left side of Eq. 99 and substituting from the Maxwell equations 14 and 15 for the various terms. Since each wave on the sheath system is separately a solution of the Maxwell equations for the required boundary conditions, Eq. 99 can be applied to the field solutions for each wave alone. Performance of the indicated differentiations, after splitting off the z dependence as noted above, results in

$$\tilde{\bar{E}} \times \frac{\partial \bar{H}}{\partial \omega} + \frac{\partial \bar{E}}{\partial \omega} \times \tilde{\bar{H}} = \tilde{\underline{E}} \times \frac{\partial \underline{H}}{\partial \omega} + \frac{\partial \underline{E}}{\partial \omega} \times \tilde{\underline{H}} - j \frac{\partial h}{\partial \omega} \left(\tilde{\underline{E}} \times \underline{H} + \underline{E} \times \tilde{\underline{H}} \right) z. \tag{100}$$

Since

$$\nabla \cdot \left[\left(\tilde{\underline{E}} \times \underline{H} + \underline{E} \times \tilde{\underline{H}} \right) z \right] = 2 \nabla \cdot \left[\mathrm{Re} \left(\tilde{\underline{E}} \times \underline{H} \right) z \right] \tag{101a}$$

or

$$\nabla\cdot\left[(\tilde{\underline{E}}\times\underline{H}+\underline{E}\times\tilde{\underline{H}})z\right]=2\,\mathrm{Re}\left[z\nabla\cdot(\underline{E}\times\tilde{\underline{H}})+\bar{a}_z\cdot(\underline{E}\times\tilde{\underline{H}})\right] \tag{101b}$$

and since the complex Poynting theorem, which is also directly obtainable from the Maxwell equations, states that for lossless systems (1, 39)

$$\nabla\cdot\bar{S}^*=\nabla\cdot\left(\frac{1}{2}\bar{E}\times\tilde{\bar{H}}\right)=j\frac{\omega}{2}(\epsilon\bar{E}\cdot\tilde{\bar{E}}-\mu\bar{H}\cdot\tilde{\bar{H}}) \tag{102}$$

it is evident, taking the real part of both sides of Eq. 102 and noting that this requires the first term on the right side of Eq. 101b to vanish, that Eq. 99 becomes

$$\nabla\cdot\left(\tilde{\underline{E}}\times\frac{\partial\underline{H}}{\partial\omega}+\frac{\partial\underline{E}}{\partial\omega}\times\tilde{\underline{H}}\right)-j\,2\,\frac{\partial h}{\partial\omega}\,\mathrm{Re}\left[a_z\cdot(\underline{E}\times\tilde{\underline{H}})\right]=-j\,(\epsilon\underline{E}\cdot\tilde{\underline{E}}+\mu\underline{H}\cdot\tilde{\underline{H}}). \tag{103}$$

Integrating Eq. 103 over the region $a\geqslant r\geqslant 0$, there results by using Eq. 95

$$\oint\bar{a}_r\cdot\left(\tilde{\underline{E}}^i\times\frac{\partial\underline{H}^i}{\partial\omega}+\frac{\partial\underline{E}^i}{\partial\omega}\times\tilde{\underline{H}}^i\right)_{r=a}dl-j\,4\,\frac{\partial h}{\partial\omega}P_z^i=-j\int_{A^i}(\epsilon\underline{E}^i\cdot\tilde{\underline{E}}^i+\mu\underline{H}\cdot\tilde{\underline{H}}^i)dA. \tag{104}$$

Similarly, for $\infty\geqslant r\geqslant a$, since the fields become exponentially or otherwise sufficiently small for $r=\infty$

$$-\oint\bar{a}_r\cdot\left(\tilde{\underline{E}}^e\times\frac{\partial\underline{H}^e}{\partial\omega}+\frac{\partial\underline{E}^e}{\partial\omega}\times\underline{H}^e\right)_{r=a}dl-j\,4\,\frac{\partial h}{\partial\omega}P_z^e=-j\int_{A^e}(\epsilon\underline{E}^e\cdot\tilde{\underline{E}}^e+\mu\underline{H}^e\cdot\tilde{\underline{H}}^e)dA. \tag{105}$$

Adding Eqs. 104 and 105, dropping the superscripts where their absence should cause no confusion, noting that only the tangential components of the fields need be retained in the line integral and that $\underline{E}_t^i=\underline{E}_t^e=\underline{E}_t$ for $r=a$, one obtains

$$\oint\bar{a}_r\cdot\left[\tilde{\underline{E}}_t\times\frac{\partial}{\partial\omega}(\underline{H}_t^i-\underline{H}_t^e)+\frac{\partial\underline{E}_t}{\partial\omega}\times(\tilde{\underline{H}}_t^i-\tilde{\underline{H}}_t^e)\right]_{r=a}dl-j\,4\,\frac{\partial h}{\partial\omega}P_z=-j\int_A(\epsilon\underline{E}\cdot\tilde{\underline{E}}+\mu\underline{H}\cdot\tilde{\underline{H}})dA. \tag{106}$$

If the tangential fields for $r=a$ are resolved in directions parallel and perpendicular to the windings of the sheath system, it is clear from the assumed boundary conditions of Eqs. 7 through 9 that $\underline{E}_t$ and $(\underline{H}_t^i-\underline{H}_t^e)$ at $r=a$ are both nonzero only in the perpendicular direction. Consequently, both vector cross products of the integrand of the line integral vanish, and with $\partial h/\partial\omega=(1/v_o)(dh/dk)=1/v_g$ from Eq. 62, Eq. 106 becomes

$$v_g=\frac{P_z}{\frac{1}{4}\int_A(\epsilon\underline{E}\cdot\tilde{\underline{E}}+\mu\underline{H}\cdot\tilde{\underline{H}})dA}. \tag{107}$$

Since the denominator of the right side of Eq. 107 is surely positive, the total average axial power flow resulting from each wave and the group velocity of the wave have the

same direction or algebraic sign, and the usual definition of v_g as the ratio of the total average real power flow to the average energy stored per unit length of the system applies.

The Source-Present Problem

G. The Gap Source

To understand more completely the significance of the many waves which occur on a sheath system, to understand the reason for calling some of these inward and others outward traveling waves as in section E, and to illustrate other points, it is necessary to solve the inhomogeneous or source-present problem. The procedure whereby this is accomplished requires that the fields which result when the sheath system is excited by an infinite line or tube source be determined first. By superimposing these cylindrical wave solutions, one can determine the total field resulting from a finite essentially spherical wave source (1, 2, 39, 48, 50).

1. Derivation of General Results.

Assume that the z component of the electric field has a discontinuity on the surface of the sheath helix which is zero everywhere except for $\ell/2 > z > -\ell/2$ where it has a value $E_n e^{-jn\theta}$ and where E_n is independent of z and θ. By the methods of Fourier integral analysis, this distribution can be represented by

$$\left(E_z^e - E_z^i\right)_{r=a} = \frac{E_n e^{-jn\theta}}{\pi} \int_C \frac{\sin \frac{h\ell}{2}}{h} e^{-jhz}\, dh = \begin{cases} E_n e^{-jn\theta}, & |z| < \frac{\ell}{2} \\ 0, & |z| > \frac{\ell}{2} \end{cases} \qquad (108)$$

The contour C is merely the entire real axis of the h plane from $-\infty$ to $+\infty$. Here, h is considered as a general complex variable and should not be confused with the axial propagation constants of the sheath helix modes, although these latter values are, of course, definite points on the real axis of the complex h plane for lossless systems. A similar remark holds for the variable ζ used below. It is assumed that the above discontinuity in the electric field is maintained by an impressed electric field which is the negative of Eq. 108. This can be considered the result of generators placed in the gap, $|z| < \ell/2$ and r = a, as shown in Fig. 14. The analysis in this section refers to what might be called an internally shielded gap source; that is, the sheath system and the generators are arranged for $|z| < \ell/2$ so that E_z^i is zero for $|z| < \ell/2$ at r = a without disturbing the sheath magnetic field boundary conditions. A less artificial choice for a gap source might have been an unshielded one in which the electric field discontinuity in the gap is in the direction of the windings. However, the type of source used here appears to lead to somewhat simpler formulas and prevents the appearance of the ordinary waveguide modes at $\psi = 0°$ and $90°$.

For E_n increasingly large and ℓ increasingly small, one can write with some

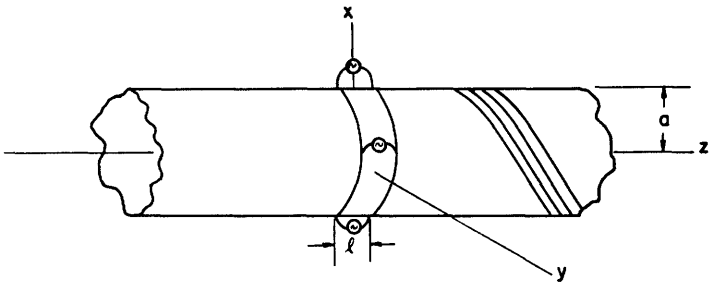

Fig. 14
Gap source driven sheath helix.

caution

$$\left(E_z^e - E_z^i\right)_{r=a} = V_n e^{-jn\theta}\, u_o(z) = \frac{V_n e^{-jn\theta}}{2\pi} \int_C e^{-jhz}\, dh \tag{109}$$

where $u_o(z)$ is the unit impulse at $z = 0$ and $V_n = E_n \ell$ is the voltage across the gap. The use of Eq. 109 in place of Eq. 108 is permissible since, although the integral in Eq. 109 is no longer convergent, the integrals to be derived throughout this discussion using Eq. 109 as the limiting form of Eq. 108 are in general convergent for $|z| > 0$. Equation 109 represents the electric field distribution in the gap as a superposition of infinitesimal z-directed electric fields of the form $(V_n e^{-jn\theta}/2\pi)\, e^{-jhz}\, dh$ existing over the entire length of the sheath helix at $r = a$. Since the system is linear, it is evident that if the fields which result when the z component of the electric field has a discontinuity of the form $(V_n/2\pi)\, e^{-jn\theta}\, e^{-jhz}$ at $r = a$ for all z can be determined, by superposing these fields one can obtain the final fields resulting from the finite gap source.

The regions for $r > a$ and $r < a$ are source-free so that the field components can still be obtained from Hertzian potentials like those given in Eqs. 31 through 34 using Eqs. 20 through 25. Also, the boundary conditions at $r = a$ are again given by Eqs. 11 through 13 using the i superscript in Eq. 12, but Eq. 10 must be modified to read

$$E_z^e - E_z^i = \frac{V_n}{2\pi} e^{-jn\theta}\, e^{-jhz} \tag{110}$$

for $r = a$, $2\pi \geq \theta \geq 0$, $+\infty > z > -\infty$. Carrying through the calculations indicated above merely leads to a set of equations precisely like Eqs. 35 through 38 except that on the right side of Eq. 35 $V_n/2\pi\zeta^2$ replaces 0. Thus, an inhomogeneous system of equations results, which can be solved for the coefficients $A_n^{i,e}$ and $B_n^{i,e}$. If these are distinguished from the ones used previously by the subscript g, there results

$$A_{ng}^i = \frac{V_n}{2\pi\zeta^2} \frac{\zeta a \cot\psi\, I_n'}{D_n} \left[nha\,(\zeta^2 a^2 + nha \cot\psi)\, K_n^2 - k^2 a^2 \zeta^2 a^2 \cot\psi\, K_n'^2\right] \tag{111}$$

$$A^e_{ng} = -\frac{V_n}{2\pi\zeta^2}\frac{\zeta a}{D_n}\left[k^2a^2\zeta^2a^2\cot^2\psi\, K'_n I'^2_n + (\zeta^2a^2 + nha\cot\psi)(\zeta a - nha\cot\psi I_n K'_n)\, I_n\right] \quad (112)$$

$$B^i_{ng} = \frac{(\zeta^2a^2 + nha\cot\psi)}{j\omega\mu a\,\zeta a\cot\psi}\frac{I_n}{I'_n}A^i_{ng} \quad (113)$$

$$B^e_{ng} = \frac{V_n}{2\pi\zeta^2}\frac{1}{j\omega\mu a D_n}\left\{nha\left[(\zeta^2a^2 + nha\cot\psi)^2 I^2_n - k^2a^2\zeta^2a^2\cot^2\psi\, I'^2_n\right]K_n\right.$$

$$\left. - k^2a^2\zeta^4a^4\cot\psi\, K'_n I_n I'_n\right\} \quad (114)$$

where

$$D_n \equiv D_n(\zeta a) = \left[(\zeta^2a^2 + nha\cot\psi)^2 I_n K_n + k^2a^2\zeta^2a^2\cot^2\psi\, I'_n K'_n\right]. \quad (115)$$

The argument of all the modified Bessel functions in Eqs. 111 through 115 above is ζa and has been omitted for convenience. The Hertzian potentials for the fields become

$$\Pi^i_{zg} = e^{-jn\theta}\int_{C_2} A^i_{ng} I_n(\zeta r)\, e^{-jhz}\, dh \quad (116)$$

$$\Pi^{*i}_{zg} = e^{-jn\theta}\int_{C_2} B^i_{ng} I_n(\zeta r)\, e^{-jhz}\, dh \quad (117)$$

$$\Pi^e_{zg} = e^{-jn\theta}\int_{C_2} A^e_{ng} K_n(\zeta r)\, e^{-jhz}\, dh \quad (118)$$

$$\Pi^{*e}_{zg} = e^{-jn\theta}\int_{C_2} B^e_{ng} K_n(\zeta r)\, e^{-jhz}\, dh. \quad (119)$$

The fields can be obtained from Eqs. 116 through 119 by using Eqs. 20 through 25. Thus, for example,

$$H^i_{zg} = -e^{-jn\theta}\int_{C_2} \zeta^2 B^i_{ng} I_n(\zeta r)\, e^{-jhz}\, dh. \quad (120)$$

The variable ζ is related to h and k in the usual way since these solutions must satisfy the wave equation, that is,

$$\zeta^2 = h^2 - k^2. \quad (121)$$

The contour C_2 is the real h axis from $-\infty$ to $+\infty$ indented around the branch points

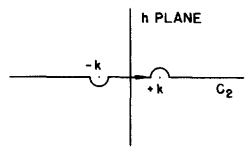

Fig. 15

Contour C_2; indentations around poles of integrand not shown.

at $\pm k$, as shown in Fig. 15, if the medium is lossless, with other proper indentations around any poles of the integrand on the real axis. These latter indentations are not shown in Fig. 15 but are discussed in detail below. If the fields obtained by using Eqs. 116 through 119 are to be the proper ones obtained from the gap distribution of Eq. 108 or Eq. 109 acting like a source, it is necessary that $\pi/2 \geq \arg \zeta \geq 0$ on C_2. Reference 2, page 415, shows an easily used procedure for following arg ζ as h varies, with arg $\zeta = 0$ and ζ positive real at $h = -\infty$. This is illustrated in Fig. 16 with

$$|\zeta| = |h-k|^{1/2} \, |h+k|^{1/2} \tag{122a}$$

$$\arg \zeta = \frac{1}{2} \arg (h-k) + \frac{1}{2} \arg (h+k). \tag{122b}$$

For lossless systems, with $\pm k$ on the real axis, arg $\zeta = 0$ for $-k > h \geq -\infty$, arg $\zeta = +\pi/2$ for $k > h > -k$, and arg $\zeta = 0$ for $h > k$.

The expressions for the current density on the surface of the sheath system are given by Eqs. 43 through 48 where now the fields produced by the gap source must be used. In this case one finds

$$K_{\parallel_g} = j\omega\epsilon \, a e^{-jn\theta} \int_{C_2} \frac{V_n}{2\pi} \frac{1}{D_n} \Big[nha \, \zeta a (K_n I_n' + I_n K_n') \cot \psi \csc \psi + \zeta^3 a^3 K_n' I_n \csc \psi \Big] e^{-jhz} \, dh \tag{123}$$

where again the modified Bessel functions all have the argument ζa. The functional notation will often be omitted throughout the remainder of this section; in all cases the argument of the modified Bessel functions is ζa unless otherwise noted. $K_{\perp_g}$ is, of course, identically zero. If one should try to evaluate $K_{\parallel_g}$ at $z = 0$, some consideration shows that the integral is no longer convergent, the integrand, in fact, going like $1/|h|$ for large h. This is to be expected since the current density caused by a finite field discontinuity between an infinitesimally small gap would, indeed, be infinite. This difficulty can be avoided by assuming a finite gap and replacing V_n in Eq. 123 by

$$V_n \frac{\sin \frac{h\ell}{2}}{\frac{h\ell}{2}}$$

as is evident from Eqs. 108 and 109. This same procedure can be used, if necessary, in the other integral representations. The input admittance for the nth mode can now

be defined as the sum of the admittances of all the infinitesimal windings making up the sheath helix, or

$$Y_n = -\int_0^{2\pi} \frac{\left[K_{\parallel_g}\right]_{z=\frac{\ell}{2}}}{V_n e^{-jn\theta}} a\,d\theta = -j\omega\epsilon a^2 \int_{C_2} \frac{N_n(\zeta a)}{D_n(\zeta a)} \frac{\sin\frac{h\ell}{2}}{\frac{h\ell}{2}} e^{-j\frac{h\ell}{2}}\,dh \qquad (124)$$

the minus sign occurring since the applied voltage is opposite to the induced voltage. $N_n(\zeta a)$ is given by the function in the brackets in Eq. 123, or

$$N_n(\zeta a) = nha\,\zeta a\,(K_n I_n' + I_n K_n') \cot\psi \csc\psi + \zeta^3 a^3 K_n' I_n \csc\psi. \qquad (125)$$

The complete and exact evaluation of the integral representations given above for the various field components is a difficult or even impossible task. Fortunately, it is the free modes only which are of most interest, and these parts of the solution can be fairly readily determined. For $|z| > 0$, Eq. 123 converges as it stands, and it becomes merely

$$K_{\parallel_g} = j\omega\epsilon a \frac{V_n e^{-jn\theta}}{2\pi} \int_{C_2} \frac{N_n(\zeta a)}{D_n(\zeta a)} e^{-jhz}\,dh. \qquad (126)$$

The only singularities of the integrand in Eq. 126 are branch points at $\pm k$ and ∞, and poles wherever $D_n(\zeta a) = 0$. But $D_n(\zeta a) = 0$ is precisely the determinantal equation 42 for the free modes which is known to have roots only at various points on the real h axis for a lossless medium, depending on the values of n, ka, and ψ. In carrying out the integration over the contour C_2 it is necessary to indent the contour properly around these poles. If the medium is assumed to be slightly lossy, the roots of $D_n(\zeta a) = 0$ move off the real axis, the branch points -k and +k move into the second and fourth quadrants, respectively, of the h plane (see Fig. 16), and the contour C_2 then becomes merely the entire real h axis from $-\infty$ to $+\infty$ without indentations. The lossless system is now considered the limiting case of the slightly lossy system, and the contour C_2 is indented in an obvious fashion as the roots and the branch points approach the real axis. Thus, in order to decide how to indent C_2 around the roots of $D_n(\zeta a)$, it is necessary to investigate $D_n(\zeta a) = 0$ in the case where the medium is slightly lossy or to obtain the required information in some equivalent manner. Assume that this has been done and that in the limit of a lossless medium the contour C_2 appears as in Fig. 17, where $-|h_a|$, $-|h_b|$, $|h_c|$, and $|h_d|$ are the various roots of $D_n(\zeta a) = 0$. In general, the roots appear only for values of $|h| > k$, as already noted in section I-E (although they can occur for $|h| = k$ in some limiting cases) and need not be symmetrically disposed about the origin. For $z > 0$, because of the e^{-jhz} factor in Eq. 126, the integrand vanishes on a circle of infinite radius in the third and fourth quadrants, and the contour

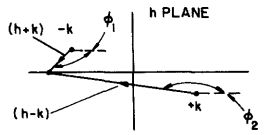

Fig. 16

Method for determining arg ζ; ϕ_1 = arg (h+k), ϕ_2 = arg (h-k).

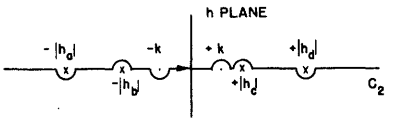

Fig. 17

Contour of integration.

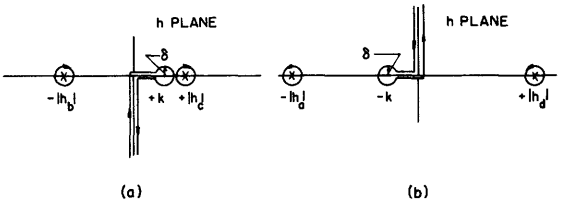

Fig. 18

(a) Modified contour for z > 0.
(b) Modified contour for z < 0.

can be deformed as in Fig. 18a. It becomes an integration around the poles of the integrand at $h = -|h_b|$ and $h = +|h_c|$, and an integration along a branch cut, which can be somewhat arbitrarily chosen. Here, it is taken along both sides of the negative imaginary axis from 0 to $-j\infty$, along both sides of the real axis from 0 to $(k-\delta)$, and around a circle of radius δ centered at +k where δ approaches zero. The contour cannot be closed at ∞ because of the branch point there, and the integrations out to the poles and back cancel each other. In a similar way, for $z < 0$ the contour can be deformed into the upper half plane, and the result appears as in Fig. 18b. It should now be clear that the $K_{\parallel g}$ which results from the gap source is a sum of the free mode terms obtained from the contributions of the poles of the integrand, plus a term contributed by the branch cut integration. This remark obviously applies to all the field components as well.

If the case for $z > 0$ is considered so that the contour shown in Fig. 18a applies, $K_{\parallel g}$ can be divided into four parts, or

$$K_{\parallel g} = K_{\parallel (fm) g} + K'_{\parallel g} + K''_{\parallel g} + K'''_{\parallel g}. \tag{127}$$

$K_{\parallel (fm) g}$ is the result of the contributions from the poles of the integrand, $K'_{\parallel g}$ results from the integration along both sides of the negative imaginary axis, $K''_{\parallel g}$ results from the integration along both sides of the real axis, and $K'''_{\parallel g}$ results from the integration around δ. It can be shown that $K'_{\parallel g}$ has the form

$$K'_{\parallel g} = \omega \epsilon a e^{-jn\theta} \frac{V_n}{2\pi} \int_0^\infty F(\alpha)\, e^{-\alpha z}\, d\alpha \tag{128}$$

where $F(\alpha)$ is, in general, a complex function of a real variable α and the parameters k, ψ, and n, and where no singularities occur in $F(\alpha)$ for $\infty > \alpha \geq 0$. $F(\alpha)$ is expressible in terms of the J_n and N_n Bessel functions (4), but since Eq. 128 has not been evaluated and there is no need for the explicit form of $F(\alpha)$, it is not given here. The important point is that in view of the bounded character of $F(\alpha)$, $K'_{\parallel g}$ becomes small like $1/z$ as z becomes increasingly large. In a similar fashion it can be shown that

$$K''_{\parallel g} = \omega\epsilon a e^{-jn\theta} \frac{V_n}{2\pi} \lim_{\delta \to 0} \int_0^{k-\delta} F(\beta) e^{-j\beta z} \, d\beta \tag{129}$$

where $F(\beta)$ is in all cases a real function of a real variable β and the parameters k, ψ, and n, and where no singularities occur in $F(\beta)$ for $k - \delta \geq \beta \geq 0$. As in the case of $F(\alpha)$, $F(\beta)$ is expressible in terms of the J_n and N_n functions, but for the discussion here it need not be given explicitly. Again, the important point is that $K''_{\parallel g}$ becomes small like $1/z$ as z becomes increasingly large. Using Eqs. 122a and 122b to find ζ on the circle of radius δ around +k in Fig. 18a, it can be shown that generally $K'''_{\parallel g}$ approaches zero as δ approaches zero. Exceptions to this rule may occur if $|h_c|$ coincides with +k, and in this case a finite value may result for $K'''_{\parallel g}$. However, these cases are best considered as limiting ones for which $|h_c|$ approaches and finally equals +k; with this precaution $K'''_{\parallel g}$ can be considered to be zero under all conditions. Since the $K_{\parallel (fm)g}$ terms have a z dependence like $e^{+j|h_b|z}$ and $e^{-j|h_c|z}$, it is clear that as z becomes increasingly large, it is only these terms which are significant, the $K'_{\parallel g}$ and $K''_{\parallel g}$ terms vanishing like $1/z$. Thus, very far away from the source only the surface current density associated with the free modes need be considered. The physical significance of the $K'_{\parallel g}$ and $K''_{\parallel g}$ terms is that they correspond to the local induction and radiation effects of the source and system for z not large. It is evident that for $z < 0$ an argument similar to the above applies, and for $z \ll 0$ only free mode fields with z dependence like $e^{+j|h_a|z}$ and $e^{-j|h_d|z}$ persist. Using the usual methods of the theory of residues in complex integration (1, 2, 50), since the poles of the integrand are simple, one obtains

$$K_{\parallel (fm)g}(z > 0) = \omega\epsilon a V_n e^{-jn\theta} \sum_{h=-|h_b|,+|h_c|,\text{etc.}} \left\{ \frac{N_n(\zeta a) e^{-jhz}}{\frac{d}{dh}\left[D_n(\zeta a)\right]} \right\} \tag{130a}$$

and

$$K_{\parallel (fm)g}(z < 0) = -\omega\epsilon a V_n e^{-jn\theta} \sum_{h=-|h_a|,+|h_d|,\text{etc.}} \left\{ \frac{N_n(\zeta a) e^{-jhz}}{\frac{d}{dh}\left[D_n(\zeta a)\right]} \right\}. \tag{130b}$$

The quantity in the braces can be evaluated, and after some manipulation one finds

$$\left\{\frac{N_n(\zeta a)e^{-jhz}}{\frac{d}{dh}\left[D_n(\zeta a)\right]}\right\}_{D_n(\zeta a)=0}$$

$$= \frac{\zeta^2 a^2}{a} \frac{\left[nha\left(\frac{I_n'}{I_n} + \frac{K_n'}{K_n}\right)\cot\psi \csc\psi + \zeta^2 a^2 \frac{K_n'}{K_n}\csc\psi\right]e^{-jhz}}{2\zeta a\,(\zeta^2 a^2 + nha\cot\psi)\,(2ha + n\cot\psi)} \qquad (131)$$

$$+ ha\left[(n^2 + \zeta^2 a^2)\,k^2 a^2 \cot^2\psi + (\zeta^2 a^2 + nha\cot\psi)^2\right]\left[\frac{I_n'}{I_n} + \frac{K_n'}{K_n}\right]$$

From Eqs. 130 and 131 the amplitudes of the surface current density associated with the different waves of the nth free mode can be obtained, and using these in Eqs. 49 through 54, one can determine the various free mode field components. Also, using these current density amplitudes in Eq. 96, one can find the average axial power flow in the free modes. The results given so far are quite general and applicable for any value of n, although it has been assumed that the θ dependence of the source is like $e^{-jn\theta}$ only. This is sufficiently general since, if the θ and the z dependence of the source are like

$$u_o(z)\sum_n V_n e^{-jn\theta}$$

the total solution can be obtained because of linearity and orthogonality in θ by merely adding the solutions obtained above for each nth harmonic term alone.

In order to complete the solution for the free modes it is necessary to decide how the contour C_2 must be indented around the poles of the integrand in Eq. 126. This is determined in the following manner. It is necessary to introduce some new notation momentarily. If the medium in which the sheath system is immersed is taken to be slightly lossy, then from Eq. 5 in place of $k^2 = \omega^2\mu\epsilon$, one can write $k^2 = \omega^2\mu\epsilon' = \omega^2\mu\epsilon - j\omega\mu\sigma = k_o^2 - jk_o v_o \mu\sigma$. k_o^2 is taken to be the value which k^2 approaches as the conductivity of the medium approaches zero. v_o is, as in section I-E, the velocity of a uniform plane wave in a lossless medium of constants μ and ϵ. The nondimensional complex variable ha can be written in terms of its real and imaginary parts as

$$ha = \beta a + j\alpha a. \qquad (132a)$$

It is evident both from the functions involved and the physical requirements of the solution that, at least in any restricted region, ha can be considered an analytic function of n, cot ψ, and ka. Of course, an explicit form for ha cannot be written, but it can be represented as

$$ha = f_n(\cot \psi,\ ka). \tag{132b}$$

For $ka = k_o a$ the solutions of Eq. 132b have already been considered. In this case the ha roots are pure real, and there can be several even for a given $\cot \psi$ and n. Calling any one of these $ha = \beta_o a$ results in

$$\beta_o a = f_n(\cot \psi,\ k_o a). \tag{133}$$

Since only positive frequencies need be considered, one can write, dropping terms of order σ^2

$$ka = +\sqrt{k_o^2 a^2 - jk_o v_o \mu\sigma a^2} \approx k_o a \left(1 - j\,\frac{1}{2}\,\frac{v_o \mu\sigma}{k_o}\right). \tag{134}$$

With ha an analytic function, an expansion can readily be written as

$$ha = \beta a + j\alpha a = f_n(\cot \psi,\ k_o a) + \left.\frac{\partial f_n}{\partial(ka)}\right]_{ka=k_o a} (ka - k_o a) + \ldots \tag{135}$$

with n and ψ constant. From Eqs. 133 and 134, Eq. 135 becomes

$$\beta a + j\alpha a \approx \beta_o a + \left.\frac{\partial f_n}{\partial(ka)}\right]_{ka=k_o a} \left(-\,j\,\frac{v_o \mu\sigma a}{2}\right) \tag{136}$$

where terms of order σ^2 are omitted. But from Eq. 62

$$\left.\frac{\partial f_n}{\partial(ka)}\right]_{ka=k_o a} = \frac{d(ha)}{d(k_o a)} = \frac{v_o}{v_g} \tag{137}$$

with v_g the group velocity. For a slightly lossy medium from Eqs. 136 and 137

$$\beta a \approx \beta_o a \tag{138a}$$

$$\alpha a \approx -\,\frac{v_o^2 \mu\sigma a}{2 v_g}. \tag{138b}$$

As expected, the real part of ha is unaltered to this order. The imaginary part is dependent on σ and approaches zero as σ approaches zero. Since $v_o^2 \mu\sigma a$ is surely positive, Eq. 138b requires the product of αa and v_g to be negative. α is, of course, the displacement of the root perpendicular to the real h axis in the h plane. v_g is already known since the manner in which the h roots vary along the real axis as k_o varies is known. Consequently, the direction of displacement of the roots for a slightly lossy system or, conversely, the manner of indentation of C_2 for a lossless system is readily obtained. Incidentally, the attenuation in the radial direction can be derived by

substituting Eq. 138 in Eq. 121.

In the remainder of this section the solutions of the determinantal equation for the sheath helix are briefly discussed in view of the above remarks. In particular, the disposition of the roots of $D_n(\zeta a) = 0$ in the h plane for various values of ψ and n as ka varies is shown. For convenience, these are shown on the assumption that the medium is slightly lossy, although it is to be understood that for the lossless case the roots and branch points appear on the real axis and C_2 is correspondingly indented. It should be clear now, in view of the way the contour is deformed for $z > 0$ and $z < 0$ (see Fig. 18), why some waves are referred to as inward and others as outward traveling waves in section I-E. Thus, for $z > 0$ a root in the fourth quadrant results in a z dependence like $e^{-j|h_c|z}$, an outward traveling wave, whereas a root in the third quadrant results in a z dependence like $e^{+j|h_b|z}$, an inward traveling wave. Similarly, for $z < 0$ a root in the second quadrant results in a z dependence like $e^{+j|h_a|z}$, an outward traveling wave, whereas a root in the first quadrant results in a z dependence like $e^{-j|h_d|z}$, an inward traveling wave. Note again, as mentioned in section I-E, that for a lossy system all free mode waves are exponentially damped at large distances from the source.

2. The Sheath Helix, n = 0

Since the n = 0 mode is somewhat special, it is treated separately. In this case Eq. 131 becomes

$$\left\{\frac{N_o(\zeta a)e^{-jhz}}{\frac{d}{dh}\left[D_o(\zeta a)\right]}\right\}_{D_o(\zeta a)=0} = \frac{\zeta^2 a^2}{a}\frac{1}{ha}\frac{-\frac{K_1}{K_o}\csc\psi\, e^{-jhz}}{4\,\zeta a + \left[k^2a^2\cot^2\psi + \zeta^2a^2\right]\left[\frac{I_1}{I_o} - \frac{K_1}{K_o}\right]}. \quad (139)$$

It is evident from Eq. 139 that for $\psi = 0°$, the sheath ring, no free mode wave is excited by the type of source considered here. Indeed, Eq. 126 shows that $K_{\|_g}$ is identically zero for all z for this case. Further, some consideration of Eqs. 116 through 119 shows that the field components resulting from the internally shielded gap source are unaffected by the presence of the sheath ring. Physically, it is evident that for n = 0 and $\psi = 0°$ there is no electric field in the direction in which current can flow. Consequently, the field components around this gap source are precisely what they would be if the sheath ring were not present. However, it should be noted that for $\psi = 0°$ the TE_{om} modes, which can exist in the interior of a perfectly conducting hollow circular cylinder, can exist in the sheath ring. Such modes correspond to values of h such that h is real and less than k in magnitude, or h is pure imaginary. For ψ any small amount larger than 0°, such values of h cannot occur. Consequently, it can be concluded that these modes are not stable on the sheath system.

For $90° > \psi > 0°$ Fig. 19 shows the position of the h roots, $\pm|h_o|$. Here, as in subsequent plots, the arrows show the relative motion of the roots as k is increased with

ψ constant. Also, the subscript and superscript notations on the h roots conform to those of section I-E. This view of the roots should be compared with that given by Figs. 8 and 9. For $\psi = 90°$, the sheath tube, there is no free mode wave for $r > a$, as noted in section I-E-2. $\psi = 90°$ with $n = 0$ corresponds in many respects to a perfectly conducting circular cylinder excited by a symmetrical gap source. It is worthy of note that for $\psi = 90°$ with $n = 0$ Eq. 124 becomes

$$Y_o = j\omega\epsilon a \int_{C_2} \frac{K_1(\zeta a)}{\zeta K_o(\zeta a)} \frac{\sin \frac{h\ell}{2}}{\frac{h\ell}{2}} e^{-j\frac{h\ell}{2}} dh. \tag{140}$$

Except for a difference in notation this is precisely the equation given on page 418 of reference 2 for the input admittance of a perfectly conducting infinite circular cylindrical wire excited in the above manner. Equation 140 gives only the external admittance for this case, and in relationship to this the remarks of section I-G-5 are pertinent.

3. The Sheath Ring, $\psi = 0°$ for $|n| \geqslant 1$

For $\psi = 0°$ Eq. 131 becomes

$$\left\{\frac{N_n(\zeta a)e^{-jhz}}{\frac{d}{dh}\left[D_n(\zeta a)\right]}\right\}_{\substack{D_n(\zeta a)=0 \\ \psi=0°}} = \frac{\zeta^2 a^2}{a} \frac{n\left(\frac{I_n'}{I_n} + \frac{K_n'}{K_n}\right)e^{-jhz}}{2n^2\,\zeta a + \left[(n^2 + \zeta^2 a^2)\,k^2 a^2 + n^2 h^2 a^2\right]\left[\frac{I_n'}{I_n} + \frac{K_n'}{K_n}\right]}. \tag{141}$$

The position of the roots is shown for this case in Fig. 20. This should be compared with Figs. 4, 5, and 6. It is interesting to note that if the frequency of the source is reduced so that the "divergence" limit $ka = (n^2 - 1)^{1/2}$ is approached from larger values of ka, then with $|h_{n,1}|$ approaching k, and ζ approaching zero, Eqs. 141 and 130 show that the amplitude of the current density of the free mode wave decreases like ζ^2.

4. The Sheath Helix, $90° > \psi > 0°$ for $n \neq 0$

In this case, since the roots are not symmetrically located about the origin, it is necessary to decide in advance whether $n > 0$ or $n < 0$ is to be considered. In the following $n > 0$ is chosen although this results in no loss of generality, as should be clear from the discussion in section I-E-3.

For $n = 1$ the position of the roots is shown in Figs. 21 and 22. These should be compared with Figs. 11a and 13a. Figs. 10a and 12a are also pertinent. ${}_n\psi_{max}$ is defined in section I-E-3 as the largest ψ for which the $|h'_{n,2}|$ and $|h'_{n,3}|$ roots occur, and, as noted there, although the precise value of ${}_1\psi_{max}$ is not available, it is known that $0.286° > {}_1\psi_{max} > 0.191°$. It can be shown that for ψ approaching 90° and ζa approaching zero, the magnitude of Eq. 131 becomes small like $\zeta^2 a^2 \times (\ln \zeta a)^2$ for the $|h'_{1,1}|$ root. This confirms the remarks

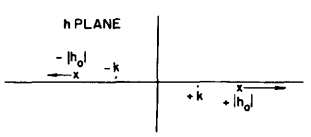

Fig. 19
The sheath helix;
$n = 0$, $90° > \psi > 0°$.

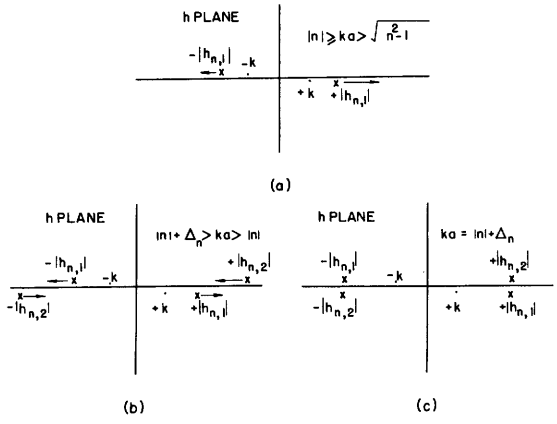

Fig. 20

The sheath ring; $\psi = 0°$, $|n| \geq 1$. (a) No roots for $ka < (n^2 - 1)^{1/2}$. (b) and (c) No roots for $ka > |n| + \Delta_n$.

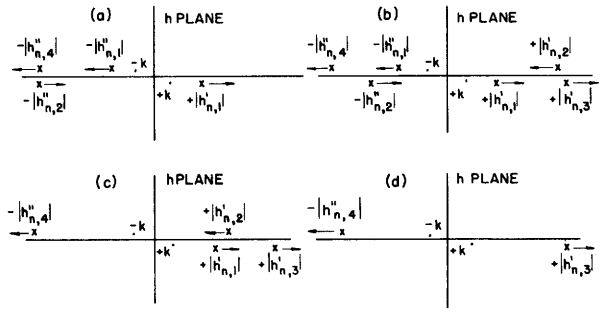

Fig. 21

The sheath helix; $n = 1$, $_n\psi_{max} > \psi > 0°$. (a) $1 >> ka > 0$. (b) ka slightly larger than 1. (c) ka slightly larger than in Fig. 21b. (d) ka larger than in Fig. 21c; similar for ka increasing.

made in section I-E-3.

Figs. 23 and 24 show the position of the roots for n = 2. These should be compared with Figs. 11b and 13b. Figs. 10b and 12b are also pertinent. The exact value of $_2\psi_{max}$ is not known, but it is less than $_1\psi_{max}$. For $n \geq 3$ the roots appear very much as they are shown in Figs. 23 and 24 for n = 2, although the $|h''_{n,1}|$ root may not occur at all, as was indicated in section I-E-3.

Some consideration of the form of the integrand in Eq. 126 and the disposition of the poles of this integrand, the zeros of $D_n(\zeta a)$, indicates that the current density amplitudes of the free mode waves approach infinity as the loss approaches zero near the points where the group velocity becomes small. In all cases this corresponds to the values of ka and cot ψ where the roots appear in juxtaposition across the real h axis as in Figs. 20c, 22b, and 23c. For lossless systems this is the point where the roots coalesce, and after which they disappear. In the case of the sheath ring, $\psi = 0°$, this occurs for $ka = |n| + \Delta_n$, or very near where the individual rings are resonant. However, even for ψ relatively large the group velocity can become zero for values of ka much smaller than $|n|$. It appears that in these cases each complete turn of the sheath helix is resonant, that is, a standing wave occurs on each turn. From this viewpoint it is possible to understand how a zero group velocity in the z direction can occur even though the phase velocity is not zero. For if standing waves occur on the turns, there is no power flow along the turns and, consequently, none in the axial direction; therefore the group velocity is zero. But if the time at which the standing waves reach their peak amplitude varies in a progressive manner from turn to turn, there is a resultant axial phase velocity which can be either positive or negative.

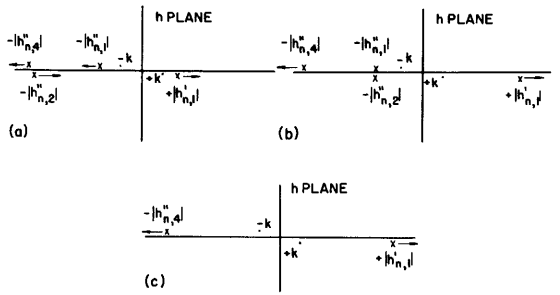

Fig. 22

The sheath helix; n = 1, $90° > \psi > {}_{n}\psi_{max}$. (a) $1 >> ka > 0$. (b) ka approximately 1 for small ψ but increasingly smaller for larger ψ. (c) ka larger than in Fig. 22b; similar for ka increasing.

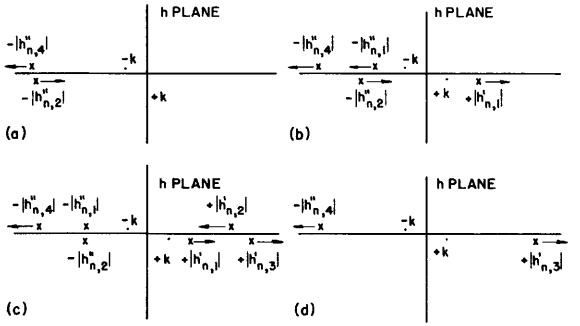

Fig. 23

The sheath helix; n = 2, ${}_{n}\psi_{max} > \psi > 0°$. (a) $1 >> ka > 0$. (b) $n > ka > {}_{n}k_{d}$. (c) ka slightly larger than in Fig. 23b and near 2. (d) ka larger than in Fig. 23c; similar for ka increasing.

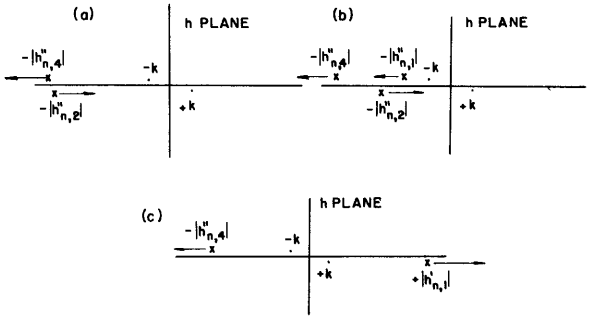

Fig. 24

The sheath helix; n = 2, $90° > \psi > {}_{n}\psi_{max}$. (a) $1 >> ka > 0$. (b) ka slightly larger than value given by Eq. 87. (c) $ka > {}_{n}k_{d}$.

5. The Sheath Tube, $\psi = 90°$

For ψ approaching 90°, ζ approaching zero, and $|h''_{n,4}|$ approaching k, it can be shown that Eq. 131 becomes

$$\lim_{\psi \to 90°} \left\{ \frac{N_n(\zeta a) e^{-jhz}}{\frac{d}{dh}\left[D_n(\zeta a)\right]} \right\}_{h = -|h''_{n,4}| = -k} = \frac{|n|}{2ka^2} e^{+jkz}, \quad |n| \geq 1. \tag{142}$$

For the limiting case of $\psi = 90°$ there can be waves with z and θ dependence like $e^{-jkz} \times e^{\pm j|n|\theta}$ with $z > 0$ and $e^{+jkz}\, e^{\pm j|n|\theta}$ with $z < 0$, all with identical amplitudes for $|n| \geq 1$. However, the waves whose coordinate dependence is like $e^{-jkz}\, e^{-j|n|\theta}$ with $z > 0$ and $e^{+jkz}\, e^{+j|n|\theta}$ with $z < 0$ are not stable (see sec. I-E).

The sheath tube also supports the TM modes which normally can exist in the interior of a perfectly conducting hollow circular cylinder (1, 2). In this case only longitudinal currents flow so that the boundary conditions (Eqs. 64 through 66) are satisfied, with the additional requirements that $H_z = 0$ everywhere and $E_\theta = 0$ for $r = a$. It can be shown that an unshielded or an externally shielded gap source excites the $TM_{n,m}$ modes. Such modes correspond to values of h such that h is real and less than k in magnitude, or h is pure imaginary. It can be shown that for ψ any small amount less than 90°, such values of h cannot occur. As a consequence, it can be concluded that these modes are not stable on the sheath tube system.

II. The Tape Helix

In this section a more physically realistic model of the helix than the sheath model is considered. This better model consists of a uniform helix wound of a tape. The symmetrical properties of a uniform helix require the field solutions to take a certain form showing that free mode solutions cannot exist in certain regions.

To obtain useful results the cases of a narrow tape helix and a narrow gap helix are solved by making appropriate approximations of the boundary conditions. The propagation constants of the free modes for both of these cases are shown to be practically identical except for small values of ka. Both inward and outward traveling waves exist for particular values of ka in a fashion reminiscent of the sheath helix solutions. The anomalous behavior of the propagation constant in the neighborhood of ka = 1 is derived directly from the theory, and excellent agreement with experimental data is obtained. Expressions for the power flow and other useful quantities are derived, and numerical results are presented for a particular case.

The multiwire helix problem is solved subject to approximations similar to those used previously, and the problem of the tape ring system is treated similarly.

Formulation and Formal Solution of the Problem

A. Definitions

As in the previous section the cylindrical coordinate system is used, and essentially all of the data given in section I-A are applicable to the analysis given. Here, however, the structure is a tape helix, that is, a helix wound of a wire which is assumed to be a perfect conductor with very small (actually, it is taken to be zero) radial extension but finite axial extension. Such a helix is shown in Fig. 25a, and a developed view is shown in Fig. 25b. p, a, and ψ are defined as before, and δ and δ' are the tape width and gap width, respectively, in the axial direction. The helix, whose axis is taken to coincide with the z axis as in Fig. 2, is assumed to be positively wound and to be infinite in extent. The medium is also taken to be infinite in extent and is assumed as before to be linear, isotropic, and homogeneous. Although the procedure to be used would be applicable even if the mediums were not the same (70), for simplicity these are again taken to be the same for $r > a$ as for $r < a$ and lossless, and to be characterized by μ, ϵ, and k as defined in section I-A. The assumption of zero radial thickness for the tape is certainly nonphysical, but if the actual thickness is very small compared with the other dimensions and with the wavelength, this approximation should influence the results to a very small degree.

B. The Field Expressions

It will be noted that the helix structure is a periodic one, and, consequently, an approach can be used which has often been employed in related problems (5, 9, 37). This is essentially an application of Floquet's theorem, which for the case here states that the fields are multiplied only by some complex constant if one moves down the helix a distance p (5, 37). This is clear since, if the helix is displaced along the z axis by a distance p, it coincides with itself, and the new fields can differ from the previous ones by only a constant factor. There is also an additional characteristic of symmetry which is made use of shortly. From the above it should be evident that a simple form of z dependence which meets the requirements of the periodic character of the structure is

$$e^{-jhz}\, e^{-jm\frac{2\pi}{p}z} = e^{-jh_m z} \tag{143}$$

where h_m is given by

$$h_m = h + m\frac{2\pi}{p} \tag{144}$$

and where m can have any integer value including zero. Since the Hertzian potentials Π_z and Π_z^* must satisfy the scalar wave equation 26, it is readily found that the θ dependence can be expressed in the form $e^{jn\theta}$, where n can be any integer including zero. The function f(r) which contains the r dependence of the elementary

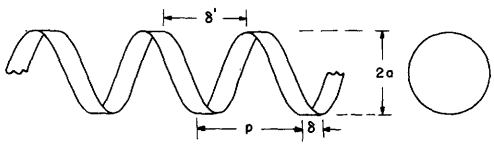

(a)

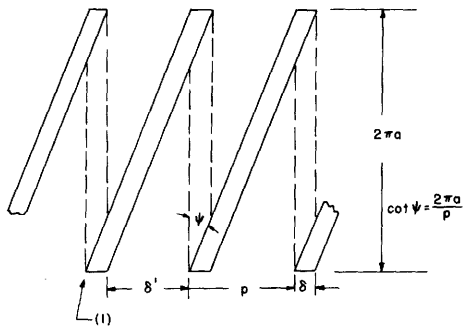

(b)

Fig. 25
Tape Helix.

solutions must then be a solution of the differential equation

$$r \frac{d}{dr}\left(r \frac{df}{dr}\right) - \left[(h_m^2 - k^2) r^2 + n^2\right] f = 0. \tag{145}$$

The solutions to Eq. 145 are the modified Bessel functions of order n and argument $\eta_m(r/a)$, where η_m is given by

$$\eta_m = \left[(h_m^2 - k^2) a^2\right]^{1/2} = \left[m^2 \cot^2 \psi + 2mha \cot \psi + h^2a^2 - k^2a^2\right]^{1/2}. \tag{146}$$

Since the fields must be finite, the I_n function is chosen for the solution for $a \geq r \geq 0$ and the K_n function for $\infty \geq r \geq a$. Further, since the complete set of functions must be used to satisfy the boundary conditions at r = a, and since the field equations are linear so that the elementary solutions can be added, the representation for Π_z becomes

$$\Pi_z^{i,e} = e^{-jhz} \sum_{m,n} A_{m,n}^{i,e} \frac{I_n}{K_n}\left(\eta_m \frac{r}{a}\right) e^{jn\theta} e^{-jm \frac{2\pi}{p} z} \tag{147}$$

where the superscripts i and e refer to the internal, $r \leq a$, and external, $r \geq a$, regions as in section I.

As mentioned above, there is an additional characteristic of symmetry which simplifies the representations. It can be readily seen that if the helix is translated along

its axis some distance less than p, it may then be rotated so that it coincides with itself. It thus appears clear that Floquet's theorem can be applied to the angular coordinate as well as to the axial coordinate. Let $z = z' + \mathfrak{z}$ or $z' = z - \mathfrak{z}$, and let $\theta = \theta' + \phi = \theta' + (2\pi/p)\mathfrak{z}$ or $\theta' = \theta - (2\pi/p)\mathfrak{z}$; $\phi = (2\pi/p)\mathfrak{z}$ is the angle through which the helix must be rotated after a translation of $\mathfrak{z}$ to make it coincide with itself. This is equivalent to putting the x' axis through the helix at $z = \mathfrak{z}$ and measuring θ' from x'. After substitution of these values of θ and z, Eq. 147 becomes

$$\prod_z^{i,e} = e^{-jh\mathfrak{z}} e^{-jhz'} \sum_{m,n} A_{m,n}^{i,e} \frac{I_n}{K_n}\left(\eta_m \frac{r}{a}\right) e^{-j(m-n)\frac{2\pi}{p}\mathfrak{z}} e^{jn\theta'} e^{-jm\frac{2\pi}{p}z'} . \qquad (148)$$

Since a rotation and a translation make the helix coincide with itself, the form of the solutions as a function θ' and z' must be the same as the form expressed as a function of θ and z. It can be seen from Eq. 148 that if this is to be true for all $\mathfrak{z}$ as well as $\mathfrak{z} = p$, it is necessary to take m = n, and for $m \neq n$ put $A_{m,n}^{i,e} = 0$. This constraint, which results when uniform helices are considered, requires that

$$\prod_z^{i,e} = e^{-jhz} \sum_m A_m^{i,e} \frac{I_m}{K_m}\left(\eta_m \frac{r}{a}\right) e^{-jm\left(\frac{2\pi}{p}z - \theta\right)} \qquad (149)$$

be taken as the representation for the electric Hertzian potential, and that an identical form

$$\prod_z^{*i,e} = e^{-jhz} \sum_m B_m^{i,e} \frac{I_m}{K_m}\left(\eta_m \frac{r}{a}\right) e^{-jm\left(\frac{2\pi}{p}z - \theta\right)} \qquad (150)$$

be taken for the magnetic Hertzian potential.

Using Eqs. 149 and 150 and 20 through 25, one can readily find the field components in terms of the $A_m^{i,e}$ and $B_m^{i,e}$ coefficients which are related by the continuity requirements of the field boundary conditions at r = a. These are, of course, that at r = a the tangential electric field is continuous everywhere, and that the discontinuity in the tangential magnetic field is proportional to the total surface current density; that is

$$\left.\begin{aligned} E_{z,\theta}^{i} &= E_{z,\theta}^{e} \\ K_\theta &= H_z^i - H_z^e \\ K_z &= H_\theta^e - H_\theta^i \end{aligned}\right\} \text{ at } r = a \qquad (151)$$

(see Eqs. 45 and 46). Since the representations for the surface current density components must have the same form as the field components

$$K_\theta = e^{-jhz} \sum_m \kappa_{\theta m} e^{-jm\left(\frac{2\pi}{p} z-\theta\right)} \tag{152}$$

and

$$K_z = e^{-jhz} \sum_m \kappa_{zm} e^{-jm\left(\frac{2\pi}{p} z-\theta\right)} \tag{153}$$

where $\kappa_{\theta m}$ and κ_{zm} are the Fourier coefficients of the current density expansions. It should be emphasized that Eqs. 152 and 153 are representations for the components of the total surface current density, that is, the sum of the current density on both sides of the infinitesimally thick perfectly conducting tape. Proceeding as above to find the field components in terms of $A_m^{i,e}$ and $B_m^{i,e}$, and using Eqs. 151, 152, and 153 to find the values of $A_m^{i,e}$ and $B_m^{i,e}$ in terms of $\kappa_{\theta m}$ and κ_{zm}, where use is made of the orthogonality of the Fourier space harmonics for $2\pi > \theta > 0$ and $p > z > 0$, one obtains after considerable algebra

$$E_r^e = \frac{e^{-jhz}}{\omega\epsilon a} \sum_m \left\{ - h_m a \eta_m I_m(\eta_m) K'_m\left(\eta_m \frac{r}{a}\right) \kappa_{zm} \right.$$

$$+ \frac{m}{\eta_m}\left[h_m^2 a^2 I_m(\eta_m) K'_m\left(\eta_m \frac{r}{a}\right) \right.$$

$$\left.\left. + \frac{a}{r} k^2 a^2 I'_m(\eta_m) K_m\left(\eta_m \frac{r}{a}\right)\right] \kappa_{\theta m} \right\} e^{-jm\left(\frac{2\pi}{p} z-\theta\right)} \tag{154}$$

$$E_\theta^e = j \frac{e^{-jhz}}{\omega\epsilon a} \sum_m \left\{ - \frac{a}{r} m h_m a I_m(\eta_m) K_m\left(\eta_m \frac{r}{a}\right) \kappa_{zm} \right.$$

$$+ \frac{1}{\eta_m^2}\left[\frac{a}{r} m^2 h_m^2 a^2 I_m(\eta_m) K_m\left(\eta_m \frac{r}{a}\right) \right.$$

$$\left.\left. + \eta_m^2 k^2 a^2 I'_m(\eta_m) K'_m\left(\eta_m \frac{r}{a}\right)\right] \kappa_{\theta m} \right\} e^{-jm\left(\frac{2\pi}{p} z-\theta\right)} \tag{155}$$

$$E_z^e = j \frac{e^{-jhz}}{\omega\epsilon a} \sum_m \left\{ \eta_m^2 I_m(\eta_m) K_m\left(\eta_m \frac{r}{a}\right) \kappa_{zm} \right.$$

$$\left. - m h_m a I_m(\eta_m) K_m\left(\eta_m \frac{r}{a}\right) \kappa_{\theta m} \right\} e^{-jm\left(\frac{2\pi}{p} z-\theta\right)} \tag{156}$$

$$H_r^e = j\, e^{-jhz} \sum_m \left\{ m \frac{a}{r} I_m(\eta_m) K_m\left(\eta_m \frac{r}{a}\right) \kappa_{zm} \right.$$

$$- \frac{h_m a}{\eta_m^2} \left[m^2 \frac{a}{r} I_m(\eta_m) K_m\left(\eta_m \frac{r}{a}\right) \right.$$

$$\left. \left. + \eta_m^2 I'_m(\eta_m) K'_m\left(\eta_m \frac{r}{a}\right) \right] \kappa_{\theta m} \right\} e^{-jm\left(\frac{2\pi}{p} z - \theta\right)} \tag{157}$$

$$H_\theta^e = e^{-jhz} \sum_m \left\{ - \eta_m I_m(\eta_m) K'_m\left(\eta_m \frac{r}{a}\right) \kappa_{zm} \right.$$

$$+ \frac{m h_m a}{\eta_m} \left[I_m(\eta_m) K'_m\left(\eta_m \frac{r}{a}\right) \right.$$

$$\left. \left. + \frac{a}{r} I'_m(\eta_m) K_m\left(\eta_m \frac{r}{a}\right) \right] \kappa_{\theta m} \right\} e^{-jm\left(\frac{2\pi}{p} z - \theta\right)} \tag{158}$$

$$H_z^e = - e^{-jhz} \sum_m \left\{ \eta_m I'_m(\eta_m) K_m\left(\eta_m \frac{r}{a}\right) \kappa_{\theta m} \right\} e^{-jm\left(\frac{2\pi}{p} z - \theta\right)}. \tag{159}$$

The prime on the I_m and K_m functions means differentiation with respect to the argument. Only the external field components are given above since the expressions for the internal components are identical except that the I_m and K_m functions are interchanged everywhere.

C. The Formal Solution

Having the proper representations of the field components, one must apply the boundary conditions to complete the solution and to find those values of h which correspond to the free modes. Since expressions are available which already satisfy the continuity requirements of the field boundary conditions at r = a, the only condition which remains is that the tangential electric field on the tape be zero. This condition can be applied by a re-expansion procedure or by a minimization of mean-square-error procedure. Both of these procedures lead to determinantal equations in the form of infinite determinants (68). A complete formal solution may therefore be obtained, although it does not appear possible or feasible to obtain useful results from this solution. Consequently, another method, which is discussed at length later in this section,has been preferred here.

D. The Forbidden Regions

Although the formal solution mentioned in the previous section appears to have little immediate practical value, the field expressions of section II-B are of considerable use in later developments, and some results which may be deduced from these expressions are of great interest.

In writing the representations for the external fields as a sum of terms whose radial dependence is of the form $K_m\left[\eta_m(r/a)\right]$, it has been tacitly assumed that η_m is real and positive. Without for the moment discussing the detailed implications of this, the necessary requirements for this condition to be met are considered next. It is assumed that h is real, and for a lossless medium k is also real. It should be recalled that the tape is assumed to be a perfect conductor. From Eq. 146

$$\eta_m = \left[(h_m^2 - k^2)a^2\right]^{1/2} > 0 \tag{160}$$

requires

$$h_m^2 a^2 > k^2 a^2 \tag{161}$$

or

$$|h_m a| > ka. \tag{162}$$

If h is assumed to be positive, Eq. 162 is surely satisfied for $m \gtrsim 0$ if $|h| > k$. For $m < 0$, however, Eq. 162 is satisfied only within restricted regions. For $m < 0$, from Eqs. 162 and 144, the condition becomes

$$|ha - |m| \cot\psi| > ka. \tag{163}$$

Examination of Eq. 163 shows that this inequality can be expressed as

$$|m| \cot\psi + ka < ha < |m| \cot\psi - ka \tag{164}$$

or

$$|m| + \frac{ka}{\cot\psi} < \frac{ha}{\cot\psi} < |m| - \frac{ka}{\cot\psi}, \quad |m| \gtrsim 1,\ h > k. \tag{165}$$

If h is negative and in magnitude larger than k, Eq. 162 is surely satisfied for $m \lesssim 0$ but only for certain restricted regions for $m > 0$. Carrying through the argument as above gives results that can be expressed in a similar manner to Eq. 165 or, finally, for both positive and negative h

$$|m| + \frac{ka}{\cot\psi} < \frac{|h|a}{\cot\psi} < |m| - \frac{ka}{\cot\psi}, \quad |m| \gtrsim 1,\ |h| > k. \tag{166}$$

The significance of Eq. 166 is most easily realized from Fig. 26 where $ka/(\cot\psi)$ has been plotted versus $ha/(\cot\psi)$. The shaded areas are the regions where the variables do not satisfy the inequality, with the boundaries being given by Eq. 166 satisfied with equal signs. The regions are labeled with the m to which they correspond. It should be noted that the entire region for $ka/(\cot\psi) > 1/2$ is shaded. Since $\cot\psi = (2\pi a)/p$, this restriction immediately becomes

$$\frac{2\pi a}{\lambda} = ka < \frac{\cot \psi}{2} = \frac{\pi a}{p}$$

or

$$p < \frac{\lambda}{2}. \tag{167}$$

The significance of the above restrictions can be seen in the following manner. Assume for the moment that a solution is possible at some $ka < (\cot \psi)/2$ with ha real and in the $|n|$th shaded region of Fig. 26. In this case, in the external field representations all the terms of the series have radial dependence like $K_m\left[\eta_m(r/a)\right]$ except one which is an $H_n^{(2)}\left[|\eta_n|(r/a)\right]$ function. But for large r this would correspond to an outgoing radial wave which can only come from an infinitely long (in the z direction) line type source located at some finite r. Such sources have not been postulated in the assumptions, and, in fact, the concern here is with the source-free problem. Thus, if a solution exists at all, it must exist with the restrictions given above and with only $K_m\left[\eta_m(r/a)\right]$ radial dependence for all the terms of the series. Therefore, free mode solutions must exist only in the unshaded regions of Fig. 26, and the shaded portions are called the forbidden regions. Another viewpoint is to recognize that the total average power flow must be the same and finite across any infinite plane perpendicular to the z axis for any free modes with h real. But an $H_n^{(2)}\left[|\eta_n|(r/a)\right]$ term would result in an average radial power flow and, consequently, a violation of the Poynting theorem if no line sources are present. In the above it was assumed that only one term might have $H_n^{(2)}$ radial dependence, although clearly the same reasoning applies if it is assumed that more than one term of this nature could exist. The exclusion of free mode solutions from the forbidden regions does not insure that solutions will exist in the allowed regions since the boundary conditions must also be matched at r = a to fulfill all the requirements for a unique solution.

In the above it has been assumed that h is real. The possibility remains that solutions may exist for h complex or pure imaginary. Although it would be expected that such solutions do not occur here as they do not for other infinite lossless open cylindrical structures, it has not been possible to prove in a rigorous fashion that such is the

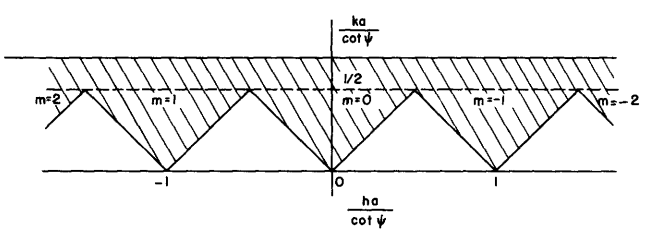

Fig. 26
Chart of forbidden regions,
ka/cot ψ vs ha/cot ψ.

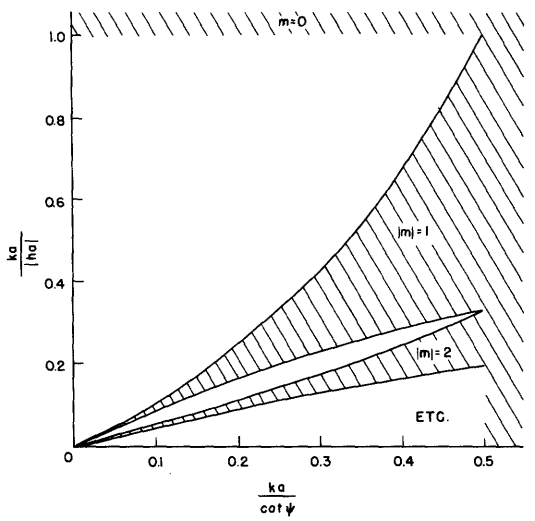

Fig. 27

Chart of forbidden regions, $ka/|ha|$ vs $ka/\cot\psi$.

case (39). It should be noted that the impossibility of the existence of complex or pure imaginary h roots can be proved for the sheath helix case by recourse to the determinantal equation (68). Attempts to use similarly the exact determinantal equation for the tape helix, were not successful. Nor did the procedures of reference 39, which included use of symmetry and violation of Poynting's theorem as the key steps, and which supplied a satisfactory proof in a similar problem, lead to a definite proof here; although with further work these steps may supply the answer. The matter of a rigorous proof for the pure realness of the h roots in the exact tape helix case must be considered still open. However, it is possible to prove from the approximate determinantal equations for the narrow tape or small wire helix and for the wide tape helix that only real h roots are possible in those cases. The proof is given in section III-D-1. It seems reasonable to suppose that this character of the h roots is maintained in the exact case also. From the results of the previous analysis and discussion it is evident that one need only consider h real with $|h| > k$ and that one can exclude the forbidden regions in seeking free mode solutions. Further, it seems clear in view of the physical symmetry of the single wound tape helix and the manner in which h and m occur in the radial argument function η_m, as well as elsewhere in the field representations, that identical solutions exist for positive and negative h.

It is often useful to consider the ratio ka/ha which corresponds to the ratio of the phase velocity of the zeroth order space harmonic to the velocity of a uniform plane wave in the medium. A plot of $ka/|h|a$ versus $ka/(\cot\psi)$ is shown in Fig. 27 and represents another type of chart for the forbidden regions. From Eq. 166 these regions correspond to values such that

$$\left|\frac{1}{|m|\,\frac{\cot\psi}{ka} - 1}\right| > \frac{ka}{|h|a} > \left|\frac{1}{|m|\,\frac{\cot\psi}{ka} + 1}\right|, \quad |m| \geq 1. \tag{168}$$

As for the sheath helix model, since it is necessary that $|h| > k$, only slow waves, referred to the z axis, can exist on the tape helix.

The limitation given in Eq. 167 shows that under no circumstances will free modes exist if $p > \lambda/2$. If each turn of the helix is considered as constituting an element of a radiating linear array, then the requirement that the spacing between elements, p, be less than $\lambda/2$ corresponds to the usual requirement for a single major lobe to exist only along the axis of the array. (See, for example, reference 56, page 275.) The forbidden

region requirement can also be interpreted in this manner and suggests the somewhat crude picture of the helix as an infinite circular diffraction device. In this case a free mode results at those frequencies for which the waves diffracted at the gap have the proper phase and amplitude so as to interfere and to prevent radiation in a radial direction.

It should be emphasized that the results of this section concerning the forbidden regions are not dependent on any approximations and would apply to the exact solution for the lossless helix problem if it were available. Further, it is evident from the remarks of section II-B that similar forbidden region restrictions exist for many types of helical structures and, actually, for all other open cylindrical periodic systems.

Some similarities between the results given here and those given elsewhere for periodic structures will, no doubt, be noted (5, 37). However, in the present case there is an upper frequency limit beyond which no free mode solutions can exist, as well as certain regions where the same restriction applies. This is in contrast to many other problems concerned with periodic structures where, although wave propagation does not occur within restricted frequency bands, exponentially damped solutions which satisfy the boundary conditions do exist in such bands. This difference is a direct consequence of the open character of the helix and the resulting need to satisfy the proper boundary condition for large r.

The Narrow Tape Approximation

E. Boundary Conditions; Derivation of Approximate Determinantal Equation

Since an exact solution to the tape helix problem seems impossible, as noted in section II-C, and since even the approximation procedure in which only a few terms of the exact infinite determinantal equation are used appears excessively burdensome, another approach is used to obtain useful numerical results. In this the tape is taken to be quite narrow so that the current distribution may be assumed with fair validity to be essentially quasi-static. By approximating the electric field boundary condition, one can then obtain a determinantal equation. In a later section the case where the tape is quite wide is considered.

If the tape is taken to be very narrow, that is, with δ small compared with a, p, and λ, it seems quite reasonable to assume that essentially all of the current flows only along the tape. In other words, in this case $K_{\parallel}$ is the major component of current density, whereas $K_{\perp}$ is small. If the point of view is taken that the fields are produced by the currents which flow, with the tape narrow and current flowing primarily in the direction of the tape, the specific distribution of current across the tape will affect to only a small degree the fields even in the near neighborhood of the wire and to a much less degree the fields on adjacent and faraway turns. Thus, if some reasonable assumptions are made concerning this current distribution, it is to be expected that only small errors will be made in the field expressions. The assumption of small $K_{\perp}$ (actually, it is taken to be

zero) is not very radical since one would expect that for narrow tapes the perpendicular or transverse currents on the outside and inside of the tape very nearly cancel each other in magnitude and phase so that the total transverse current density, $K_\perp$, is exceedingly small. Further, if a solution is obtained for the helix problem on the assumption of zero $K_\perp$ which leads to a nonzero value of $E_\perp$ on the tape, then for a narrow tape only a small transverse current density would be required to cancel this finite $E_\perp$; and this would perturb the zero $K_\perp$ solution only slightly. The above arguments may be expressed in a somewhat more rigorous fashion (68).

If an inexact current distribution on the tape is assumed, the tangential electric field can no longer be made zero everywhere on the tape, and this boundary condition can be only approximately satisfied. This may be done in several ways. One could, for example, require the average value, or better the mean-square value, of the tangential electric field on the tape to be a minimum, with the propagation constant h which gives this minimum taken as the solution. However, another procedure is used here which leads to a somewhat simpler determinantal equation for calculative purposes than the above possibilities and which appears to be a quite adequate approximation. In this it is required that $E_{||}$ be zero along the center of the tape; in other words, one of the boundary conditions is matched exactly along a line. As noted before, for a narrow tape the dominant current density is $K_{||}$, and, loosely speaking, it is $E_{||}$ which forces this current to flow along the tape. Thus, if the most important boundary condition is completely satisfied on a line, one may hope to obtain a reasonably good approximation to the exact case where this condition must be satisfied over a surface. Ignoring the boundary condition for $E_\perp$ on the tape is not very serious for a narrow tape since, as already pointed out, if the approximate solution leads to a finite $E_\perp$ there, only a very small $K_\perp$, which alters the solution only slightly, will neutralize it. The satisfaction of the $E_{||} = 0$ condition merely along a line may seem like only a fair approximation, but if this condition is met, it can be expected that $E_{||}$ is also zero, or very nearly so, on a surface in the neighborhood of this line which is almost a narrow tape. Since the exact cross sectional shape of the conductor should affect the characteristics of the solution only slightly, particularly if the largest transverse dimension of this shape is small compared with a, p, and λ, it may be concluded that this approximation also exerts at most only a small influence on the final result. It should be mentioned that this approximation method, which proceeds by assuming a quasi-static distribution of the magnetic (or electric) field under conditions where such an assumption is quite valid and then by matching the electric (or magnetic) field condition along a line, has often been used in boundary value problems (36).

To apply the above approximation procedure, the expression for $E_{||}$ is needed for $r = a$ in terms of $K_{||_m}$ and $K_{\perp_m}$. Since

$$K_{\theta,z} = e^{-jhz} \sum_m \kappa_{\theta,zm}\, e^{-jm\left(\frac{2\pi}{p} z-\theta\right)} \qquad (152,153)$$

$$K_{\parallel,\perp} = e^{-jhz} \sum_m \kappa_{\parallel,\perp_m}\, e^{-jm\left(\frac{2\pi}{p} z-\theta\right)} \qquad (169,170)$$

where $\kappa_{\parallel_m}$ and $\kappa_{\perp_m}$ are the Fourier coefficients of the current density expansions, and since

$$K_{\parallel} = K_z \sin\psi + K_\theta \cos\psi \qquad (47)$$

$$K_{\perp} = K_z \cos\psi - K_\theta \sin\psi \qquad (48)$$

there results immediately from orthogonality

$$\kappa_{\parallel_m} = \kappa_{zm} \sin\psi + \kappa_{\theta m} \cos\psi \qquad (171)$$

$$\kappa_{\perp_m} = \kappa_{zm} \cos\psi - \kappa_{\theta m} \sin\psi \qquad (172)$$

and

$$\kappa_{zm} = \kappa_{\parallel_m} \sin\psi + \kappa_{\perp_m} \cos\psi \qquad (173)$$

$$\kappa_{\theta m} = \kappa_{\parallel_m} \cos\psi - \kappa_{\perp_m} \sin\psi. \qquad (174)$$

Also

$$E_{\parallel} = E_z \sin\psi + E_\theta \cos\psi \qquad (175)$$

$$E_{\perp} = E_z \cos\psi - E_\theta \sin\psi. \qquad (176)$$

Using Eqs. 173 and 174 in Eqs. 155 and 156 to obtain E^e_θ and E^e_z in terms of $\kappa_{\parallel_m}$ and $\kappa_{\perp_m}$, and then using Eq. 175 to obtain $E^e_\parallel$, one obtains finally

$$E^e_\parallel = j\frac{e^{-jhz}\sin^2\psi}{\omega\epsilon a}\sum_m \Bigg\{\Bigg(\left[\eta_m^2 - mh_m a\left(1+\frac{a}{r}\right)\cot\psi + \frac{a}{r}m^2h_m^2a^2\frac{\cot^2\psi}{\eta_m^2}\right] I_m(\eta_m)K_m\left(\eta_m\frac{r}{a}\right)$$

$$+ k^2a^2\cot^2\psi\, I'_m(\eta_m)K'_m\left(\eta_m\frac{r}{a}\right)\Bigg)\kappa_{\parallel_m}$$

$$+\Bigg(\left[\eta_m^2\cot\psi + mh_m a\left(1-\frac{a}{r}\cot^2\psi\right) - \frac{a}{r}m^2h_m^2a^2\frac{\cot\psi}{\eta_m^2}\right] I_m(\eta_m)K_m\left(\eta_m\frac{r}{a}\right)$$

$$- k^2a^2\cot\psi\, I'_m(\eta_m)K'_m\left(\eta_m\frac{r}{a}\right)\Bigg)\kappa_{\perp_m}\Bigg\} e^{-jm\left(\frac{2\pi}{p}z-\theta\right)}. \qquad (177)$$

For narrow tapes a reasonable assumption is that the magnitude of the current density $K_{\parallel}$ is constant across the tape. For this

$$K_{\parallel} = e^{-jhz} \sum_m \kappa_{\parallel_m} e^{-jm\left(\frac{2\pi}{p} z-\theta\right)} \approx \begin{cases} Ae^{-jhz} e^{j(h-\beta_{\parallel})\left(z - \frac{p}{2\pi}\theta\right)}, & \frac{p}{2\pi}\theta + \delta > z > \frac{p}{2\pi}\theta \\ 0, \text{ elsewhere} \end{cases} \tag{178}$$

with A an undetermined constant. The factor $e^{j(h-\beta_{\parallel})\left(z - \frac{p}{2\pi}\theta\right)}$ is included for some generality to account for a possible linear phase shift of the current density across the tape, with $\beta_{\parallel}$ real, positive, and independent of θ and z. The point $z = 0$, $\theta = 0$ is chosen somewhat arbitrarily as point (1) in Fig. 25b. Note that the form of the assumed current distribution has been chosen so that the phase variation of the current density in z for constant θ is dependent on $\beta_{\parallel}$ alone. The current is taken to flow in the positive θ and z directions along the tape. The constant A may be related to the amplitude of the total current $|I|$ which flows in the direction of the tape by

$$|I| = \left| \int_{\text{tape}} K_{\parallel}\, dl \right| \tag{179}$$

where l is measured perpendicular to the tape edges. Using the right side of Eq. 178 in Eq. 179 and assuming the constant phase front of the current density is perpendicular to the tape edges (for this $\beta_{\parallel} = h \sin^2\psi$ (see sec. II-L)), one obtains after some transformations and change of variable

$$A = \frac{|I|}{\delta \cos\psi}. \tag{180}$$

The assumption of some other phase variation for the current density in place of the one used above makes very little difference if δ is small. Using Eq. 180 in Eq. 178, multiplying both sides of Eq. 178 by $e^{jn\left(\frac{2\pi}{p} z-\theta\right)}$, and integrating on z from 0 to p, one obtains

$$\begin{aligned} {}_1\kappa_{\parallel_m} &= \frac{|I|}{p \cos\psi} e^{j\left(h - \beta_{\parallel} + m\frac{2\pi}{p}\right)\frac{\delta}{2}} \frac{\sin\left[\left(h - \beta_{\parallel} + m\frac{2\pi}{p}\right)\frac{\delta}{2}\right]}{\left[\left(h - \beta_{\parallel} + m\frac{2\pi}{p}\right)\frac{\delta}{2}\right]} \\ &= \frac{|I|}{p \cos\psi} e^{j\left(h - \beta_{\parallel} + m\frac{2\pi}{p}\right)\frac{\delta}{2}} {}_1D_m. \end{aligned} \tag{181}$$

The subscript 1 is used to distinguish the current density Fourier coefficients of this approximation from those of another type which are derived shortly, and ${}_1D_m$ is defined in an obvious manner. Since $K_\perp$ is taken to be zero

$$ {}_1K_{\perp_m} = 0. \tag{182} $$

A more reasonable assumption than a constant for the variation of the current density is one for which the distribution approximates that on an isolated narrow thin tape. With this approximation $K_{||}$ is taken as becoming infinitely large in an inverse square root manner as the tape edges are approached, with $K_\perp$ again taken to be zero (see sec. II-L). For this assumption

$$ K_{||} = e^{-jhz} \sum_m K_{||_m} e^{-jm\left(\frac{2\pi}{p} z - \theta\right)} \approx \begin{cases} Ae^{-jhz} e^{j(h-\beta_{||})\left(z - \frac{p}{2\pi}\theta\right)} \dfrac{\delta}{\sqrt{\left(z - \frac{p}{2\pi}\theta\right)\left(\delta - z + \frac{p}{2\pi}\theta\right)}} \\ \qquad \text{for } \frac{p}{2\pi}\theta + \delta > z > \frac{p}{2\pi}\theta \\ 0, \text{ elsewhere.} \end{cases} \tag{183} $$

The comments following Eq. 178 apply here also, except that in this case A has a slightly different value. Using the right side of Eq. 183 in Eq. 179 and the same assumptions employed to derive Eq. 180, one obtains for this

$$ A = \frac{|I|}{\pi\delta \cos\psi}. \tag{184} $$

Using Eq. 184 in Eq. 183 and proceeding in the usual fashion, one obtains

$$ {}_2K_{||_m} = \frac{|I|}{p \cos\psi} e^{j\left(h - \beta_{||} + \frac{2\pi m}{p}\right)\frac{\delta}{2}} J_o\left[\left(h - \beta_{||} + \frac{2\pi m}{p}\right)\frac{\delta}{2}\right] $$

$$ = \frac{|I|}{p \cos\psi} e^{j\left(h - \beta_{||} + m\frac{2\pi}{p}\right)\frac{\delta}{2}} {}_2D_m \tag{185} $$

where J_o is the ordinary Bessel function and ${}_2D_m$ is defined in an obvious manner. In obtaining Eq. 185 it is necessary, after making a change of variable, to use

$$ \int_0^1 \frac{\cos bx}{\sqrt{1 - x^2}}\, dx = \frac{\pi}{2} J_o(b). \tag{186} $$

(See reference 3, page 48.) In Eq. 185 the subscript 2 is used to distinguish the results of this approximation from those of the previous constant density assumption. Note that ${}_1K_{\parallel_m}$ and ${}_2K_{\parallel_m}$ are similar in form and not too unlike in actual value since (sin z)/z and $J_o(z)$ are much the same, at least for small z. This confirms the remarks made previously, and more will be said of this later. Since $K_\perp$ is taken to be zero, for this approximation also

$$ {}_2K_{\perp_m} = 0. \tag{187}$$

Insertion of Eq. 181 or Eq. 185 and Eq. 182 or Eq. 187 in Eq. 177 yields for $E_\parallel^e$ for either approximate current distribution

$$E_\parallel^e \approx je^{-jhz}\frac{\sin\psi\tan\psi}{p\omega\epsilon a}|I|\, e^{j(h-\beta_\parallel)\frac{\delta}{2}}\sum_m\left\{\left[\eta_m^2 - mh_m a\left(1+\frac{a}{r}\right)\cot\psi\right.\right.$$

$$\left.\left.+\frac{a}{r}m^2h_m^2a^2\frac{\cot^2\psi}{\eta_m^2}\right]I_m(\eta_m)K_m\left(\eta_m\frac{r}{a}\right)+k^2a^2\cot^2\psi\, I'_m(\eta_m)K'_m\left(\eta_m\frac{r}{a}\right)\right\}{}_{1,2}D_m\, e^{jm\frac{\pi\delta}{p}}e^{-jm\left(\frac{2\pi}{p}z-\theta\right)} \tag{188}$$

If $E_\parallel^e$ is required to be zero along the center of the tape, the substitutions r = a and $z = (p/2\pi)\,\theta + \delta/2$ in Eq. 188 yield

$$E_\parallel^e\left(r=a, z=\frac{p}{2\pi}\theta+\frac{\delta}{2}\right)=0 \approx j\, e^{-j\left(\frac{hp}{2\pi}\theta+\beta_\parallel\frac{\delta}{2}\right)}\frac{\sin\psi\tan\psi}{p\omega\epsilon a}|I|\times$$

$$\sum_m\left\{\left(\eta_m-\frac{mh_m a\cot\psi}{\eta_m}\right)^2 I_m(\eta_m)K_m(\eta_m)\right.$$

$$\left.+k^2a^2\cot^2\psi\, I'_m(\eta_m)K'_m(\eta_m)\right\}{}_{1,2}D_m \tag{189}$$

Since the right side of Eq. 189 consists of a complex factor whose magnitude is independent of h, times a real series, it is clear that if Eq. 189 is to be satisfied, the series must be zero. Since

$$\left(\eta_m-\frac{mh_m a\cot\psi}{\eta_m}\right)^2=\eta_m^2-2h_m am\cot\psi+\frac{m^2h_m^2a^2\cot^2\psi}{\eta_m^2}$$

$$=h^2a^2-k^2a^2+k^2a^2\frac{m^2\cot^2\psi}{\eta_m^2} \tag{190}$$

there results finally for the approximate determinantal equation for the narrow tape helix

for either assumed current distribution

$$0 \approx \sum_m \left\{ \left(h^2a^2 - k^2a^2 + k^2a^2 \frac{m^2\cot^2\psi}{\eta_m^2} \right) I_m(\eta_m) K_m(\eta_m) \right.$$

$$\left. + k^2a^2 \cot^2\psi \, I'_m(\eta_m) K'_m(\eta_m) \right\} {}_{1,2}D_m. \qquad (191)$$

F. General Solution of the Approximate Determinantal Equation

To obtain useful numerical results some procedure is required for determining those values of h, real and in magnitude greater than k, which satisfy the determinantal equation 191 for specific values of ka, cot ψ, and δ. The procedure used here is a combination of analytical, numerical, and graphical methods which are briefly described below.

For the purpose of simplifying the determinantal equation somewhat, it is assumed that $\beta_{11} = h$. This is equivalent to assuming that the constant phase front of the current distribution on the tape occurs for constant z. Although this would be expected to be a sufficiently satisfactory assumption for large ψ, it might be thought to be quite poor for small ψ. However, it can be shown that the more realistic assumption of a current distribution constant phase front which is perpendicular to the tape edges makes very little difference even for small ψ if the tape is narrow. With $\beta_{11} = h$, ${}_1D_m$ becomes

$${}_1D_m(\beta_{11} = h) = \frac{\sin mx}{mx} \qquad (192)$$

where the parameter x is defined as

$$x = \frac{\pi\delta}{p} \qquad (193)$$

and should not be confused with the coordinate axis. Only the constant magnitude current density assumption is considered for the moment. It is shown in section II-L that the use of ${}_2D_m$ alters the final result only in a minor way.

Since the determinantal equation is in the form of an infinite series, a means of summing this series must be found. Further, examination shows that for large m the terms vary like $(\sin mx)/m^2x$, which means that the series converges very slowly and thus is not very suitable for numerical work in its present form. To improve this a well-known procedure is used in which a series, whose terms for large m are essentially equal to those of the series whose sum is desired, is added to and then subtracted term by term from the latter. If the sum of the terms in the series which is added and subtracted is known, the desired series is transformed to the sum of a known function plus a remainder series which is more rapidly convergent than the original one. The increase in the rate of convergence depends on how rapidly the terms in the subtracted

series approach those of the original.

Using the following representations (discussed at length in reference 68), one has to a very good approximation for $|m| \geq 1$

$$I_m(\eta_m)K_m(\eta_m) \approx \frac{1}{2} \frac{1}{\left(m^2 + \eta_m^2\right)^{1/2}} \tag{194}$$

$$I'_m(\eta_m)K'_m(\eta_m) \approx -\frac{1}{2} \frac{\left(m^2 + \eta_m^2\right)^{1/2}}{\eta_m^2}. \tag{195}$$

Using Eqs. 192, 194, and 195 in Eq. 191 in the manner described above, separating out the m = 0 term since Eqs. 194 and 195 are not sufficiently good approximations for this, and converting the sum over negative m to a sum over positive m results in

$$0 \approx \zeta^2 a^2 I_o(\zeta a)K_o(\zeta a) + k^2 a^2 \cot^2\psi\, I'_o(\zeta a)K'_o(\zeta a) + \frac{1}{2}\sum_{m=1}^{\infty}\left\{\left(h^2a^2 - k^2a^2\right.\right.$$

$$\left.\left. + k^2a^2 \frac{m^2\cot^2\psi}{\eta_{+m}^2}\right) \frac{1}{\left(m^2 + \eta_{+m}^2\right)^{1/2}} - k^2a^2\cot^2\psi \frac{\left(m^2 + \eta_{+m}^2\right)^{1/2}}{\eta_{+m}^2}\right\} \frac{\sin mx}{mx}$$

$$+ \frac{1}{2}\sum_{m=1}^{\infty}\left\{\left(h^2a^2 - k^2a^2 + k^2a^2 \frac{m^2\cot^2\psi}{\eta_{-m}^2}\right) \frac{1}{\left(m^2 + \eta_{-m}^2\right)^{1/2}}\right.$$

$$\left. - k^2a^2\cot^2\psi \frac{\left(m^2 + \eta_{-m}^2\right)^{1/2}}{\eta_{-m}^2}\right\} \frac{\sin mx}{mx} + \sum_{m=1}^{\infty} R(\eta_{-m}) + \sum_{m=1}^{\infty} R(\eta_{+m}). \tag{196}$$

In Eq. 196

$$\eta_o = \zeta a = \sqrt{h^2a^2 - k^2a^2} \tag{197}$$

(see Eq. 30)

$$\eta_{+m} = \left[m^2\cot^2\psi + 2mha\cot\psi + h^2a^2 - k^2a^2\right]^{1/2} \tag{198}$$

$$\eta_{-m} = \left[m^2\cot^2\psi - 2mha\cot\psi + h^2a^2 - k^2a^2\right]^{1/2} \tag{199}$$

with $m \geq 1$, and

$$R(\eta_{\pm m}) = \left\{ \left(h^2a^2 - k^2a^2 + k^2a^2 \frac{m^2\cot^2\psi}{\eta^2_{\pm m}} \right) \left[I_m(\eta_{\pm m}) K_m(\eta_{\pm m}) - \frac{1}{2} \frac{1}{\left(m^2 + \eta^2_{\pm m}\right)^{1/2}} \right] \right.$$

$$\left. + k^2a^2\cot^2\psi \left[I'_m(\eta_{\pm m}) K'_m(\eta_{\pm m}) + \frac{1}{2} \frac{\left(m^2 + \eta^2_{\pm m}\right)^{1/2}}{\eta^2_{\pm m}} \right] \right\} \frac{\sin mx}{mx}. \qquad (200)$$

Because of the symmetrical position of h and m in Eq. 196, it can be observed that if Eq. 196 has any solutions for h positive, it will also have identical solutions for h negative and of the same magnitude. This confirms a remark made in section II-D, at least to this approximation. Since only $h > k$ need be considered in view of the above, from Eq. 198

$$\eta_{\pm m} > \left[m^2\cot^2\psi + 2mka\cot\psi \right]^{1/2}. \qquad (201)$$

Because of the limitation $(\cot\psi)/2 > ka$ and since $m \geq 1$ in Eq. 201, some consideration shows that for any practical value of ψ, $\eta_{\pm m}$ is sufficiently large so that Eqs. 194 and 195 are exceedingly good approximations for all ka, ha, and m. This in turn means that all the $R(\eta_{\pm m})$ terms are very small compared with their corresponding terms in the first sum in Eq. 196, and, therefore, the sum

$$\sum_{m=1}^{\infty} R(\eta_{+m})$$

can be omitted with negligible error. However, since η_{-m} can become very small (it is zero at the edges of the mth forbidden region) the sum

$$\sum_{m=1}^{\infty} R(\eta_{-m})$$

must not be omitted. Fortunately, it turns out that, in general, only one term of this series is significant, and even this occurs only near the boundary of a forbidden region. Dropping

$$\sum_{m=1}^{\infty} R(\eta_{+m})$$

and simplifying the expressions in the braces in the first two sums of Eq. 196 by combining terms in k^2a^2, one obtains

$$0 \approx \zeta^2 a^2 I_o(\zeta a) K_o(\zeta a) + k^2 a^2 \cot^2\psi\, I_o'(\zeta a) K_o'(\zeta a)$$

$$+ \frac{(h^2 a^2 - k^2 a^2 \csc^2\psi)}{2} \sum_{m=1}^{\infty} \left[\frac{1}{\left(m^2 + \eta_{+m}^2\right)^{1/2}} + \frac{1}{\left(m^2 + \eta_{-m}^2\right)^{1/2}} \right] \frac{\sin mx}{mx}$$

$$+ \sum_{m=1}^{\infty} R(\eta_{-m}). \tag{202}$$

Both

$$\frac{1}{\left(m^2 + \eta_{+m}^2\right)^{1/2}} \text{ and } \frac{1}{\left(m^2 + \eta_{-m}^2\right)^{1/2}}$$

go like $1/(m \csc\psi)$ for large m so that after adding and subtracting $1/(m \csc\psi)$ from each term in the brackets in the first sum in Eq. 202, there results

$$0 \approx \zeta^2 a^2 I_o(\zeta a) K_o(\zeta a) + k^2 a^2 \cot^2\psi\, I_o'(\zeta a) K_o'(\zeta a) + \frac{(h^2 a^2 - k^2 a^2 \csc^2\psi)}{\csc\psi} \frac{1}{x} \sum_{m=1}^{\infty} \frac{\sin mx}{m^2}$$

$$+ \frac{(h^2 a^2 - k^2 a^2 \csc^2\psi)}{2} \sum_{m=1}^{\infty} \left[\frac{1}{\left(m^2 + \eta_{+m}^2\right)^{1/2}} + \frac{1}{\left(m^2 + \eta_{-m}^2\right)^{1/2}} - \frac{2}{m \csc\psi} \right] \frac{\sin mx}{mx}$$

$$+ \sum_{m=1}^{\infty} R(\eta_{-m}). \tag{203}$$

The dominant term in

$$\frac{1}{x} \sum_{m=1}^{\infty} \frac{\sin mx}{m^2}$$

is $\ln(e/x)$. For narrow tapes it is sufficient to use just the dominant term, and Eq. 203 becomes

$$0 \approx \zeta^2 a^2 I_o(\zeta a) K_o(\zeta a) + k^2 a^2 \cot^2\psi\, I_o'(\zeta a) K_o'(\zeta a) + \frac{(h^2 a^2 - k^2 a^2 \csc^2\psi)}{\csc\psi} \ln \frac{e}{x}$$

$$+ \frac{(h^2 a^2 - k^2 a^2 \csc^2\psi)}{2} \sum_{m=1}^{\infty} \left[\frac{1}{\left(m^2 + \eta_{+m}^2\right)^{1/2}} + \frac{1}{\left(m^2 + \eta_{-m}^2\right)^{1/2}} - \frac{2}{m \csc\psi} \right] \frac{\sin mx}{mx}$$

$$+ \sum_{m=1}^{\infty} R(\eta_{-m}). \tag{204}$$

Since the terms in the first series in Eq. 204 vary as $(\sin mx)/m^4x$ for large m, Eq. 204 might be used as it stands for numerical computation. However, in view of the wide range of ha and ka which must be investigated and because of the rather inconvenient form of the terms, a suitable approximation for this series is highly desirable. This may be derived by approximating the $(\sin mx)/mx$ term by a simple algebraic factor, which agrees exceedingly well with $(\sin mx)/mx$ even for relatively large m with x small, and by changing the summation to an integration. For small x this process leads to a quite good approximation which is derived in reference 68. The final expression is rather complicated and is therefore not repeated here.

It will be recalled that Eq. 204 is the modified expression for E_{11} at the center of the tape. If this field is considered the result of the current which flows, a physical interpretation can be given for the various terms in Eq. 204. The first two terms are from the m = 0 term of the series and give the average field from the current in all the turns. Note that the first two terms alone are the determinantal equation for the zeroth mode of the sheath helix. The third term in Eq. 204 is logarithmic in the tape width and comes from the large order terms in Eq. 191. It is essentially the field resulting from the current in the near neighborhood of the point at the center of the tape. Although not so obvious, the fourth term in Eq. 204 may be interpreted as the portion of the field at the center of the tape contributed by the adjacent turns, whereas the final term is interpreted as the rest of the field resulting from the turns very far away. This interpretation for the final term is confirmed by noting that for m = 1, at least, the field determined from $R(\eta_1)$ near $\eta_1 = 0$ has the same character, namely logarithmic, as when the field on a turn resulting from the current in turns very far away is simply calculated by using the usual dipole far field radiation expressions. Except for this result, the simple calculation has little interest and is not shown here.

Since the first two terms in Eq. 204 give precisely the determinantal equation for the zeroth mode of the sheath helix, it is evident from the discussion in section I-E-3 that the sum of these is essentially zero over a wide range of frequencies for $|h|a = ka \csc \psi$ or $ka/(|h|a) = \sin \psi$. For this value of $|h|a$ the other terms in Eq. 204 are also zero with the exception of the final remainder term, which is very small except near $\eta_m = 0$. Consequently, to this approximation, the single wound narrow tape helix has solutions which are very near those for the zeroth mode of the sheath helix except for the effect of the forbidden regions. This will be seen more clearly in the next section where a particular case is discussed. An interesting aspect of Eq. 204 is that it shows quite clearly why the infinitesimal thin wire diameter solution of reference 17 and the usual zeroth mode sheath helix solution of references 7, 9, 10, and 11, which is discussed in the previous section, agree so well in the range of frequencies where the asymptotic solution $|h|a = ka \csc \psi$ is valid.

G. Numerical Results for $\psi = 10°$ and $x = 0.1$; Comparison with Published Experimental Results

Calculations for the case of $\psi = 10°$ and $x = 0.1$ have been carried through in detail, and the propagation constants which result are shown in Figs. 28 and 29. $\psi = 10°$ was chosen as a representative value for which the solutions would exhibit their general properties. $x = 0.1$ was chosen since it was felt that this value is sufficiently small so that the approximations should be quite valid. Since the tape width appears to make only a small difference in the results, this choice of x is not a significant restriction. As in the sheath helix case, several waves can exist at a particular frequency. In Figs. 28 and 29 the t subscript on the h values refers to the tape solutions, the numerical subscript 0, 1, 2 refers to the dominant character of the fields for $r >> a$ associated with a particular solution, and the prime superscript is used to distinguish between solutions with the same numerical subscript. Since a solution is now made up of an entire set of space harmonics, it becomes difficult to speak of modes in the same sense as was used in the sheath helix case in the previous section. However, if one considers the field structure for $r >> a$, it is usually found that one of the space harmonics of a wave is much larger than all the others, and the number of this space harmonic might be considered as a mode number. This has been done, in so far as possible, by labeling the various h_t solutions, as will be evident soon.

In Fig. 28 the solid and dotted lines refer to waves which would be observed if one were located at $z >> 0$ or $z << 0$, respectively, with a source at $z = 0$. As in the sheath helix case the reasons for this are understood best by considering the source-present or driven helix, and this is done in the following section. Note that Fig. 28b is essentially symmetrical about the $ka/\cot\psi$ axis, so that for every wave in the positive z direction there is a similar wave in the negative z direction. However, it is physically clear, as is also evident from the field expressions, that these waves rotate in opposite θ directions. Fig. 28b and the solutions shown there are to be interpreted in the following manner. If an observation point is located at $z >> 0$ so that the radiation field from a source at $z = 0$ is negligible, then waves with propagation constants $-|h''_{t1}|$, $|h_{to}|$, and $|h'_{t1}|$ could be detected at low frequencies. As the frequency increases, a point is reached where the $-|h''_{t1}|$ and $|h_{to}|$ waves have propagation constants of the same magnitude, but their group velocities are zero. The usual group velocity concept and its relationship to the axial power flow are completely valid here, as will be proved in section II-I. v_g/v_o is, of course, given by

$$\frac{d\left(\frac{ka}{\cot\psi}\right)}{d\left(\frac{ha}{\cot\psi}\right)}.$$

No power is propagated by the $-|h''_{t1}|$ and $|h_{to}|$ waves at this point, $ka = 0.77$, and this evidently corresponds to a standing wave. However, the $|h'_{t1}|$ wave is also present, and

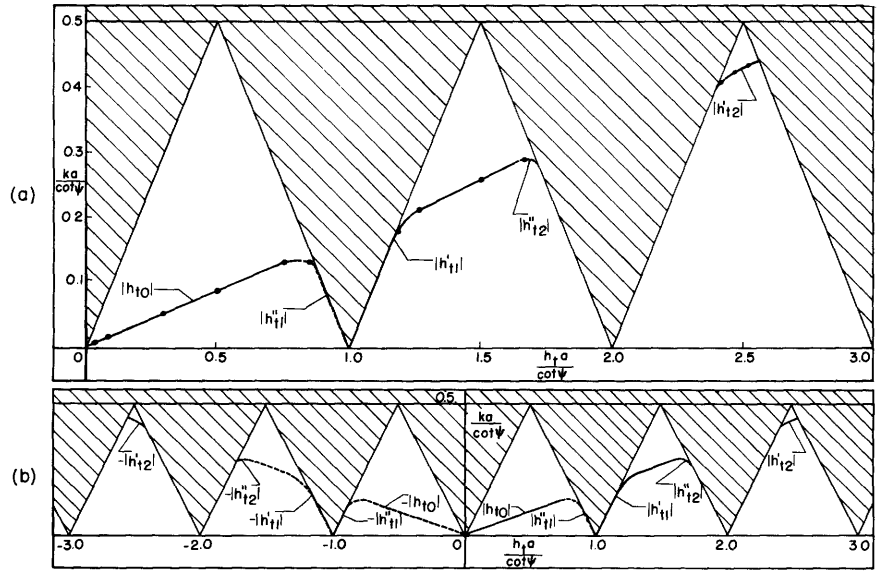

Fig. 28

The narrow tape helix;
$ka/\cot\psi$ vs $h_t a/\cot\psi$ for $\psi = 10°$, $x = 0.1$.

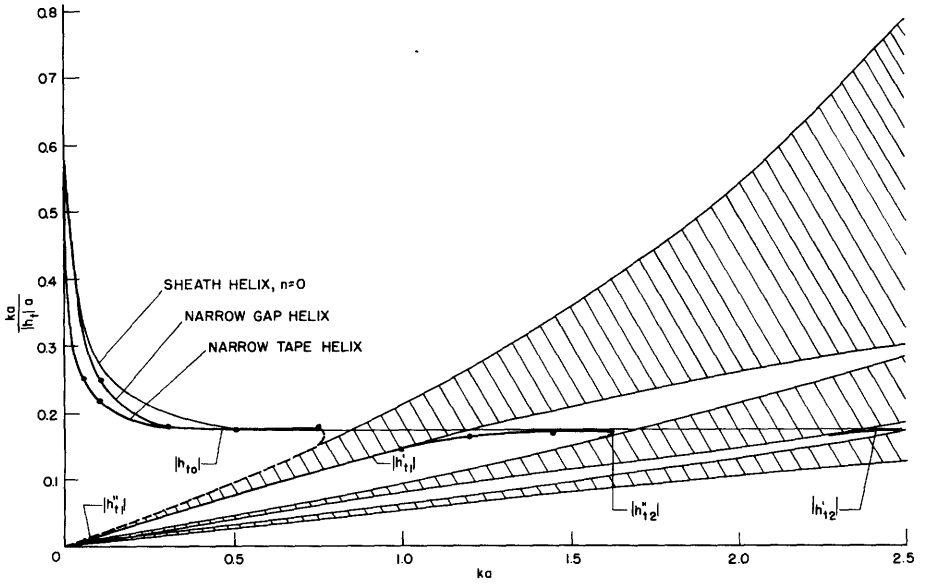

Fig. 29

$ka/|h_t|a$ vs ka for $\psi = 10°$, $x = 0.1$ for the narrow tape helix;
$\psi = 10°$, $x' = 0.1$ for the narrow gap helix (see sec. II-J);
and for $\psi = 10°$ for the sheath helix from reference 10.

as the frequency is increased further, it is the only wave which exists until ka = 1.61, after which the $-|h''_{t2}|$ wave appears. The $|h'_{t1}|$ and $-|h''_{t2}|$ waves exist together until ka = 1.64 at which point standing waves occur again. From 2.26 > ka > 1.64 no free mode propagation occurs; for 2.49 > ka > 2.26 only the $|h'_{t2}|$ wave exists; while for ka > 2.49 there are no free mode waves. If one is located at $z << 0$, the action is similar to the above except that the dotted lines in Fig. 28b are traced.

By using Eqs. 156, 173, 174, 181, and 192 with ${}_1\kappa_{\perp_m} = 0$, the following expression for E_z^e to this approximation can be readily obtained

$$E_z^e \approx j \frac{|I| e^{-jhz}}{p\omega\epsilon a} \sum_m \left[mha + \zeta^2 a^2 \tan \psi\right] I_m(\eta_m) K_m\left(\eta_m \frac{r}{a}\right) \frac{\sin mx}{mx} e^{jmx} e^{-jm\left(\frac{2\pi}{p} z - \theta\right)} \quad (205)$$

or

$$E_z^e \approx \sum_m A_m e^{-jh_m z}$$

which defines A_m. The ratio of the phase velocity, ${}_m v$, of the various space harmonics of a wave to the velocity, v_o, of a uniform plane wave in the medium is given by

$$\frac{{}_m v}{v_o} = \frac{ka}{h_m a} = \frac{ka}{m \cot \psi + ha} = \frac{\frac{ka}{\cot \psi}}{m + \frac{ha}{\cot \psi}}. \quad (206)$$

Note that ${}_m v/v_o$ can be positive or negative. Figure 30 shows the values of ${}_m v/v_o$ for $1 \geq m \geq -2$ for the various waves. Figure 31 shows the E_z^e space harmonic amplitude ratios in decibels at r = 2a; that is, it is a plot of $20 \log_{10}|A_m/A_n|$. The $-|h''_{t2}|$ wave is not shown in this latter plot since it is of minor interest, and since for it the m = +2 harmonic is by far the dominant one. All the space harmonics which are of sufficient amplitude to appear in Fig. 31 are plotted there. It is evident that even for r = 2a only a few space harmonics are significant.

Section II-I shows, from a consideration of the power flow associated with each wave, that the amplitudes of the $|h''_{t1}|$ and $|h'_{t1}|$ waves can be expected to be much less than the amplitude of the $|h_{to}|$ wave over most of the range ka < 0.75. Although the actual amplitudes depend on the configuration of the source and can be determined only by solving the driven helix problem, within relatively broad limits the $|h_{to}|$ wave is the dominant one at low frequencies. Assume that one were to measure E_z^e at r = 2a with a small detecting dipole. If Figs. 30 and 31 are considered together, it is evident that for ka < 0.5, at least, a space harmonic wave with no angular variation and with a phase velocity ratio like

$$\left.\frac{{}_o v}{v_o}\right] |h_{to}|$$

would be observed. For $0.77 > ka > 0.5$ a space harmonic wave whose phase velocity ratio is like

$$\left[\frac{-1^{v}}{v_o}\right]|h_{to}|$$

and whose angular variation is like $e^{-j\theta}$ would be observed, although this would probably be a region of some confusion. For $1.5 > ka > 0.77$ a space harmonic wave whose phase velocity ratio is like

$$\left[\frac{-1^{v}}{v_o}\right]|h'_{t1}|$$

and whose angular variation is like $e^{-j\theta}$ would be observed, although near the upper limit of this region there would be some mixing of space harmonics of almost equal amplitude. Over most of the range $1.64 > ka > 1.5$ the dominant space harmonic has an angular variation like $e^{-j2\theta}$, although it can be expected that this region would again be one of some confusion because of the mixture of space harmonics of nearly equal amplitude. For $2.26 > ka > 1.64$ no free mode wave propagation would be observed, while for most of the range $2.49 > ka > 2.26$ a space harmonic wave whose phase velocity ratio is like

$$\left[\frac{-2^{v}}{v_o}\right]|h'_{t2}|$$

and whose angular variation is like $e^{-j2\theta}$ would be observed. However, the $m = -2$ and $m = -3$ space harmonics are not very different in amplitude over all of this region, and it would probably be one of some confusion.

Figure 30 shows the phase velocity ratios of some sheath helix modes which were obtained from solutions of Eq. 42 for $\psi = 10°$. Over restricted frequency ranges most of the dominant space harmonic waves associated with the tape helix have phase velocities which correspond quite closely to the phase velocities of particular sheath helix modes. Thus, if E_z^e around a helix were observed in the above fashion, one might conclude that sheath helix modes exist but only over restricted frequency ranges. This was precisely the sort of action noted in reference 24. Although an exact comparison is not possible because of a lack of data, it is thought that the above offers an explanation of why such action occurs. Although only the E_z^e field is discussed above, the other field components have space harmonic amplitudes at $r = 2a$ which act in a similar, although not identical, fashion. For $r >> a$ the ratios $|A_m/A_n|$ are much larger than at $r = 2a$, and the transitions between the dominant space harmonics are more abrupt. These transitions occur in E_z^e at $r = 2a$ and in all the field components for $r >> a$ near $ka = 0.5$, 1.5, and 2.45, as shown in Fig. 31. For $r < a$ the higher order space harmonics also damp out rapidly although for $r << a$ only the zeroth space harmonic may be significant. Indeed, for $r = 0$ only that harmonic is nonzero for all the waves.

The numbering of the space harmonics in Figs. 30 and 31 is for $z > 0$ using the solid line solutions of Fig. 28b. If $z < 0$ is considered, the dotted line solutions of Fig. 28b are used, and the numbering of the space harmonics is reversed since the field rotates in the opposite θ direction. For $ka < 0.5$ the dominant space harmonics in the $|h'_{t1}|$ and

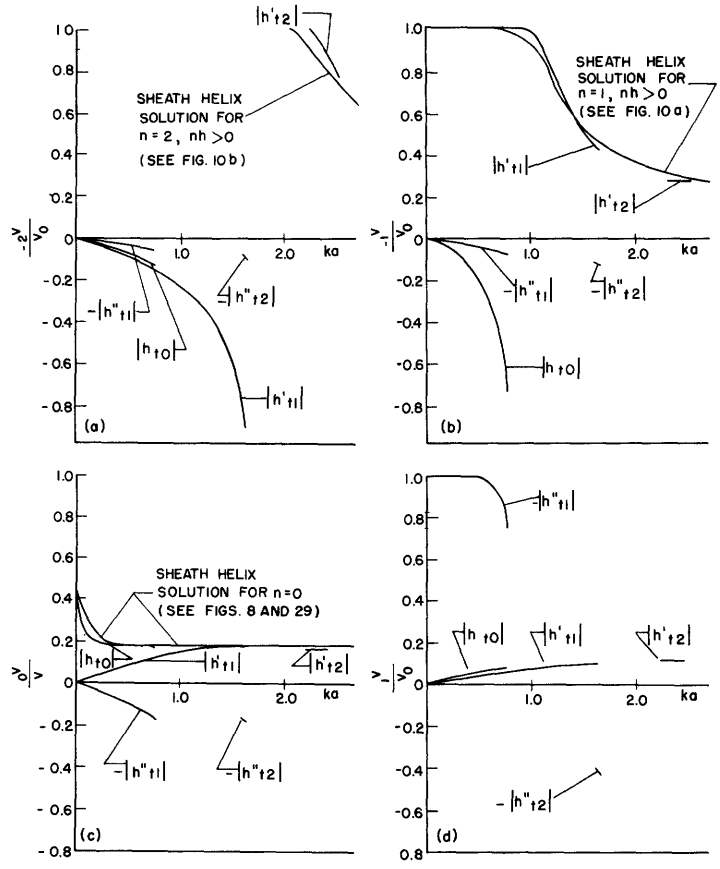

Fig. 30

The narrow tape helix;

(a) $-2^{V}/v_o$ vs ka

(b) $-1^{V}/v_o$ vs ka

(c) o^{V}/v_o vs ka

(d) $1^{V}/v_o$ vs ka

For all cases, $\psi = 10°$, $x = 0.1$, $z > 0$.

$-|h''_{t1}|$ waves are those for which m = -1 and m = +1, respectively, and these have phase velocity ratios which are very close to unity. It would appear that these waves are essentially perturbed uniform plane waves which are circularly or elliptically polarized, and rotating and traveling in opposite directions; however, sufficiently accurate values of $\eta_{\pm 1}$ were not available for confirming that the field components approach the proper form. If this supposition is correct, it explains why at low frequencies the $|h'_{t1}|$ and $|h''_{t1}|$ waves would be excited to very small amplitudes only by any finite source.

From Figs. 29 and 30c it can be seen that for ka < 0.4 or (ka/cot ψ) < 0.07 the dominant m = 0 harmonic has a phase velocity ratio which is somewhat less than that given by the sheath helix zeroth mode solution. References 22 and 23 have reported measurements which agree quite closely with the zeroth mode sheath helix solution for 0.05 > (ka/cot ψ) > 0.003 if the mean radius of the physical helix is used as the radius of the sheath helix. The theory presented here for the narrow tape helix thus appears to

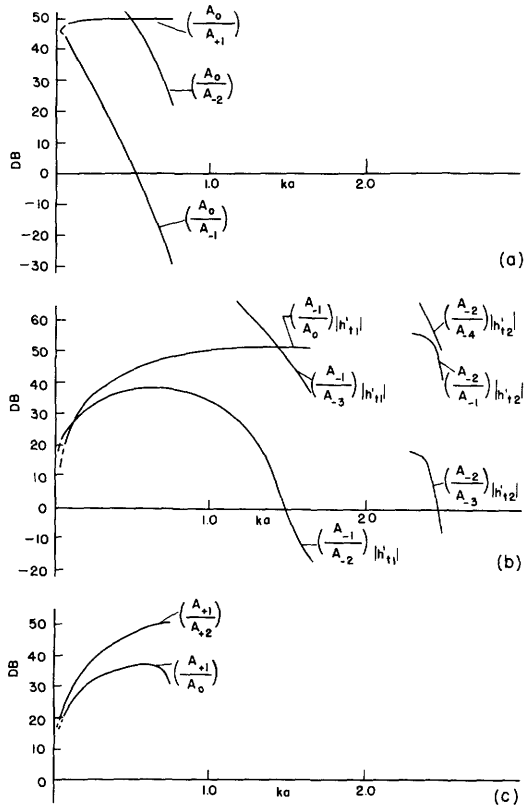

Fig. 31

The narrow tape helix $z > 0$; (a) space harmonic amplitudes of E_z^e for the $|h_{to}|$ wave at $r = 2a$ vs ka, $\psi = 10°$, $x = 0.1$. (b) space harmonic amplitudes of E_z^e for the $|h'_{t1}|$ and $|h'_{t2}|$ waves at $r = 2a$ vs ka, $\psi = 10°$, $x = 0.1$. (c) space harmonic amplitudes of E_z^e for the $-|h''_{t1}|$ wave at $r = 2a$ vs ka, $\psi = 10°$, $x = 0.1$.

predict phase velocity ratios which are too low for ka/cot ψ small. However, increasing the tape width, δ, changes the phase velocity ratio in a direction so as to make for better agreement. It seems quite likely that if a wider tape were assumed, with some deterioration in the validity of the approximations, closer agreement between the tape solution and the experimentally measured phase velocity ratios would occur. This matter is considered further in section II-J. Although reference 22 reported no wave other than the usual slow one for a wide range of frequencies (but for (ka/cot ψ) < 0.04), exciting conditions, and terminating conditions, reference 23 reported a fast wave, one with a phase velocity ratio near unity, coexisting with the slow wave. It would appear that this fast wave was either the m = -1 or m = +1 space harmonic of the $|h'_{t1}|$ or $-|h''_{t1}|$ wave (see Figs. 30b and 30d). Reference 23 pointed out that the fast wave disappeared (or became of sufficiently small amplitude so as not to be observed) when the exciting arrangement was altered.

Instead of considering the propagation constant and phase velocity of the waves referred to the z axis, it is possible to refer these to a line measured along or parallel to the helix itself. Since this line is given by $(2\pi/p)z - \theta$ = constant, it is evident that the propagation constant β along this line is given by

$$\beta = h \sin \psi. \tag{207}$$

A phase velocity ratio v_β/v_o can now be defined in the usual manner so that

$$\frac{v_\beta}{v_o} = \frac{k}{\beta} = \frac{ka}{ha \sin \psi}. \tag{208}$$

Figure 32 shows v_β/v_o for the different waves as a function of ka. Also shown are some experimental points given in references 25 and 32. These were obtained by moving a

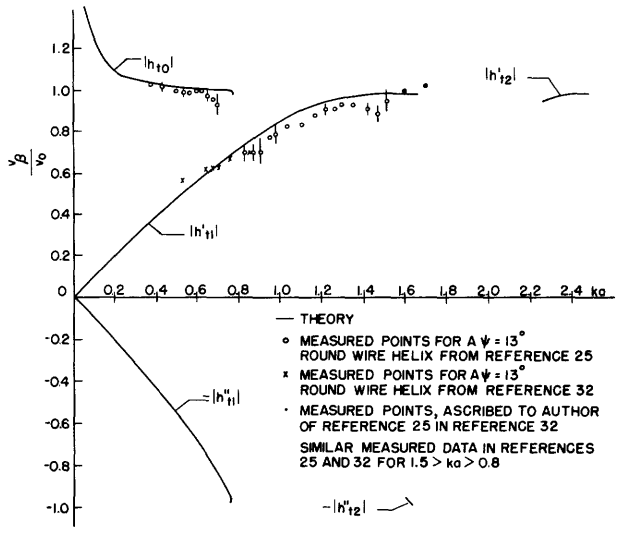

Fig. 32

The narrow tape helix $z > 0$; v_β/v_o vs ka, $\psi = 10°$, $x = 0.1$.

search probe along the surface of a round wire helix. The experimental technique is described in detail in reference 32. Reference 33 shows experimental curves for other helices for $13.6° > \psi > 6.5°$. All of these exhibit essentially the same characteristics shown by the experimental points in Fig. 32 for $\psi = 13°$. In particular, as the frequency is increased, the ratio v_β/v_o at first remains near unity over a relatively wide range; then, a break occurs in which there is evidently the mixing of several waves; and, afterwards, the ratio v_β/v_o is observed to be less than unity and to increase towards unity.

Although the agreement between the values predicted from the theory and those measured experimentally is rather good, some possible limitations should be noted. The most obvious is that the experimental data is for $\psi = 13°$, whereas the theoretical curves in Fig. 32 are for $\psi = 10°$. Calculations have not been carried through in detail, but some careful estimates indicated that for $\psi = 13°$ the theoretical v_β/v_o curve from the $|h'_{t1}|$ wave agrees even more closely with the experimental points. The difference is small, being of the order of 4 percent for $1.2 > ka > 0.8$. The theoretical v_β/v_o curve from the $|h_{to}|$ wave is altered even less for $0.7 > ka > 0.4$. Although the theory applies to a narrow tape helix, whereas the experimental helix was a round wire one, this difference also seems to change the results an insignificant amount for $ka > 0.5$. A more serious objection to comparing the experimental and theoretical results is that the former were obtained from a helix of finite length, whereas the latter apply to a helix of infinite length. However, since the experimental data refer to the average phase velocity obtained from measurements over the third to sixth turn of a seven-turn helix, and since reference 25 noted that in this region the end effects were rather small, it would appear that comparisons are still valid. Although radiation from a finite length helix alters the phase distribution from that which exists on an infinite length helix, one would

expect that over the center portion of a helix of several turns radiation effects would be minor.

Reference 25 shows no $|h'_{t1}|$ wave for ka < 0.8, but reference 32 requires, in addition to an $|h_{to}|$ wave, an outward traveling wave of quite small amplitude and with the phase velocity ratios shown in Fig. 32 to obtain agreement with experimentally measured phase velocities for 0.8 > ka > 0.54. No $-|h''_{t1}|$ wave has been reported, and it is thought that this wave may normally be of sufficiently small amplitude for ka < 0.7 so as to avoid detection. Further, for ka < 0.5 the theoretical solutions for the $|h'_{t1}|$ and $|h''_{t2}|$ waves are quite dependent on the assumption of a helix of infinite length, and it is to be expected that these solutions would be altered for a finite length helix. One other possible shortcoming of the theory should be noted. References 25 and 32 note some evidence for a wave of the $|h''_{t2}|$ type, but traveling outward rather than inward and existing for 1.6 > ka > 1.3. The theory does not predict such a wave. No measurements have been reported for ka > 1.7 so no experimental confirmation of the existence of the $|h'_{t2}|$ free mode wave is possible.

Although the theoretical results do not appear to agree completely with all the observed results, the rather close correspondence between theory and experiment is rather satisfying and suggests that the approximations used are reasonably valid. It should be mentioned that when these results (essentially Fig. 29) were derived, it was thought that they were quite new and original. However, at the time this report was being written, the writer's attention was called to reference 51 in which very similar results were obtained through the integral equation approach. This approach, which leads to results equivalent to those obtained by the characteristic function method used in this section is discussed in the next section.

H. Other Roots; Generalization for Other Values of ψ

It is interesting to inquire whether other free modes besides those discussed in the previous section exist, or, in other words, are there any other values of h which satisfy Eq. 202 or Eq. 204? The following discussion shows the unlikelihood of any other roots for the approximate determinantal equation, although it certainly cannot be thought of as a rigorous proof. Consider the right side of Eq. 202 or Eq. 204 plotted as a surface, say f(ha, ka), versus the coordinates ka and ha with x and ψ constant, and h > k. The ka versus $h_t a$ curve then becomes the locus of the intersection of this surface, f(ha, ka), with the plane f(ha, ka) = 0. The first two terms in Eq. 202 merely form the sheath helix zeroth mode solution which is known to have only one locus or line of intersection with the f(ha, ka) = 0 plane (see sec. I-E-3 and Fig. 9), and for all but small values of ka this occurs for ha $\approx$ +ka csc ψ. The first series in Eq. 202 is an essentially positive quantity for x small, and it is clear that the entire term is zero only for ha = +ka csc ψ. In general, the major effect of this term is to make the locus approach the ha = +ka csc ψ line more closely for small values of ka. The last series in Eq. 202 is small everywhere except for ha = $|m|\cot\psi \pm$ ka, and, even here, it is significant only for

$|m| = 1$. In this latter case $R(\underline{\eta}_1)$ becomes logarithmically large so that the surface f(ha, ka) always crosses zero near both boundaries of the $|m| = 1$ forbidden region, at least for small ka. The higher order terms, $R(\underline{\eta}_m)$, may cause additional zero crossings of f(ha, ka) near $ha = |m| \cot \psi \pm ka$, but this would appear to happen, if at all, only for quite small values of $|m|$. The above remarks are the reasons for believing that no other real roots, besides those shown, exist for the approximate determinantal equation for the narrow tape helix. The question of complex or pure imaginary roots has already been considered in section II-D.

The preceding discussion concerning the existence of the roots suggests a simple method whereby the free mode solutions can be obtained without carrying out the lengthy calculative process described in reference 68. This method consists merely of drawing the lines $ka/\cot \psi = \sin \psi \; (|h|a/\cot \psi)$ in Fig. 26 in the allowed regions and then joining these lines smoothly with lines drawn along the boundaries of the $|m| = 1$ forbidden regions. Figure 28 illustrates the meaning of this procedure. The simple method will result in values of $|h|$ for the $|h_{to}|$ wave which are too large for ka small. These may be improved for ka not too small by averaging them with the values obtained in this region from the zeroth mode sheath solution alone. Figure 29 indicates why this procedure seems valid. Although the method described above misses the $|h''_{t2}|$ wave and undoubtedly predicts incorrect band limits for the free mode solutions between the higher order allowed regions for small ψ, its simplicity is appealing and its accuracy is probably sufficient for many purposes for all practical values of ψ. The effect of the tape width is not specifically considered in this simple construction although the averaging procedure mentioned above accounts for the influence of this parameter in an approximate manner. It is worthwhile noting that some experiments performed by Mr. L. Stark of these laboratories indicate that the simple procedure described above gives reasonably accurate predictions of the performance of the $|h_{to}|$ wave. The writer wishes to thank Mr. Stark for this information.

I. Power Flow; Relative Axial Electric Field; Power Loss

It is useful first to prove that the group velocity and total average real axial power flow for free mode waves in the tape helix case have the same algebraic sign as they do in the sheath helix case. The proof follows the steps given by Eqs. 99 through 107 since these formulas are quite general and apply to the tape helix case also. The boundary conditions for the tape helix at r = a require that $\underline{E}_t = 0$ on the tape and that $(\underline{H}_t^i - \underline{H}_t^e) = 0$ between the tape; and these conditions are invariant with frequency. Consequently, the line integral in Eq. 106 is zero, and Eq. 107 and the usual definition of group velocity follow directly. The group velocities of the space harmonics of a given wave are identical since they are all associated with the same wave. This is evident from

$$\frac{v_g}{v_o} = \frac{m v_g}{v_o} = \frac{d(ha + m \cot \psi)}{d(ka)} = \frac{d(ha)}{d(ka)}. \tag{209}$$

Figure 33 shows the group velocities of the various waves for the particular case of $\psi = 10°$ and $x = 0.1$ discussed in section II-G. These were obtained from an enlarged plot of the type shown in Fig. 28 using Eq. 209. Because of the approximations involved, the values of v_g/v_o at the points a, b, and c in Fig. 33 must be considered doubtful; in particular, point a may be at $v_g/v_o = 1$.

The average real axial power flow associated with the free modes of the tape helix can be calculated in the usual fashion using the field expressions 154 through 159 and 95. The power flow in the different waves can be calculated separately. The reasons for this are given in section I-F for the sheath helix case and are still valid here. Using Eqs. 173 and 174 with $\kappa_{\perp_m} = 0$ in the field expressions and then these latter in Eq. 95, one obtains (ref. 68) after considerable manipulation the following approximate expression for the power flow for the narrow tape case

$$P_z \approx \frac{\pi a^2 \sin^2\psi}{\omega\epsilon a} \sum_m K_m I_m \left[h_m a \left\{ \frac{q_m^2}{\eta_m^3} \left[\frac{1}{2}\left(\frac{I'_m}{I_m} + \frac{K'_m}{K_m} \right) + \frac{1}{\eta_m} \right] \right.\right.$$

$$\left.\left. + \frac{k^2 a^2 \cot^2\psi}{\eta_m} \left[-\frac{1}{\eta_m} \frac{K'_m I'_m}{K_m I_m} + \frac{1}{2}\left(1 + \frac{m^2}{\eta_m^2} \right)\left(\frac{I'_m}{I_m} + \frac{K'_m}{K_m} \right) \right] \right\} \right.$$

$$\left. + \frac{m q_m \left(h_m^2 a^2 + k^2 a^2 \right)}{\eta_m^4} \cot\psi \right] |\kappa_{\parallel_m}|^2 \qquad (210)$$

where q_m is given by

$$q_m = \eta_m^2 - m h_m a \cot\psi = \zeta^2 a^2 + mha \cot\psi. \qquad (211)$$

In Eq. 210 the argument of the modified Bessel functions is η_m, and the functional notation is omitted for convenience. Some examination shows that exclusive of the $|\kappa_{\parallel_m}|^2$ factor the higher order terms in Eq. 210 decrease only like $1/|m|$. Of course, with the $|\kappa_{\parallel_m}|^2$ factor the series converges but too slowly to be useful for computation. In order to improve the convergence, Eq. 210 can be transformed in the same manner as the approximate determinantal equation. The details are shown in reference 68 along with other data useful for calculating the value of Eq. 210.

For the particular case of $\psi = 10°$ and $x = 0.1$, with the constant current density constant z phase front approximation, the results obtained from Eq. 210 are shown in Fig 34. $(\mu/\epsilon)^{1/2}$ is the intrinsic impedance of the medium and is 120π ohms for free

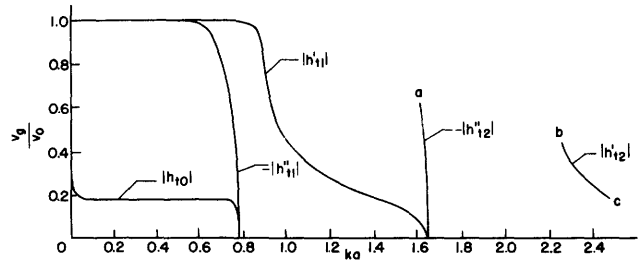

Fig. 33

The narrow tape helix z > 0; v_g/v_o vs ka, $\psi = 10°$, x = 0.1 (see text concerning a, b, c).

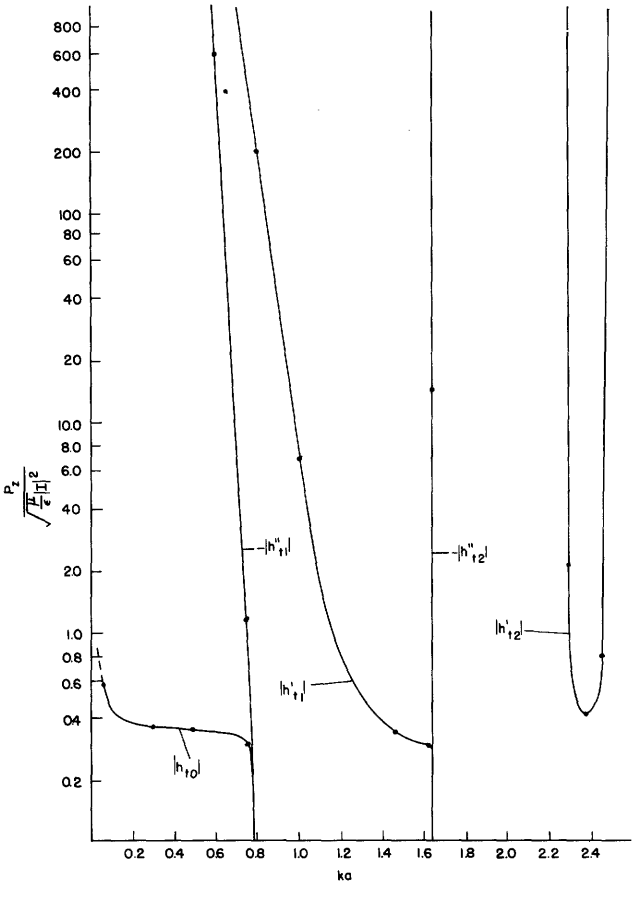

Fig. 34

The narrow tape helix z > 0; total average axial power flow vs ka, $\psi = 10°$, x = 0.1.

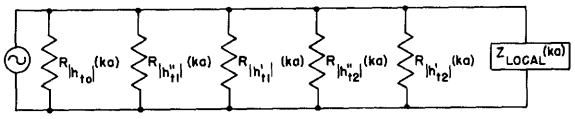

Fig. 35

Equivalent Circuit.

space. If the helix is excited by a finite source, for example, a voltage generator in series with the tape, the equivalent circuit may be drawn as in Fig. 35. $R_{|h_{to}|}(ka)$, $R_{|h''_{t1}|}(ka)$, etc. represent the impedances of the free mode waves which are essentially resistive and are functions of ka; and $Z_{local}(ka)$ represents the impedance resulting from the local radiation and induction fields near the source. The real average power orthogonality of the free mode waves is sufficient to show that the equivalent circuit can be drawn as in Fig. 35, although it can also be deduced in a more rigorous fashion from the results of the next section concerning the source-present helix problem. Although not described in section I, similar results apply to the sheath helix case, as can be realized from Eq. 124 and the discussion in section I-G. The impedances or admittances of the free mode waves result from the contributions of the poles of the integrand, whereas $Z_{local}(ka)$ or $Y_{local}(ka)$ results from the contribution of the branch cut integration. Reference 2, page 423, gives an excellent description of similar results obtained for the somewhat simpler case of the common open two wire transmission line. Although the actual values of $R_{|h_{to}|}(ka)$, $R_{|h''_{t1}|}(ka)$, etc. may be defined in several ways, and although the currents which flow through them will depend to a considerable extent on the actual configuration of the source, it seems clear that the ratio $P_z/|I|^2$ is at least a measure of the relative ease with which the different waves are excited by any finite source. It is therefore evident from Fig. 34 that the $|h''_{t1}|$ and $|h'_{t1}|$ waves are excited to much smaller amplitudes than the $|h_{to}|$ wave for the particular case of $\psi = 10°$ and $x = 0.1$ for $ka < 0.7$. It would appear that these same conclusions are applicable to other values of ψ and x. This explains the remarks made in section II-G concerning the amplitudes of the different waves. Figures 34 and 35 show that the points of zero group velocity correspond to zero values for $R_{|h_{to}|}(ka)$, $R_{|h''_{t1}|}(ka)$, etc. and explains, perhaps, the meaning of these resonance points. However, it can be expected that for a physical helix, that is, for one in which the wire has a finite conductivity, the characteristics of the power flow curves or the values of $R_{|h_{to}|}(ka)$, etc. will be modified at these points.

In traveling-wave tubes using helices, the magnitude of the axial electric field at the center of the helix is often of considerable interest (9). From the expressions for E_z^i and P_z for the sheath helix obtained from Eqs. 51 and 96 and the solutions for the zeroth sheath helix mode given in reference 10, $|E_z^i(r = 0)|^2/P_z$ for the sheath helix is readily calculated. This ratio can be determined more easily, perhaps, using curves available in reference 9. To within the approximations used here, for the narrow tape helix it is evident from Eq. 205 that

$$|E_z^i(r = 0)| \approx \frac{|I|}{p\omega\epsilon a} \zeta^2 a^2 \tan\psi \, K_o(\zeta a). \tag{212}$$

By substitution of the values of $|h_{to}|a$ in Eq. 212 and by use of the values of

$$\frac{P_z}{\sqrt{\frac{\mu}{\epsilon}}\,|I|^2}$$

given in Fig. 34, the ratio $|E_z^i(r = 0)|^2/P_z$ for the $|h_{to}|$ wave for the narrow tape helix for which $\psi = 10°$ and $x = 0.1$ can be obtained. Figure 36 shows the ratios of the magnitudes of the axial electric fields for $r = 0$ in the sheath and narrow tape helices, assuming the total average power flow, the mediums, and the pitch angle are the same for both cases. Note that the axial electric field at $r = 0$ given by the narrow tape helix approximation is somewhat smaller than that predicted by the sheath helix model over the range of ka where the axial phase velocity is relatively constant. Calculations have been carried out only for the $|h_{to}|$ wave. Reference 22 noted, as interpreted by this writer, that the measured axial electric field at $r = 0$ in a helix at $ka = 0.2$ was from 1.6 to 3.4 db less than predicted by the sheath model. The agreement with the value given in Fig. 36 by the narrow tape approximation is quite good. However, it is felt that this agreement is somewhat, although not entirely, coincidental since the helix on which the experiments were performed was a round wire helix whose pitch angle was 5° and whose diameter was 13 percent of the mean helix diameter and 50 percent of its pitch.

In concluding this section, an estimate of the power loss resulting from the finite conductivity of the conductor is given. It is assumed that the tape is sufficiently thick so that currents flowing on the inside and outside of the tape do not interact. In other words, the frequency and conductivity of both are taken to be sufficiently high so that the skin depth is much smaller than the tape thickness and the tape width (1). It is assumed further that the current divides equally between the inside and outside of the tape. This is essentially equivalent to neglecting the interaction of adjacent turns or to assuming that the current distribution is similar to what it would be on a straight, infinitely long tape. This assumption is certainly in error, but it should not be too serious if the tape width is small. It is also assumed that the transverse current is negligible and that only one wave has any significant amplitude at a particular frequency. Using the above assumptions and the constant current density approximation, one readily finds the power loss per unit axial length of the helix to be given by

$$P_L \approx \frac{|I|^2}{2\delta \sin 2\psi} \sqrt{\frac{\omega\mu_t}{2\sigma_t}} \tag{213}$$

where μ_t and σ_t are the conductivity and permeability, respectively, of the tape material. The inverse square root density approximation leads to the following approximate expression for the loss

$$P_L \approx \frac{1}{\pi^2} \ln\left|\frac{\delta \cos\psi}{\Delta}\right| \frac{|I|^2}{\delta \sin 2\psi} \sqrt{\frac{\omega\mu_t}{2\sigma_t}}. \tag{214}$$

In this, Δ is the tape thickness, and it is assumed that the power loss only up to within a distance Δ of the edges need be considered. This is admittedly quite crude, but such an assumption is necessary to avoid obtaining an infinite power loss and can be partly justified by considering an elliptical rather than a flat tape conductor. For $\cos\psi \approx 1$ and for $1000 > (\delta/\Delta) > 10$, Eqs. 213 and 214 differ only by a factor near 2, so that Eq. 213 is probably adequate for the present purposes. For a circular wire helix with the above assumptions one obtains

$$P_L \approx \frac{|I|^2}{4\pi b \sin\psi} \sqrt{\frac{\omega\mu_t}{2\sigma_t}} \tag{215}$$

where b is the radius of the wire.

If the loss is small, an axial attentuation constant can be defined in the usual way (1, 2) as

$$\text{Attenuation Constant} = \frac{1}{2} \frac{P_L}{P_z}. \tag{216}$$

Calling C the value of

$$\frac{P_z}{\sqrt{\frac{\mu}{\epsilon}}\,|I|^2}$$

obtained from Fig. 34 or a similar plot for other pitch angles, using Eq. 213 in Eq. 216, and taking $\mu = \mu_t$, one obtains after some manipulation

$$\text{Attenuation Constant} \approx \frac{1}{Cx} \frac{1}{(4a \sin\psi)^2} \sqrt{\frac{ka}{2\sigma_t \sqrt{\frac{\mu}{\epsilon}}}}\, a \tag{217}$$

in nepers per unit length. x is the parameter defined by Eq. 193. As an example, for

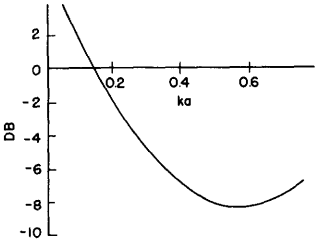

Fig. 36

$20 \log_{10} \left\{\left[|E_z^i(r = 0)|\ |h_{to}|, \text{ tape}\right] / \left[|E_z^i(r = 0)|\ |h_o|, \text{ sheath}\right]\right\}$ vs ka;
$\psi = 10°$ for both, $x = 0.1$ for tape helix, P_z identical for both.

free space where $(\mu/\epsilon)^{1/2} = 120\pi$ ohms, for $x = 0.1$, $ka = 0.2$, $C = 0.376$, $\psi = 10°$, $\sigma_t = 5.6 \times 10^7$ mhos/meter for copper, and $a = 0.035$ meters, Eq. 217 gives an attenuation constant of 0.0182 nepers/meter. No check with experimental data has been made. In the above the common assumption has been made that the loss is small so that the propagation characteristics are affected only slightly (1,2). Reference 52 has pointed out that at extremely low frequencies the loss will considerably alter the characteristics from those found for the lossless case.

The Narrow Gap Approximation

J. Boundary Conditions; Derivation and Solution of Approximate Determinantal Equation

An approximate treatment of the tape helix when the tape is narrow has been given. It is possible to use similar methods to determine the propagation and other characteristics of the helix when the tape is quite wide, or when the gap width, δ', shown in Fig. 25, is assumed to be small compared with a, p, and λ. In this case it is obviously no longer possible to assume that $K_\perp$ is zero. However, since $\delta' \ll \lambda$, the distribution of the electric field in the gap is essentially quasi-static, and some reasonable assumptions concerning this should lead to field expressions which are nearly correct.

Since $E_{||}$ must be zero at the tape edges, it seems clear from physical considerations that it must be quite small everywhere in the gap. Therefore, a fair approximation should result if $E_{||}$ is taken to be zero in the gap. However, since $E_{||}$ must also be zero on the tape if it is a perfect conductor, the assumption that $E_{||} = 0$ in the gap means that $E_{||} = 0$ everywhere for $r = a$. Because the tape is assumed to be of infinitesimal thickness, $E_\perp$ in the gap must become infinitely large in an inverse square root manner as the tape edges are approached, and a distribution which acts in this manner alone should be a good approximation. However, it might be assumed instead that $E_\perp$ in the gap is constant in magnitude, and this leads to results which are quite similar to those obtained from the more realistic inverse square root distribution. If an approximate tangential electric field distribution in the gap is assumed, the requirement that the tangential magnetic field be continuous at all points through the gap can no longer be satisfied. The property which characterizes the narrow gap helix is that no current cross the gap from turn to turn; for this $K_\perp$ (gap) = 0, or $H_{||}$ must be continuous through the gap. Although this boundary condition might be approximately satisfied in several ways, the simplest expression results if this condition is imposed only along a line in the center of the gap. The similarity between the assumptions concerning $E_{||}$, $K_\perp$, and $E_\perp$ in the gap for the narrow gap case, and those concerning $K_\perp$, $E_{||}$, and $K_{||}$, respectively, on the tape for the narrow tape case should be noted.

It is clear that $E_\perp$ at $r = a$ can be expressed in the form

$$E_{\perp}(r = a) = e^{-jhz} \sum_{m} \epsilon_{\perp_m} e^{-jm\left(\frac{2\pi}{p} z - \theta\right)} \tag{218}$$

where the $\epsilon_{\perp_m}$ are the Fourier coefficients of the perpendicular electric field expansion. If $E_{\perp}$ in the gap is assumed to be constant in magnitude, then

$$E_{\perp}(r = a) = e^{-jhz} \sum_{m} \epsilon_{\perp_m} e^{-jm\left(\frac{2\pi}{p} z - \theta\right)} \approx \begin{cases} Ae^{-jhz} e^{j(h-\beta_{11})\left[z - \frac{p}{2\pi}\theta - (p-\delta')\right]} \\ \text{for } \frac{p}{2\pi}\theta + p > z > \frac{p}{2\pi}\theta + p - \delta' \\ 0, \text{ elsewhere.} \end{cases} \tag{219}$$

β_{11} has exactly the same meaning here as in Eq. 178 with which Eq. 219 should be compared, and the point $z = 0$, $\theta = 0$ is again chosen as point (1) in Fig. 25b. If $E_{\perp}$ in the gap is assumed to vary in an inverse square root manner, then

$$E_{\perp}(r = a) = e^{-jhz} \sum_{m} \epsilon_{\perp_m} e^{-jm\left(\frac{2\pi}{p} z - \theta\right)} \approx \begin{cases} Ae^{-jhz} e^{j(h-\beta_{11})\left[z - \frac{p}{2\pi}\theta - (p-\delta')\right]} \times \\ \dfrac{\delta'}{\left\{\left[z - \frac{p}{2\pi}\theta - (p-\delta')\right]\left[\delta' - z + \frac{p}{2\pi}\theta + (p-\delta')\right]\right\}^{1/2}} \\ \text{for } \frac{p}{2\pi}\theta + p > z > \frac{p}{2\pi}\theta + p - \delta' \\ 0, \text{ elsewhere.} \end{cases} \tag{220}$$

Eq. 220 should be compared with Eq. 183. A in Eq. 219 has a different value than A in Eq. 220. These can be related to the amplitude of the voltage across the gap in each case by

$$|V| = \left| \int_{\text{gap}} E_{\perp}(r = a)\, dl \right|. \tag{221}$$

Equation 221 is similar to Eq. 179. Proceeding exactly as in section II-E, assuming the constant phase front of the electric field is perpendicular to the gap edges, although this makes very little difference if δ' is small, one finds that

$${}_1\epsilon_{\perp_m} = \frac{|V|}{p \cos\psi} e^{-jm \frac{2\pi}{p} \delta'} e^{j\left(h - \beta_{11} + m \frac{2\pi}{p}\right) \frac{\delta'}{2}} {}_1D'_m \tag{222}$$

for the constant magnitude gap field, and

$${}_2\epsilon_{\perp_m} = \frac{|V|}{p \cos\psi} e^{-jm \frac{2\pi}{p} \delta'} e^{j\left(h - \beta_{11} + m \frac{2\pi}{p}\right) \frac{\delta'}{2}} {}_2D'_m \tag{223}$$

for the inverse square root gap field. Equations 222 and 223 should be compared with Eqs. 181 and 185. ${}_1D'_m$ and ${}_2D'_m$ are identical to ${}_1D_m$ and ${}_2D_m$ except that δ in the latter is replaced by δ'. The subscripts 1 and 2 have the same significance as in section II-E.

Since E_{11} is taken to be zero everywhere for r = a, after some reduction Eq. 177 gives, because of the orthogonality of the space harmonics,

$$\kappa_{11_m} \approx -\nu_m \kappa_{\perp_m} \tag{224a}$$

where

$$\nu_m = \frac{\left[(\eta_m^2 + mh_m a \tan\psi)(\eta_m^2 - mh_m a \cot\psi) - k^2 a^2 \eta_m^2 \frac{I'_m(\eta_m) K'_m(\eta_m)}{I_m(\eta_m) K_m(\eta_m)}\right]}{\left[(\eta_m^2 - mh_m a \cot\psi)^2 + k^2 a^2 \eta_m^2 \cot^2\psi \frac{I'_m(\eta_m) K'_m(\eta_m)}{I_m(\eta_m) K_m(\eta_m)}\right]} \cot\psi. \tag{224b}$$

Using Eqs. 155, 156, 173, 174, and 176, one can readily show that

$$E_{\perp}(r = a) = j \frac{e^{-jhz}}{\omega \epsilon a} \sin\psi \cos\psi \sum_m (a_m \kappa_{11_m} + b_m \kappa_{\perp_m}) e^{-jm\left(\frac{2\pi}{p} z - \theta\right)} \tag{225}$$

where

$$a_m = \left[(\eta_m^2 - mh_m a \cot\psi)(\eta_m^2 + mh_m a \tan\psi) \frac{I_m(\eta_m)K_m(\eta_m)}{\eta_m^2} \right.$$

$$\left. - k^2a^2 I'_m(\eta_m)K'_m(\eta_m) \right] \tag{226}$$

$$b_m = \left[(\eta_m^2 + mh_m a \tan\psi)^2 \frac{I_m(\eta_m)K_m(\eta_m)}{\eta_m^2} + k^2a^2\tan^2\psi\, I'_m(\eta_m)K'_m(\eta_m) \right] \cot\psi. \tag{227}$$

Substitution of Eq. 224a in Eq. 225 gives

$$E_\perp(r = a) \approx j \frac{e^{-jhz}}{\omega\epsilon a} \sin\psi \cos\psi \sum_m (b_m - a_m \nu_m)\kappa_{\perp m} e^{-jm\left(\frac{2\pi}{p} z - \theta\right)}. \tag{228}$$

But $E_\perp(r = a)$ is also expressed by Eq. 218 so that from the values of $\epsilon_{\perp m}$ given by Eq. 222 or Eq. 223 the following approximation for $\kappa_{\perp m}$ results

$$_{1,2}\kappa_{\perp m} = -j \frac{\omega\epsilon a |V|}{p \sin\psi \cos^2\psi} e^{j(h-\beta_{11})\frac{\delta'}{2}} \frac{e^{-jm\frac{\pi\delta'}{p}}}{b_m - a_m\nu_m} {}_{1,2}D'_m. \tag{229}$$

From Eqs. 224b, 226, and 227 one finds after considerable manipulation that

$$\frac{1}{b_m - a_m\nu_m} = \frac{\cos\psi \sin^3\psi}{k^2a^2\eta_m^2 I'_m(\eta_m)K'_m(\eta_m)I_m(\eta_m)K_m(\eta_m)} \left[\left(h^2a^2 - k^2a^2 \right.\right.$$

$$\left.\left. + k^2a^2 \frac{m^2\cot^2\psi}{\eta_m^2} \right) I_m(\eta_m)K_m(\eta_m) + k^2a^2\cot^2\psi\, I'_m(\eta_m)K'_m(\eta_m) \right]. \tag{230}$$

Since

$$K_\perp = e^{-jhz} \sum_m \kappa_{\perp m} e^{-jm\left(\frac{2\pi}{p} z - \theta\right)} \tag{170}$$

if one uses Eq. 229 in Eq. 170 and requires that $K_\perp = 0$ at the center of the gap, or where $z = (p/2\pi)\,\theta + p - \delta'/2$, the following approximate determinantal equation for the narrow gap case is obtained

$$K_{\perp}\left(z = \frac{p}{2\pi}\theta + p - \frac{\delta'}{2}\right) = 0 \approx -j\frac{\omega\epsilon a|V|}{p\sin\psi\cos^2\psi} e^{j\left(h\delta' - \beta_{11}\frac{\delta'}{2} - \frac{hp}{2\pi}\theta - hp\right)} \sum_m \frac{{}_{1,2}D'_m}{b_m - a_m\nu_m}. \tag{231}$$

The right side of Eq. 231 consists of a complex factor whose magnitude is independent of h times a real series; and if Eq. 231 is to be satisfied, the series must be zero. Substituting Eq. 230 in Eq. 231, multiplying by 1/4 for convenience, and dropping all other multiplying factors which do not affect the solution, one obtains

$$0 \approx \sum_m \frac{1}{-4\eta_m^2 I'_m(\eta_m)K'_m(\eta_m)I_m(\eta_m)K_m(\eta_m)} \left[\left(h^2a^2 - k^2a^2 + k^2a^2\frac{m^2\cot^2\psi}{\eta_m^2}\right) I_m(\eta_m)K_m(\eta_m) + k^2a^2\cot^2\psi\, I'_m(\eta_m)K'_m(\eta_m)\right] {}_{1,2}D'_m. \tag{232}$$

Except for $-4\eta_m^2 I'_m(\eta_m)K'_m(\eta_m)I_m(\eta_m)K_m(\eta_m)$, Eq. 232 is identical to the approximate determinantal equation for the narrow tape helix given in Eq. 191 if the gap width, δ', in the former is equal to the tape width, δ, in the latter. But further, the factor $-4\eta_m^2 I'_m(\eta_m)K'_m(\eta_m)I_m(\eta_m)K_m(\eta_m)$ is exceedingly close to unity for $\eta_m \geq 0$ and $|m| \geq 1$, and it can be put equal to unity in Eq. 232 for $|m| \geq 1$ with negligible error (68). Only the m = 0 term is appreciably altered by this factor, and even this occurs only for η_o and, therefore, ka small. The discussion in section II-F concerning the numerical solution of Eq. 191 is directly applicable to Eq. 232 also.

If the constant field constant z phase front distribution is assumed so that

$${}_1D'_m = \frac{\sin mx'}{mx'} \tag{233}$$

where x' is given by

$$x' = \frac{\pi\delta'}{p} \tag{234}$$

(see Eqs. 192 and 193), the numerical results available from the narrow tape helix calculations can be used with only minor modifications. The effects of using ${}_2D'_m$ and some other assumption concerning the gap field phase front are considered in section II-L and are shown to be small. The $ka/|h_t|a$ ratios which result for the narrow gap helix for $\psi = 10°$ and $x' = 0.1$ are shown in Fig. 29. Note that only for the $|h_{to}|$ wave for $ka < 0.3$ are the results for the narrow gap and narrow tape case distinguishable. It is evident from the previous discussion, Eq. 232, and from Eq. 202 or Eq. 204 that as δ' becomes smaller, the $ka/|h_{to}|a$ solution for the narrow gap case for ka small approaches the asymptotic value $\sin\psi$ more closely. This also occurs for the narrow tape case as δ is made smaller. It appears, therefore, that as the tape width is

increased from a very small value to a very large one, the $ka/|h_{to}|a$ ratio for small ka increases, approaches a maximum, and then decreases. The decrease occurs at a slower rate than the increase for a proportionate change in tape width because of the $-4\eta_o^2 I_o'(\eta_o)K_o'(\eta_o)I_o(\eta_o)K_o(\eta_o)$ factor which divides the m = 0 term in the wide tape determinantal equation. It also seems quite possible that the maximum $ka/|h_{to}|a$ ratio for small ka differs only slightly from the zeroth mode sheath helix solution and may occur in the region where $\delta \approx \delta' \approx p/2$. This action of the $|h_{to}|$ wave solution may explain why the experimentally measured values of $ka/|h_{to}|a$ for small ka agree so well with the zeroth mode sheath solution since the helices on which experiments were performed were wound of round wire whose diameter was about 50 percent of the pitch (22, 23). The radial extension of the wire in the helices used for the measurements may also have been an influencing factor. This factor is obviously not accounted for in the tape helix theory.

Since the $ka/|h_t|a$ solutions for both the narrow tape and narrow gap helices are essentially identical except for the $|h_{to}|$ wave for small ka, the various phase and group velocities are also very nearly alike. Consequently, the curves of Figs. 28, 30, 32, and 33 are quite indicative of the results obtained for $\psi = 10°$ and $x' = 0.1$, and specific curves for the narrow gap case are not shown. Many of the remarks in sections II-G and II-H concerning the narrow tape helix apply to the narrow gap helix as well. It can be expected that the relative amplitudes of the space harmonics for the two cases will be somewhat altered although the general characteristics are certainly maintained. This is evident from the fact that the dominant harmonic is determined primarily by the values of η_m, and these will be nearly the same in both cases. Incidentally, it is clear from Eqs. 175, 176, 218, 222, and 223 that

$$E_z^e \approx \frac{|V|}{p} e^{j(h-\beta_{11})\frac{\delta'}{2}} e^{-jhz} \sum_m e^{-jm\frac{\pi}{p}\delta'} {}_{1,2}D_m' \frac{K_m\left(\eta_m \frac{r}{a}\right)}{K_m(\eta_m)} e^{-jm\left(\frac{2\pi}{p}z-\theta\right)}. \quad (235)$$

E_z^i is given by an identical expression except that I_m replaces K_m. Calculations for numerical values of $E_z^{i,e}$ for the narrow gap case have not been performed.

K. Power Flow; Tape Current; Power Loss

It is possible to derive an approximate expression for the real average axial power flow for the narrow gap helix in a manner quite analogous to that used in section II-I for the narrow tape helix. Here, however, since both components of surface current density occur, the procedure is somewhat more involved. The details are shown in reference 68. The approximate expression for the power flow in the narrow gap helix case is

$$P_z \approx \pi a^2 \frac{\omega\epsilon a}{k^4 a^4} \sin^2\psi \tan^2\psi \sum_m \frac{q_m^2}{\eta_m^4} \frac{I_m K_m}{I_m'^2 K_m'^2} \left[h_m a \left\{ \frac{q_m'^2}{\eta_m^3} \left[\frac{1}{2} \left(\frac{I_m'}{I_m} + \frac{K_m'}{K_m} \right) + \frac{1}{\eta_m} \right] \right.\right.$$

$$\left.\left. + \frac{k^2 a^2 \cot^2\psi}{\eta_m} \left[-\frac{1}{\eta_m} \frac{K_m' I_m'}{K_m I_m} + \frac{1}{2} \left(1 + \frac{m^2}{\eta_m^2} \right) \left(\frac{I_m'}{I_m} + \frac{K_m'}{K_m} \right) \right] \right\} \right.$$

$$\left. + m(h_m^2 a^2 + k^2 a^2) \cot\psi \frac{q_m'}{\eta_m^4} \right] |\epsilon_{\perp m}|^2. \qquad (236)$$

The argument of the modified Bessel functions is η_m and the functional notation is omitted for convenience as usual. In Eq. 236 q_m' is given by

$$q_m' = -k^2 a^2 \cot^2\psi \frac{\eta_m^2}{q_m} \frac{I_m' K_m'}{I_m K_m} \qquad (237)$$

and q_m is given as before by Eq. 211.

It should be noted that Eq. 236 has a form which is very similar to Eq. 210, the approximate power flow equation for the narrow tape case. No numerical calculations have been carried through using Eq. 236, but the same procedure used to obtain results from Eq. 210 can obviously be used for such calculations. If one of the approximate forms for $\epsilon_{\perp m}$, Eq. 222 or Eq. 223, is substituted in Eq. 236, it can be expressed in the form

$$P_z = \sqrt{\frac{\epsilon}{\mu}} |V|^2 D.$$

In this, D is a nondimensional number depending on the value of the series. Since the equivalent circuit for the narrow tape helix shown in Fig. 35 applies to the narrow gap case also, D as a function of ka will have its poles and zeros interchanged with those of the function

$$\frac{P_z}{\sqrt{\frac{\mu}{\epsilon}} |I|^2}$$

shown in Fig. 34.

In the narrow tape case the current $|I|$, defined by Eq. 179, is the amplitude controlling factor. In the narrow gap case the voltage $|V|$, defined by Eq. 221, performs this role. It may prove useful to relate these in at least an approximate fashion so that the two cases can be compared. The following calculation uses Eq. 179 to obtain $|I|$ assuming $|V|$ is known, although a quite analogous calculation using Eq. 221 could be

used to go in the other direction. Relating $\kappa_{\perp_m}$ and $\epsilon_{\perp_m}$ through Eqs. 218 and 228, using this expression for $\kappa_{\perp_m}$ with Eqs. 224 and 230 in Eq. 169, and, finally, inserting this expression for $K_{\parallel}$ in Eq. 179, one obtains

$$|I| \approx \frac{\omega \epsilon a \sin\psi \cos\psi}{k^2 a^2} \left| \int_0^{(p-\delta')\cos^2\psi} \sum_m P_m \epsilon_{\perp_m} e^{-j\left(h_m z + \frac{p}{2\pi a^2} z\right)} \sec\psi \, dz \right|. \quad (238)$$

The fact that the integration proceeds along a line perpendicular to the tape edges has been used in Eq. 238. Also, P_m is given by

$$P_m = \frac{1}{\eta_m^2} \frac{1}{I'_m K'_m} \left[mha(\cot\psi + \tan\psi) + \zeta^2 a^2 - k^2 a^2 \left(\frac{m^2}{\eta_m^2} + \frac{I'_m K'_m}{I_m K_m} \right) \right]. \quad (239)$$

Using Eq. 222 or Eq. 223 in Eq. 238, performing the integration, using trigonometric identities involving the sum and differences of angles, and dropping unimportant phase factors give after some manipulation

$$_{1,2}|I| = \frac{\omega \epsilon a |V|}{2\pi k^2 a^2 \cot\psi} \left| \sum_m P_{m\ 1,2} D'_m \frac{(\cos my' + \cos mx')\sin z' + (\sin my' - \sin mx')\cos z'}{m + \tau} \right.$$

$$\left. - j \sum_m P_{m\ 1,2} D'_m \frac{(\sin my' + \sin mx')\sin z' + (\cos mx' - \cos my')\cos z'}{m + \tau} \right|. \quad (240)$$

In Eq. 240 x' is given by Eq. 234, and y', and z', and τ by

$$y' = 2\pi \left(1 - \frac{x'}{\pi}\right) \cos^2\psi + x' \quad (241)$$

$$z' = \pi \left(1 - \frac{x'}{\pi}\right) \tau \cos^2\psi \quad (242)$$

$$\tau = \tan^2\psi \, (1 + ha \cot\psi). \quad (243)$$

The convergence of Eq. 240 can be improved by the usual procedure of adding and subtracting asymptotic forms. This has been done only for the constant field,constant z phase front distribution. The details are shown in reference 68 and are not repeated here. No numerical results are available.

The use of assumptions very similar to those discussed at the end of section II-I makes possible the calculation of the loss resulting from the finite conductivity of the tape in the narrow gap case. The power loss per unit axial length of the helix is given by

$$P_L = \frac{1}{2p}\sqrt{\frac{\omega\mu_t}{2\sigma_t}}\left[\int_{\substack{\text{one turn}\\ \text{of tape}}} (|H_\theta^i|^2 + |H_z^i|^2 + |H_\theta^e|^2 + |H_z^e|^2)dA\right]. \tag{244}$$

Using the approximations for $\kappa_{\parallel_m}$ and $\kappa_{\perp_m}$ given in section II-J, solving for $\kappa_{\theta m}$ and κ_{zm}, inserting these in the appropriate field expressions from Eqs. 154 through 159, and then these in Eq. 244, one might obtain an explicit expression for P_L. This is clearly a very tedious task, and it was not thought worthwhile carrying through the calculation for this report. If the inverse square root gap voltage distribution is assumed, the series expressing P_L may not converge. If such is the case, it may be necessary to use the artifice suggested in section II-I following Eq. 214 or to consider the results obtainable from the constant gap voltage distribution as adequate.

Although numerical results are not available for the quantities considered here, with the exception of P_L it should be relatively easy to obtain such results from the formulas which are available (68). These have been mentioned here for purposes of comparison with the narrow tape case and for reference in case of future interest.

Further Consideration of Approximations

L. Effects of the Amplitude and Phase Approximations

To derive an approximate determinantal equation for the narrow tape case, it was necessary to make an assumption concerning the current density distribution on the tape. Similarly, for the narrow gap case the distribution of the electric field in the gap was assumed. Both constant amplitude and inverse square root approximations were considered although numerical results for only the former have been presented so far. Also, some simplifications concerning the phase of the current density on the tape or the electric field in the gap were made. Here these matters are discussed further.

Before doing this some remarks about the inverse square root distribution are of interest. It would be expected that such a distribution would be a very good approximation for particular components very near the edges of the tape since in any small region the wave equation is closely approximated by Laplace's equation (36, 38). This expectation is confirmed from general considerations of the behavior of an electromagnetic field in the neighborhood of a sharp edge (53). Such considerations show that, in general

$$\left.\begin{aligned} E_{\parallel} &= 0(R^{1/2}) \qquad (245a)\\ H_{\parallel} &= 0(1) \qquad (245b)\\ K_{\perp} &= 0(1) \qquad (245c) \end{aligned}\right\} \text{ for } R \to 0$$

where R is the distance from the edge, and 0 is the usual order symbol. All other field components become singular like $R^{-1/2}$ as R approaches zero, or

$$\left.\begin{aligned} E_{\perp} &= 0(R^{-1/2}) \qquad (246a)\\ H_{\perp} &= 0(R^{-1/2}) \qquad (246b)\\ K_{\parallel} &= 0(R^{-1/2}) \qquad (246c) \end{aligned}\right\} \text{for } R \to 0.$$

For an electromagnetic wave normally incident on a surface with an edge of infinitesimal thickness, it can be shown that an even greater restriction than Eq. 245c applies, namely

$$K_{\perp} = 0(R^{1/2}) \qquad (247)$$

and it seems likely that Eq. 247 applies to waves of arbitrary incidence as well (53).

From using the inverse square root and constant z phase front approximation so that

$$_2D_m(\beta_{\parallel} = h) = J_o(mx) \qquad (248)$$

(compare with Eq. 192), an equation exactly like Eq. 203 results except that $J_o(mx)$ replaces (sin mx)/mx everywhere. It should be recalled that $J_o(0) = 1$ and $J_o(-mx) = J_o(mx)$. The third term in this equation is

$$\sum_{m=1}^{\infty} \frac{J_o(mx)}{m} \text{ instead of } \frac{1}{x} \sum_{m=1}^{\infty} \frac{\sin mx}{m^2}$$

aside from the multiplier independent of x. The dominant term in this Schlömilch series is $\ln(2/x)$, and for $x = 0.1$ this term alone represents the series to better than 0.01 percent (68). For the constant density assumption the equivalent term which represents

$$\frac{1}{x} \sum_{m=1}^{\infty} \frac{\sin mx}{m^2}$$

is $\ln(e/x)$. Since $x = \pi\delta/p$, it is evident that the only change in the local field term in the approximate determinantal equation resulting from the different assumed distributions is a change in the effective width of the tape. For example, $x = 0.10$ for the constant amplitude distribution is equivalent to $x = 0.0735$ for the inverse square root distribution.

Since the fourth term in Eq. 203 represents the contribution to $E_{\parallel}$ from adjacent turns, it would be expected from physical considerations that the assumed current distribution would have only a minor influence on this term. Although a reduction in effective tape width in a similar ratio to that noted above appears desirable, because of the rapid convergence of the term in the brackets in the fourth term in Eq. 203, the effect of this change is generally negligible (68). Since $J_o(mx)$ almost equals (sin mx)/mx for small m and x, the $R(\eta_m)$ terms are not altered to any appreciable degree by either

choice of current density distribution. Thus, the only difference in the solutions for the approximate determinantal equation caused by the different amplitude but constant z phase front approximations is a slight change in the tape width to which such solutions apply in the ratio 2/e.

If Eq. 248 is used in place of Eq. 192 to calculate the power flow from Eq. 210, it can be shown (68) that the only significant difference caused by the different amplitude but constant z phase front approximations is a change in the effective tape width in the ratio 2/2.241. This ratio is slightly different from that required for similarity in the determinantal equation, although for small x the numerical effect is quite small.

In order to simplify the sums encountered in the approximate determinantal and power flow equations, it has been assumed, so far, that $\beta_{11} = h$, or that the constant phase front of the current density on the narrow tape is in a plane of constant z. Although this should be quite satisfactory for a narrow tape, a better approximation, and one which could possibly be applied to relatively wide tapes, is one in which the constant phase front is perpendicular to the tape edges. From Eq. 178 or Eq. 183 and Fig. 25b it can be shown that this requires that

$$\frac{hp}{2\pi}\theta_1 - \beta_{11}z_1 + \beta_{11}\frac{p}{2\pi}\theta_1 = \frac{hp}{2\pi}\theta_2 - \beta_{11}z_2 + \beta_{11}\frac{p}{2\pi}\theta_2 \tag{249}$$

where

$$z_2 - z_1 = \delta\cos^2\psi \tag{250}$$

$$a(\theta_1 - \theta_2) = \delta\sin\psi\cos\psi. \tag{251}$$

Using Eqs. 250 and 251 in Eq. 249 results in

$$\beta_{11} = h\sin^2\psi. \tag{252}$$

If Eq. 252 is used instead of $\beta_{11} = h$, by the same procedure whereby Eq. 204 is derived from Eq. 191, a quite similar approximate determinantal equation for the narrow tape helix with the constant amplitude assumption can be derived (68). This equation and the one which results if the inverse square root distribution is used with Eq. 252 have been investigated (68). It has been found that the roots of these determinantal equations are insignificantly different from those of Eq. 204. The effect of using Eq. 252 rather than $\beta_{11} = h$ on the power flow has not been considered in detail. However, it is clear that for small x, at least, the effect is negligibly small.

Although the influence of the amplitude and phase distribution on only the narrow tape solution is considered in the previous discussion, it should be obvious, in view of the results of section II-J, that the conclusions apply to the narrow gap case as well. The fact that different amplitude and phase distributions alter the free mode solutions for the tape helix only slightly is a reminder that the powerful variational techniques for solving electromagnetic wave boundary value problems might prove useful here (50). Although such methods have been used in a variety of problems, none appear to be of

the type where both TE and TM waves are required on an open transmission system. The possibility of applying variational procedures to obtain solutions for such systems seems worthy of future investigation.

Related Problems

M. Multiwire Helices

The methods used in the previous sections can be applied to the problem of a helix wound with several wires or tapes. Although it is possible to derive an exact formal expression for the determinantal equation in this case as mentioned in section II-C for the single tape helix, this expression is of little practical use. Consequently, the assumptions discussed in section II-E are used. The constant amplitude constant z phase front current density approximation for narrow tapes is used in the analysis given in this section, although it should be clear that any of the other approximations, including the narrow gap one, lead to practically identical results.

The developed view of a four-wire helix as an example of a multiwire helix is shown in Fig. 37. One of the wires has been darkened as an aid in following the windings, but this has no other significance. Figure 37 is to be compared with Fig. 25b. In a multiwire helix each wire forms a helix of pitch p, pitch angle ψ, and there are N wires uniformly spaced in the pitch distance. δ and δ' are taken, as before, to be the tape width and gap width, respectively, in the axial or z direction. It is to be expected from the results of the sheath helix theory and from the general theory of multiwire transmission systems that several different types of free modes occur on a multiwire helix. These are distinguished by the relative phase of the currents flowing in the different wires at any given cross section of constant z, and one may anticipate that the propagation constants for the different modes are dissimilar functions of frequency. As before, the tapes are assumed to be perfect conductors, and the medium for $r > a$ is taken to be the same as that for $r < a$ and lossless.

1. The Zeroth Mode

If the currents in all the tapes are in phase at a cross section of constant z and all have the same amplitude, the system can be rotated through an angle of any multiple of $2\pi/N$ with no change in the fields. Further, if the system is shifted axially a distance p/N, the new fields can differ from the previous ones by only a constant factor. Proceeding exactly as in section II-B, one can readily show that the electric Hertzian potential must be of the form

$$\Pi_z^{i,e} = e^{-jhz} \sum_m A_{mN}^{i,e} \frac{I_{mN}}{K_{mN}} \left(\eta_{mN} \frac{r}{a}\right) e^{-jmN\left(\frac{2\pi}{p} z - \theta\right)} \tag{253}$$

with an identical form for the magnetic Hertzian potential. The summation index m runs, as before, by integer values... -2, -1, 0, 1, 2,.... Some consideration shows

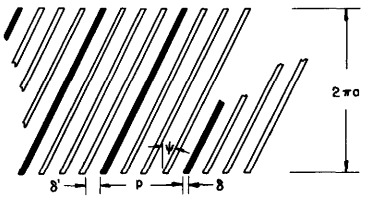

Fig. 37
Multiwire helix; $\cot \psi = 2\pi a/p$.

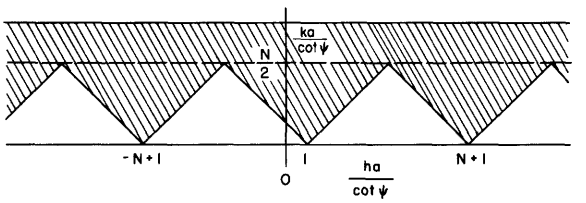

Fig. 38
Chart of forbidden regions
for multiwire helix for zeroth mode.

that the exact field expressions in this case are those given by Eqs. 154 through 159 if there m is replaced by mN. The significance of the above may, perhaps, be further realized from the expansion for the approximate current distribution. Since each of the windings is a uniform helix, Eq. 169 applies, and with the assumptions taken here

$$e^{-jhz}\sum_m \kappa_{\parallel_m} e^{-jm\left(\frac{2\pi}{p}z-\theta\right)} \approx \frac{|I|}{\delta \cos\psi} e^{-jhz}$$

$$\text{for} \begin{cases} \frac{2\pi}{p}z + 2x > \theta > \frac{2\pi}{p}z \\ \vdots \\ \frac{2\pi}{p}z + n\frac{2\pi}{N} + 2x > \theta > \frac{2\pi}{p}z + n\frac{2\pi}{N} \\ \vdots \\ \frac{2\pi}{p}z + (N-1)\frac{2\pi}{N} + 2x > \theta > \frac{2\pi}{p}z + (N-1)\frac{2\pi}{N} \end{cases}$$

$$0, \text{ elsewhere} \qquad (254)$$

where $x = \pi\delta/p$, as before. Proceeding in the usual way, one obtains

$$_1\kappa_{\parallel_m} = \frac{|I|}{p\cos\psi} e^{-jmx}\frac{\sin mx}{mx} N, \quad m = \ldots -2N, -N, 0, N, 2N, \ldots \qquad (255a)$$

or

$$_1\kappa_{\parallel_m} = \frac{|I|}{p\cos\psi} e^{-jmNx}\frac{\sin mNx}{mx}, \quad m = \ldots -2, -1, 0, 1, 2, \ldots . \qquad (255b)$$

The subscript 1 has the same meaning as in Eqs. 181 and 192 with which Eq. 255 should be compared. The difference in the sign of the exponential is the result of a different choice for the coordinate origin. $|I|$ is the amplitude of the total current flowing in the direction of the tape on each one. From Eq. 255 it is again evident, as already deduced from considerations of symmetry, that the summations in the field and current density representations proceed in steps of N, or in successive integer steps of m if m is replaced by mN.

Since only the mNth harmonics appear in the field representations with m = ... -2, -1, 0, 1, 2, ..., the forbidden region restriction is correspondingly modified. From an analysis similar to that given in section II-D one obtains the plot shown in Fig. 38 for the case being considered here. This should be compared with Fig. 26, and the obvious relationships noted. The limitation given by Eq. 167 can be generalized, and one has

$$ka < \frac{N}{2} \cot \psi$$

or

$$p < N \frac{\lambda}{2}. \tag{256}$$

If in Fig. 27 the abscissa is labeled $ka/(N \cot \psi)$ rather than $ka/\cot \psi$, it can be used as it stands for $N > 1$. Instead of doing this, one might change the scale so that the point 1/2 in Fig. 27 becomes N/2 with the abscissa label remaining $ka/\cot \psi$.

If Eq. 255 is substituted in Eq. 177 with $\kappa_{\perp_m} = 0$, and it is required that $E^e_{11} = 0$ for r = a at the center of all the tapes, that is, at $\theta = (2\pi/p)\, z + x, \ldots, (2\pi/p)\, z + x + n\,(2\pi/N), \ldots, (2\pi/p)\, z + x + (N-1)(2\pi/N)$, the following single approximate determinantal equation results from the satisfaction of this boundary condition at each point

$$0 \approx \sum_{m=..-1,0,1..} \left\{ \left[h^2a^2 - k^2a^2 + k^2a^2 \frac{m^2N^2\cot^2\psi}{\eta^2_{mN}} \right] I_{mN}(\eta_{mN}) K_{mN}(\eta_{mN}) \right.$$

$$\left. + k^2a^2\cot^2\psi\, I'_{mN}(\eta_{mN}) K'_{mN}(\eta_{mN}) \right\} \frac{\sin mNx}{mNx}. \tag{257}$$

Equation 257 should be compared with Eq. 191. An unimportant multiplying factor has been dropped in deriving Eq. 257. If N is now allowed to become increasingly large with Nx approaching a finite limit ($\pi > Nx > 0$), it can be shown (68) that all the terms in Eq. 257 for $m \neq 0$ become of order 1/N. In the limit of $N = \infty$, the only finite term remaining in Eq. 257 is the term for which m = 0. This is exactly the determinantal equation, Eq. 83, for the zeroth mode of the sheath helix, and the relationship between this sheath mode and the multiwire helix mode being considered here is thereby established. Note that in the limit of $N = \infty$, the only forbidden region restriction which remains for any finite value of ka is merely that $|h|a > ka$.

If N is large one may write

$$|I| = \frac{|K_{\parallel}|}{N} p \cos\psi \tag{258}$$

where $|K_{\parallel}|$ is the magnitude of the surface current density in the direction of the wires. Substitution of Eq. 258 in Eq. 255, Eq. 255 in Eqs. 173 and 174 with $\kappa_{\perp_m} = 0$, and the resulting expressions for κ_{zm} and $\kappa_{\theta m}$ in Eq. 154 through Eq. 159 yields, for $r \neq a$ as N becomes infinitely large since the $m \neq 0$ terms in the field representations become exponentially small, exactly the sheath helix field expressions given by Eqs. 49 through 54 with $n = 0$. For $r = a$ the higher harmonic amplitudes become increasingly large although of increasingly rapid variation as N increases. It is clear that the proper solutions for the sheath system are obtained by determining the limiting expressions for $r \neq a$ as N becomes increasingly large.

For finite N use of the procedure described in section II-F transforms Eq. 257 to the following form

$$0 \approx \zeta^2 a^2 I_o(\zeta a) K_o(\zeta a) + k^2 a^2 \cot^2\psi\, I_o'(\zeta a) K_o'(\zeta a)$$

$$+ \frac{(h^2 a^2 - k^2 a^2 \csc^2\psi)}{2} \sum_{m=1}^{\infty} \left[\frac{1}{(m^2 N^2 + \eta_{+mN}^2)^{1/2}} + \frac{1}{(m^2 N^2 + \eta_{-mN}^2)^{1/2}} \right] \frac{\sin mNx}{mNx}$$

$$+ \sum_{m=1}^{\infty} R(\eta_{-mN}). \tag{259}$$

Since $N \geq 2$ for a multiwire helix, the second series in Eq. 259 contains no terms with modified Bessel functions of first order. From this it can be shown (68) that for the multiwire helix in this mode no h root exists corresponding to the $|h_{t1}''|$ solution for $N = 1$. Also, the portion of the $|h_{t1}'|$ solution along the $|m| = 1$ (really $|m|N = 1$) boundary disappears; in fact, the forbidden region of this order no longer occurs. Since $\pi > Nx > 0$, the first series in Eq. 259 is essentially 1/N times as large as the corresponding term in Eq. 202. In view of all this, the simple procedure suggested in section II-H with the omission of the step for putting in the solutions along the $|m|N = 1$ boundary will give quite accurate results. Further, even for N as small as 2 it is perhaps better to use the sheath solution in the low frequency region rather than the average value as suggested in section II-H. Some experiments performed by Mr. L. Stark of these laboratories using a helix operating in the zeroth mode with $N = 2$ indicate that this simple procedure gives quite accurate predictions concerning the characteristics of this mode. The writer wishes to thank Mr. Stark for this information.

The power flow for the multiwire helix in this mode can be readily calculated using Eq. 255 and the procedures described here and in reference 68.

2. The Higher Modes

It is simplest and it appears sufficient to consider only a particular case in detail here. The mode to be discussed is the one for which the currents in the tapes at a cross section of constant z differ in phase progressively by $2\pi/N$ radians but have the same amplitude. The meaning of this is made clear in Fig. 39 for N = 2, 3, 4 where the relative phase of the currents at a particular instant of time is indicated by the vectors in the conventional manner for simple harmonic varying quantities. Since each winding is a uniform helix, with the assumptions taken here one has

$$e^{-jhz}\sum_m \kappa_{\parallel m} e^{-jm\left(\frac{2\pi}{p}z-\theta\right)} \approx \begin{cases} \frac{|I|}{\delta\cos\psi}e^{-jhz}, & \frac{2\pi}{p}z + 2x > \theta > \frac{2\pi}{p}z \\ \cdots \\ \frac{|I|}{\delta\cos\psi}e^{-jhz}e^{-jn\frac{2\pi}{N}}, & \frac{2\pi}{p}z + 2x + n\frac{2\pi}{N} > \theta > \frac{2\pi}{p}z + n\frac{2\pi}{N} \\ \cdots \\ \frac{|I|}{\delta\cos\psi}e^{-jhz}e^{-j(N-1)\frac{2\pi}{N}}, & \frac{2\pi}{p}z + 2x + (N-1)\frac{2\pi}{N} > \theta > \frac{2\pi}{p}z + (N-1)\frac{2\pi}{N} \\ 0, \text{ elsewhere.} \end{cases} \tag{260}$$

From Eq. 260

$$1\kappa_{\parallel m} = \frac{|I|}{p\cos\psi}e^{-jmx}\frac{\sin mx}{mx}\frac{e^{-j(m+1)2\pi}-1}{e^{-j(m+1)\frac{2\pi}{N}}-1} \tag{261a}$$

or

$$1\kappa_{\parallel m} = \frac{|I|}{p\cos\psi}e^{-jmx}\frac{\sin mx}{mx}N, \quad \begin{matrix} m = -1 + nN \\ n = \ldots -2, -1, 0, 1, 2, \ldots . \end{matrix} \tag{261b}$$

Note that the m = -1 harmonic always exists, although the absence or presence of the higher harmonics is determined by N. Since many of the space harmonics are absent, the forbidden region restriction is modified. It is readily determined that in this case the ha/cot ψ, ka/cot ψ plane appears as in Fig. 40. Although the order of the harmonics present has been determined from an approximate distribution, the same results hold for the exact case if the currents in the tapes vary in phase in the assumed manner.

Substitution of Eq. 261 in Eq. 177 with $\kappa_{\perp m} = 0$ and imposition of the boundary condition that $E^e_{\parallel} = 0$ for r = a at the center of all the tapes lead to the following single approximate determinantal equation

$$0 \approx \sum_n \left\{ \left(h^2a^2 - k^2a^2 + k^2a^2m^2 \frac{\cot^2\psi}{\eta_m^2} \right) I_m(\eta_m) K_m(\eta_m) \right.$$

$$\left. + k^2a^2 \cot^2\psi \, I'_m(\eta_m) K'_m(\eta_m) \right\} \frac{\sin mx}{mx} \qquad (262)$$

where $m = -1 + nN$ and $n = \ldots -2, -1, 0, 1, 2, \ldots$. If now N is allowed to become increasingly large with Nx approaching a finite limit, it can be shown (68) that all the terms in Eq. 262 for $n \neq 0$ or $m \neq -1$ become of order 1/N, so that in the limit of $N = \infty$ only the term for m = -1 remains. If the substitution

$$\frac{ha}{\cot\psi} = \frac{\hbar a}{\cot\psi} + 1 \qquad (263a)$$

or

$$h = \hbar + \frac{2\pi}{p} \qquad (263b)$$

is made in Eq. 262, some consideration of Eq. 190 shows that with $\eta_{-1}^2 = \hbar^2a^2 - k^2a^2$ playing the role of ζ^2a^2, and $\hbar a$ playing the role of ha, the remaining term in Eq. 262 becomes precisely the determinantal equation for the sheath helix, Eq. 42, with n = 1 there. The relationship of the transformation implied by Eq. 263 to a shift in the abscissa axis of Fig. 40 should be noted. Using Eqs. 258 and 261 and proceeding exactly as in section II-M-1, one can readily show that for $N = \infty$ the general field expressions become the sheath helix field expressions for n = 1 with the correspondence between the various quantities noted above. The relationship between the sheath helix mode for n = 1 and the particular assumed multiwire helix mode considered here is consequently established. Note again that in the limit of $N = \infty$ the only forbidden region restriction which remains for any finite value of ka is that $|\hbar|a > ka$.

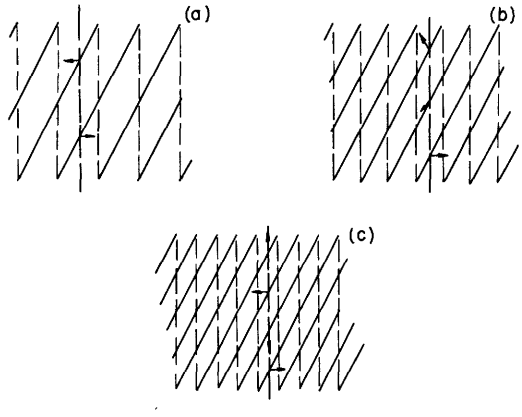

Fig. 39
Relative phase of currents:
(a) N = 2, (b) N = 3, (c) N = 4.

The manner in which the solutions for all the higher modes on multiwire helices can be determined is now evident. It is assumed that the phases of equal amplitude currents in the wires or tapes differ by $n[s(2\pi/N)]$ at any cross section of constant z, and proceeding in a manner which should be very clear by now, one obtains an approximate determinantal equation. In this, s is essentially the sequence number, which can be positive or negative and is fixed for any

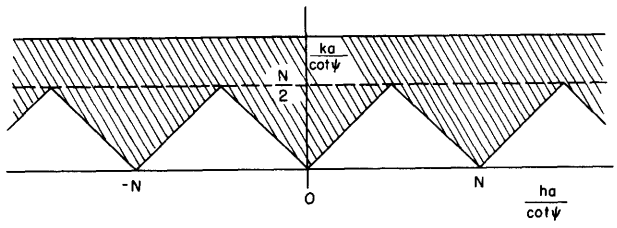

Fig. 40

Chart of forbidden regions for multiwire helix for first mode.

particular mode; n refers to a particular tape and runs from 0 to N - 1; whereas N is the number of conductors. In the limit of $N = \infty$, through the use of a transformation quite similar to that given by Eq. 263 for the case considered here, the sheath helix equations are obtained. For finite N the approximate determinantal equation can be solved by the methods already described, and the other properties of the system can also be readily determined. Since the summation in any of the determinantal equations for the higher modes is no longer symmetrical in the summation index, the loci of roots are no longer symmetrically disposed in the ha, ka plane. This would also be expected from the results given in section I concerning the higher modes on the sheath helix.

N. The Tape Ring System

In the sheath helix system it is possible to allow ψ to be zero and so obtain what is called in section I the sheath ring. Of course, for a physical helix the smallest pitch angle is limited by the tape width or wire diameter. However, a relatively realistic system does correspond to the sheath ring, and this can be analyzed by the methods described. The tape ring system is considered to consist of an infinite series of circular rings of radius a, coaxial with the z axis and uniformly spaced a distance p apart. Each ring has a width δ in the axial direction, and the edges are separated by a distance δ' so that $\delta + \delta' = p$. Each ring is made of tape taken to have infinitesimal thickness in the radial direction and assumed to be perfectly conducting. The assumptions concerning the medium in which the tape ring system is immersed are identical to those already made for the tape helix.

By an argument quite similar to that of section II-B it is determined that the electric Hertzian potential can be written as

$$\Pi_z^{i,e} = e^{-jhz}\, e^{jn\theta} \sum_m A_m^{i,e} \frac{I_n}{K_n}\left(\eta_m \frac{r}{a}\right) e^{-jm\frac{2\pi}{p}z} \tag{264}$$

with a similar form for the magnetic Hertzian potential. Equation 264 should be compared with Eq. 149. η_m is given by Eq. 146. In this, ψ loses its significance as a pitch angle and becomes only a convenient parameter. In the tape ring system the θ, z constraint which is imposed on the field representations for uniform helices is no longer present. In Eq. 264, n is not dependent on m, and it is clear from physical considerations that independent solutions may exist for each n. It is also clear that in Eq. 264 n may be positive or negative, so that solutions with θ dependence like $\sin n\theta$ or $\cos n\theta$ may be obtained by linear combination. The current density can also

be expressed in a form similar to Eq. 264; namely

$$K_{\theta,z} = e^{-jhz}\, e^{jn\theta} \sum_m \kappa_{\theta,zm}\, e^{-jm\frac{2\pi}{p}z} \tag{265}$$

Use may be made of the considerable similarity between the tape ring problem and the tape helix problem which is quite obvious. The field expressions given by Eqs. 154 through 159 are valid in the case here if one changes $e^{+jm\theta}$ there to $e^{+jn\theta}$ here, the order of the modified Bessel functions m there to n here, and m there, if it occurs by itself as an ordinary algebraic multiplier, to n here. Thus, for example, E_θ^e for the tape ring system becomes

$$E_\theta^e = j\frac{e^{-jhz}}{\omega\epsilon a} e^{jn\theta} \sum_m \left\{ -\frac{a}{r} nh_m a I_n(\eta_m) K_n\left(\eta_m \frac{r}{a}\right) \kappa_{zm} \right.$$

$$\left. + \frac{1}{\eta_m^2}\left[\frac{a}{r} n^2 h_m^2 a^2 I_n(\eta_m) K_n\left(\eta_m \frac{r}{a}\right) + \eta_m^2 k^2 a^2 I_n'(\eta_m) K_n'\left(\eta_m \frac{r}{a}\right)\right] \kappa_{\theta m} \right\} e^{-jm\frac{2\pi}{p}z}. \tag{266}$$

If the rings are narrow so that K_θ and K_z can be considered to act like $K_{||}$ and $K_\perp$, respectively, in the narrow tape helix case, one can readily obtain

$$_{1,2}\kappa_{\theta m} = \frac{|I|}{p} e^{jmx}\, {}_{1,2}D_m(\beta_{||} = h) \tag{267a}$$

$$_{1,2}\kappa_{zm} = 0. \tag{267b}$$

The notation has exactly the same significance as that used in section II-E and needs no further explanation. The $\beta_{||} = h$ assumption seems the most reasonable one to use here. Substituting Eq. 267 in Eq. 266 and requiring that $E_\theta^e = 0$ at r = a along the center of the rings lead to the following approximate determinantal equation

$$0 \approx \sum_m \frac{1}{\eta_m^2}\left[n^2 h_m^2 a^2 I_n(\eta_m) K_n(\eta_m) + k^2 a^2 \eta_m^2 I_n'(\eta_m) K_n'(\eta_m)\right] {}_{1,2}D_m(\beta_{||} = h). \tag{268}$$

If now p is allowed to become increasingly small, since x approaches a finite limit ($\pi > x > 0$), it can be shown (68) that all the terms in Eq. 268 for $m \neq 0$ become of order p. Thus, in the limit of p = 0, the only finite term remaining in Eq. 268 is the one for which m = 0, and this is the determinantal equation, Eq. 56, for the sheath ring. The sheath ring field expressions follow from the tape ring field expressions by a similar substituting and limiting process.

If the rings are wide so that the gaps are narrow, a procedure quite like that of section II-J leads to the following form for the approximate determinantal equation

$$0 \approx \sum_m \frac{1}{-4\eta_m^2 I_n'(\eta_m)K_n'(\eta_m)I_n(\eta_m)K_n(\eta_m)} \frac{1}{\eta_m^2}\left[n^2 h_m^2 a^2 I_n(\eta_m)K_n(\eta_m)\right.$$

$$\left. + k^2 a^2 \eta_m^2 I_n'(\eta_m)K_n'(\eta_m)\right]_{1,2} D_m'(\beta_{11} = h). \tag{269}$$

No calculations have been performed using Eq. 268 or 269, but it is clear that these equations can be solved by the methods already described. Since the order of the modified Bessel functions in Eqs. 268 and 269 remains fixed, it may be possible to simplify the procedure. Note that a forbidden region restriction quite like the one in force for the zeroth mode multiwire helix also applies here, and that in the limiting case of $p = 0$ the only restriction which remains for any finite ka is that $|h|a > ka$.

III. The Integral Equation Solution

The fields surrounding a helical line carrying a current of exponential form is determined from the integral expression for the Hertzian potential. The results are equivalent to those obtained by the procedure used in section II. Several different ways of approximating the boundary conditions also lead to essentially identical results.

By using the integral expression for the electric field along a wire in terms of the current which flows, a formula for the current produced on an infinite helical wire by a series voltage source is obtained. Although the complete evaluation of this is not attempted, the free mode portion is examined. It is shown that for $\psi = 90°$ the expression for the current reduces essentially to the known proper form for this case. Finally, the influence of loss in the wire is indicated.

The Source-Free Problem

A. Derivation of the Fields from an Assumed Current Distribution

Here the fields surrounding a helix carrying an assumed current distribution are derived from an integral expression for the vector potential, and the results are compared with those obtained in the previous section. No originality is claimed for the following derivation for the method is exactly like that used in reference 16. Here, however, contrary to the procedure used in reference 16, the propagation constant is considered an unknown which must be determined by the boundary conditions. The work of references 17 and 51 is also pertinent.

It is assumed that a current of the form

$$I(s') = |I|\, e^{-j\beta s'} \tag{270}$$

flows along a helical line defined by

$$x' = a \cos \theta' \tag{271}$$

$$y' = a \sin \theta' \tag{272}$$

$$z' = s' \sin \psi = \frac{p}{2\pi} \theta' . \tag{273}$$

s' is the distance measured along the helical line, and a and ψ are as shown in Figs. 2 and 3. The prime refers to points on the helix, and θ' is the cylindrical angular coordinate which can be considered to vary from $-\infty$ to $+\infty$ as implied in Eq. 273. β in Eq. 270 is taken to be real. An electric Hertzian potential $\bar{\Pi}$ can be written for the case here as (1)

$$\bar{\Pi} = -j \frac{|I|}{4\pi\omega\epsilon} \int_{-\infty}^{\infty} \bar{a}_{\parallel} e^{-j\beta s'} \frac{e^{-jkR}}{R} ds' . \tag{274}$$

All the field components can be derived from this potential alone, that is, with $\bar{\Pi}^* = 0$, through the use of Eqs. 16 and 17. $\bar{a}_{\parallel}$ is given by Eq. 3, or, equivalently, by

$$\bar{a}_{\parallel} = -\bar{a}_x \cos \psi \sin \theta' + \bar{a}_y \cos \psi \cos \theta' + \bar{a}_z \sin \psi. \tag{275}$$

$\bar{a}_x$ and $\bar{a}_y$ are unit vectors in the x and y directions. In Eq. 274 R is given by

$$R = \left[(x-x')^2 + (y-y')^2 + (z-z')^2 \right]^{1/2} \tag{276a}$$

$$R = \left[r^2 + a^2 - 2ar \cos(\theta-\theta') + \left(z - \frac{p}{2\pi} \theta' \right)^2 \right]^{1/2} \tag{276b}$$

where x, y, z or r, θ, z define the point of observation. To insure convergence of the integral in Eq. 274, the medium may be assumed to be slightly lossy, after which the loss may be considered to approach zero. Since

$$\bar{a}_x = \bar{a}_r \cos \theta - \bar{a}_\theta \sin \theta \tag{277}$$

$$\bar{a}_y = \bar{a}_r \sin \theta + \bar{a}_\theta \cos \theta \tag{278}$$

one obtains for Eq. 275

$$\bar{a}_{\parallel} = \bar{a}_r \cos \psi \sin(\theta-\theta') + \bar{a}_\theta \cos \psi \cos(\theta-\theta') + \bar{a}_z \sin \psi. \tag{279}$$

Using Eqs. 276b and 279 in Eq. 274 and making a change of variable, first to θ' and then to ξ, where

$$\xi = \theta' - \frac{2\pi}{p} z \tag{280}$$

one obtains for Eq. 274

$$\bar{\Pi} = -j \frac{|I|}{4\pi\omega\epsilon} a \sec\psi \, e^{-j\beta z \sec\psi} \int_{-\infty}^{\infty} e^{-j\beta a\xi \sec\psi} \left[\bar{a}_r \cos\psi \sin(\rho-\xi) \right.$$

$$\left. + \bar{a}_\theta \cos\psi \cos(\rho-\xi) + \bar{a}_z \sin\psi \right] \frac{e^{-jkR}}{R} d\xi. \tag{281}$$

In Eq. 281

$$\rho = \theta - \frac{2\pi}{p} z \tag{282}$$

and

$$R = \left[r^2 + a^2 - 2ar\cos(\rho-\xi) + \xi^2 a^2 \tan^2\psi \right]^{1/2}. \tag{283}$$

It can be shown (1, 2, 3) that

$$\frac{e^{-jkR}}{R} = \int_0^{\infty} J_o\left[\chi\sqrt{r^2 + a^2 - 2ar\cos(\rho-\xi)} \right] \frac{e^{-a|\xi|\tan\psi\sqrt{\chi^2 - k^2}}}{\sqrt{\chi^2 - k^2}} \chi d\chi \tag{284}$$

and

$$J_o\left[\chi\sqrt{r^2 + a^2 - 2ar\cos(\rho-\xi)} \right] = \sum_{m=-\infty}^{\infty} J_m(\chi r) J_m(\chi a) e^{jm(\rho-\xi)}. \tag{285}$$

Using Eqs. 284 and 285 in Eq. 281, one obtains after interchanging the operations of summation and integration

$$\bar{\Pi} = -j \frac{|I|}{4\pi\omega\epsilon} a \sec\psi \, e^{-j\beta z \csc\psi} \sum_m \int_0^{\infty} \frac{\chi d\chi J_m(\chi r) J_m(\chi a)}{\sqrt{\chi^2 - k^2}} \int_{-\infty}^{\infty} e^{-j\beta a\xi \sec\psi} \times$$

$$\left[\bar{a}_r \cos\psi \sin(\rho-\xi) + \bar{a}_\theta \cos\psi \cos(\rho-\xi) + \bar{a}_z \sin\psi \right] e^{jm(\rho-\xi)} e^{-a \tan\psi |\xi| \sqrt{\chi^2 - k^2}} d\xi. \tag{286}$$

At this stage it is useful to recall that β can be related to h, the propagation constant along the z axis, through

$$\beta = h \sin\psi. \tag{207}$$

Carrying out the integration on ξ in Eq. 286 and then using Eq. 207, one finds that

$$\bar{\Pi} = -j \frac{|I|}{4\pi\omega\epsilon} a^2 \cot\psi \, e^{-jhz} \sum_m \int_0^{\infty} \chi d\chi J_m(\chi r) J_m(\chi a) \left\{ -j\bar{a}_r \left(\frac{e^{j(m+1)\rho}}{a^2\chi^2 + \eta_{m+1}^2} \right.\right.$$

$$\left. - \frac{e^{j(m-1)\rho}}{a^2\chi^2 + \eta_{m-1}^2} \right) + \bar{a}_\theta \left(\frac{e^{j(m+1)\rho}}{a^2\chi^2 + \eta_{m+1}^2} + \frac{e^{j(m-1)\rho}}{a^2\chi^2 + \eta_{m-1}^2} \right) + \bar{a}_z \tan\psi \left(\frac{2e^{jm\rho}}{a^2\chi^2 + \eta_m^2} \right) \Bigg\}. \tag{287}$$

In Eq. 287 η_m is exactly the quantity defined in Eq. 146 and used throughout the previous section. It can be shown (3) that

$$\int_0^\infty \frac{\chi J_m(\chi r) J_m(\chi a)}{\chi^2 + \frac{\eta_n^2}{a^2}} d\chi = I_m(\eta_n) K_m\left(\eta_n \frac{r}{a}\right), \quad r \geq a \tag{288}$$

so that the final result for $\bar{\bar{\Pi}}$ becomes after some rearrangement and the use of Eq. 282

$$\bar{\bar{\Pi}}^e = -j \frac{|I|}{4\pi\omega\epsilon} \cot\psi \, e^{-jhz} \sum_m \left\{ -j\bar{a}_r \left[I_{m-1}(\eta_m) K_{m-1}\left(\eta_m \frac{r}{a}\right) - I_{m+1}(\eta_m) K_{m+1}\left(\eta_m \frac{r}{a}\right) \right] \right.$$

$$+ \bar{a}_\theta \left[I_{m-1}(\eta_m) K_{m-1}\left(\eta_m \frac{r}{a}\right) + I_{m+1}(\eta_m) K_{m+1}\left(\eta_m \frac{r}{a}\right) \right]$$

$$\left. + \bar{a}_z \, 2\tan\psi \, I_m(\eta_m) K_m\left(\eta_m \frac{r}{a}\right) \right\} e^{-jm\left(\frac{2\pi}{p} z - \theta\right)}. \tag{289}$$

Since Eq. 288 applies only for $r \geq a$, a superscript e is affixed to $\bar{\bar{\Pi}}$. An identical formula applies for $r \leq a$, except that the I_m and K_m functions are interchanged everywhere.

For purposes of comparison it is sufficient to find $E_{||}^e$. By substitution of Eq. 289 in Eq. 16, which is simplified by the use of Eq. 18, E_z^e and E_θ^e can be found. $E_{||}^e$ is then obtained by inserting these in Eq. 175. There results finally after considerable manipulation

$$E_{||}^e = j \frac{|I| \sin\psi \tan\psi}{p\omega\epsilon a} e^{-jhz} \sum_m \left\{ \left[\eta_m^2 - mh_m a \left(1 + \frac{a}{r}\right) \cot\psi \right. \right.$$

$$\left. + \frac{a}{r} m^2 h_m^2 a^2 \frac{\cot^2\psi}{\eta_m^2} \right] I_m(\eta_m) K_m\left(\eta_m \frac{r}{a}\right)$$

$$\left. + k^2 a^2 \cot^2\psi \, I'_m(\eta_m) K'_m\left(\eta_m \frac{r}{a}\right) \right\} e^{-jm\left(\frac{2\pi}{p} z - \theta\right)}. \tag{290}$$

It should now be recognized that Eq. 290 agrees exactly with Eq. 188 if in the latter one puts $\delta = 0$. But this implies from Eqs. 169 and 181 or Eq. 185 that

$$K_{\parallel}\left(\lim_{\delta \to o}\right) = \frac{|I|}{p \cos \psi} \sum_{m} e^{-jm\left(\frac{2\pi}{p} z - \theta\right)} \qquad (291)$$

with $K_{\perp} = 0$, of course. Equation 291 can be recognized as the nonconvergent Fourier series expansion for an impulse of integrable area $|I|/\cos \psi$ along the line $(2\pi/p)z = \theta$. Thus, the equivalence and relationship between the fields derived by the characteristic function approach of the previous section and those obtained from the integral expression 274 are established. It is obvious that the other field component expressions which can be obtained from Eq. 289 agree with those given in the previous section if Eq. 291 is used there.

B. Approximate Matching of the Boundary Conditions; Comparison with the Narrow Tape Case

Since the series representations for the field components obtained in the previous section are those resulting from an assumed current flowing along a line, it is obvious from physical considerations that they must become divergent as the line is approached. From the asymptotic forms for the products of the modified Bessel functions it can be shown that the representations converge for $r > a$ and $r < a$ and are conditionally convergent for $r = a$ if $(2\pi/p)z - \theta \neq 0$. Reference 17 discusses the matter of convergence of these series in considerable detail. If the current does not flow on a helical line, but rather on the surface of a small diameter perfectly conducting wire, the fields should be only slightly different from those found for the line current. Thus, if the condition that the tangential electric field be zero on the entire surface of the wire is imposed, a quite good approximation to the physical situation should result. However, this too is quite difficult to do, and further approximations must be made. Several methods of approximately matching the tangential electric field boundary condition on the wire in the wire direction are now considered. In the absence of any source this field component must be zero, and the application of this requirement results in a determinantal equation for the free mode propagation constants.

In the following it is assumed that the wire diameter is 2b and that the axis of the wire coincides with the helical line defined by Eqs. 271, 272, and 273. It is also assumed that b is much smaller than a, p, and λ. One method of satisfying the electric field boundary condition in an approximate manner is to require the value of $E_{\parallel}$ for $r = a$ averaged over the wire to be zero. Although $E_{\parallel}$ is divergent for $r = a$ and $\theta = (2\pi/p)z$, the divergence is only logarithmic and, consequently, integrable. If it is assumed that the phase of the current on the wire is essentially constant in a plane of constant z, one obtains on putting

$$\left[E_{\parallel}^{e}\,(r = a)\right]_{\text{average}}$$

equal to zero after dropping unimportant constants

$$0 \approx \sum_m \left\{ \left(\eta_m - \frac{m h_m a \cot\psi}{\eta_m} \right)^2 I_m(\eta_m) K_m(\eta_m) + k^2 a^2 \cot^2\psi \, I'_m(\eta_m) K'_m(\eta_m) \right\} {}_1\mathfrak{S}_m \quad (292)$$

where

$${}_1\mathfrak{S}_m = \frac{1}{\frac{4\pi b \sec\psi}{p}} \int_{\frac{2\pi}{p}(z-b\sec\psi)}^{\frac{2\pi}{p}(z+b\sec\psi)} e^{-jm\left(\frac{2\pi}{p}z-\theta\right)} d\theta = \frac{\sin\left(m\frac{2\pi b}{p}\sec\psi\right)}{m\frac{2\pi b}{p}\sec\psi}. \quad (293)$$

2b sec ψ is merely the maximum wire dimension in the z direction. Comparing Eq. 292 with Eq. 191 and Eq. 293 with Eq. 192 shows that if 2b sec ψ is considered equivalent to δ, Eq. 292 is exactly like the determinantal equation obtained for the narrow tape case for the approximations implied in Eqs. 191 and 192. Instead of averaging over the wire, one might require the average value of E_{11}^e at $\theta = (2\pi/p)(z \pm b \sec\psi)$ and r = a to be zero. In this case an equation like Eq. 292 results except that in place of ${}_1\mathfrak{S}_m$ a factor ${}_2\mathfrak{S}_m$ occurs, where

$${}_2\mathfrak{S}_m = \cos m\left(\frac{2\pi b}{p}\sec\psi\right). \quad (294)$$

If Eq. 294 is used in place of the (sin mx)/mx distribution factor, it can be shown (68) that this approximation merely alters the effective diameter of the wire.

Finally, one might impose the condition $E_{11}^e\left[r = a + b,\ \theta = (2\pi/p)z\right] \approx 0$. In this case one has from Eq. 290

$$0 \approx \sum_m \left\{ \left[\eta_m^2 - m h_m a \left(1 + \frac{1}{1+\Delta}\right)\cot\psi + \frac{1}{1+\Delta} m^2 h_m^2 a^2 \frac{\cot^2\psi}{\eta_m^2} \right] I_m(\eta_m) K_m\left[\eta_m(1+\Delta)\right] \right.$$

$$\left. + k^2 a^2 \cot^2\psi \, I'_m(\eta_m) K'_m\left[\eta_m(1+\Delta)\right] \right\} \quad (295)$$

where now $\Delta = b/a$. Although the presence of Δ in the algebraic multiplier as well as in the argument of K_m and K'_m in Eq. 295 complicates matters somewhat, it is still possible to make a quite satisfactory approximation if Δ is small. Some examination shows that if $\Delta \ll 1$, it has negligible effect on the value of the algebraic multiplier, and, consequently, it can be put equal to zero there. It can be shown (68) that since only h > k need be considered, Eq. 295 can be transformed in the usual fashion to the following form:

$$0 \approx \zeta^2 a^2 I_o(\zeta a) K_o\left[\zeta a(1+\Delta)\right] + k^2 a^2 \cot^2\psi\, I_o'(\zeta a) K_o'\left[\zeta a(1+\Delta)\right]$$

$$+ \frac{(h^2 a^2 - k^2 a^2 \csc^2\psi)}{\csc\psi} \sum_{m=1}^{\infty} \frac{e^{-m\Delta \csc\psi}}{m}$$

$$+ (h^2 a^2 - k^2 a^2 \csc^2\psi) \sum_{m=1}^{\infty} \left\{ I_m(\eta_{+m}) K_m\left[\eta_{+m}(1+\Delta)\right] \right.$$

$$\left. + I_m(\eta_m) K_m\left[\eta_m(1+\Delta)\right] - \frac{e^{-m\Delta \csc\psi}}{m \csc\psi} \right\} + \sum_{m=1}^{\infty} \mathcal{R}(\eta_{-m}). \qquad (296)$$

In Eq. 296

$$\sum_{m=1}^{\infty} \mathcal{R}(\eta_m)$$

is a remainder series whose characteristics are very similar to those of

$$\sum_{m=1}^{\infty} R(\eta_m)$$

in Eq. 196.

Since

$$\sum_{m=1}^{\infty} \frac{e^{-mz}}{m} = -\ln(1 - e^{-z}) = \ln\frac{1}{z} + \frac{z}{2} - \frac{1}{24} z^2 + \ldots \qquad (297)$$

(see reference 4, equation 601), it is clear that Eq. 296 becomes essentially equivalent to Eq. 204. It is therefore evident that the solutions of the two equations are practically equal except for a very minor difference equivalent to a small change in the cross sectional dimensions of the conductor.

At the end of section II-G reference was made to a recently published work which presented results similar to those obtained in section II for the propagation constants of the free mode waves on a narrow tape helix (51). The method of solution described in reference 51 is very nearly like that indicated here and in section III-A, and the approximate determinantal equation given there is almost identical to Eq. 295 here. The procedure for solving the equation presented there is a numerical and graphical one related to the one used here, although in reference 51 it appears that the series are summed directly rather than after some transformations as done here. These latter transformations make the calculations much simpler, of course, and permit the generalizations discussed in section II-H. Only one case is presented in reference 51, and this is very near the case considered here. Also, it is shown there that agreement with

the experimental results given in reference 27 can be obtained. However, reference 51 does not point out that the $\pm|h''_{t1}|$ wave is an inward rather than an outward traveling wave, and no mention is made of the fact that free mode solutions exist between the higher order forbidden regions. The matters of power flow, space harmonic phase velocity, group velocity, power loss, etc. are not considered there, and, as already noted, no attempt is made to simplify the calculative procedure. Of course, the very similar results of references 16 and 17 have already been noted, although the manner in which the boundary conditions are approximated in those references did not lead to the more complete results given in this report.

The Source-Present Problem

C. Integral Equation for E_{11}

In the analysis given here, it is necessary to start with the integral expression for the electric field on the surface of a conductor of small cross sectional area in terms of the total current in the conductor and the various parameters. Although this has been derived in several places, it is useful to review the derivation here (1, 6, 54, 58). From the expression for the electric Hertzian potential in the form (1, 56)

$$\bar{\Pi}(x) = \frac{-j}{4\pi\omega\epsilon} \int_{V'} \bar{J}(x') \frac{e^{-jkR}}{R} dV' \tag{298}$$

it is shown from Eq. 16, with $\bar{\Pi}^* = 0$, that

$$\bar{E}(x) = \frac{-j}{4\pi\omega\epsilon} \int_{V'} \left\{ \left[\bar{J}(x') \cdot \nabla' \right] \nabla' + k^2 \bar{J}(x') \right\} \frac{e^{-jkR}}{R} dV'. \tag{299}$$

Here, x and x' stand for the three coordinates at the points of observation and integration, respectively, $\bar{J}(x')$ is the vector current density per unit area flowing in the volume V', R is given by Eq. 276a, and ∇' is

$$\nabla' = \bar{a}_x \frac{\partial}{\partial x'} + \bar{a}_y \frac{\partial}{\partial y'} + \bar{a}_z \frac{\partial}{\partial z'}. \tag{300}$$

In deriving Eq. 299 use is made of the fact that

$$\nabla' f(R) = -\nabla f(R) \tag{301}$$

where f(R) is a function of R, and ∇ is

$$\nabla = \bar{a}_x \frac{\partial}{\partial x} + \bar{a}_y \frac{\partial}{\partial y} + \bar{a}_z \frac{\partial}{\partial z}. \tag{302}$$

If the current is assumed to flow in a wire of small transverse dimensions so that the current only in the direction of the wire is significant, it is evident that Eq. 299 is very closely approximated by

$$\bar{E}(x) \approx \frac{-j}{4\pi\omega\epsilon} \int_{s'} \left\{ \left[I(s')\bar{a}_{s'} \cdot \nabla' \right] \nabla' + k^2 I(s')\bar{a}_{s'} \right\} \frac{e^{-jkR}}{R} ds' \qquad (303)$$

where $\bar{a}_{s'}$ is a vector along the axis of the wire, s' is the distance measured along the axis of the wire, and I(s') is the total current flowing through a cross section of the wire at s'. It is assumed that the transverse dimensions of the wire are small compared with the radius of curvature, which is considered to be continuous, and with the wavelength.

Since $\bar{a}_{s'} \cdot \nabla' = (\partial/\partial s')$, where $\partial/\partial s'$ means the derivative in the direction of s', that is, along $\bar{a}_{s'}$, and since ∇' outside the brackets in Eq. 303 operates on e^{-jkR}/R only, Eq. 303 becomes

$$\bar{E}(x) \approx \frac{-j}{4\pi\omega\epsilon} \left\{ -\nabla \int_{s'} I(s') \frac{\partial}{\partial s'} \left(\frac{e^{-jkR}}{R} \right) ds' + k^2 \int_{s'} \bar{a}_{s'} I(s') \frac{e^{-jkR}}{R} ds' \right\}. \qquad (304)$$

Integrating the first term in Eq. 304 by parts, one obtains

$$\int_{s'} I(s') \frac{\partial}{\partial s'} \left(\frac{e^{-jkR}}{R} \right) ds' = \left[I(s') \frac{e^{-jkR}}{R} \right]_{s'_1}^{s'_2} - \int_{s'} \frac{e^{-jkR}}{R} \frac{\partial I(s')}{\partial s'} ds' \qquad (305)$$

where s'_1 and s'_2 are the extremities of the wire. If Eq. 305 is inserted in Eq. 304, one obtains an approximate expression for the electric field resulting from the current flowing in a wire of finite length. If the wire is assumed to be infinite in length so that s'_2 and s'_1 are at plus and minus infinity, respectively, and if I(s') is bounded, then the first term in Eq. 305 vanishes. For a circuit of infinite length Eq. 304 becomes

$$\bar{E}(x) \approx \frac{-j}{4\pi\omega\epsilon} \left\{ \int_{-\infty}^{\infty} \frac{\partial I(s')}{\partial s'} \nabla \left(\frac{e^{-jkR}}{R} \right) ds' + k^2 \int_{-\infty}^{\infty} \bar{a}_{s'} I(s') \frac{e^{-jkR}}{R} ds' \right\}. \qquad (306)$$

If the point of observation is on the surface of the conductor at a point s, with s the distance measured along a line on the surface of the wire essentially parallel to its axis and with $\bar{a}_s$ a unit vector along this line, then the electric field at s and in the direction of the wire is from Eq. 306

$$E_{\parallel}(s) = \bar{a}_s \cdot \bar{E}(x) \approx \frac{-j}{4\pi\omega\epsilon} \left\{ \int_{-\infty}^{\infty} \frac{\partial I(s')}{\partial s'} \frac{\partial}{\partial s} \left(\frac{e^{-jkR}}{R} \right) ds' + k^2 \int_{-\infty}^{\infty} \bar{a}_s \cdot \bar{a}_{s'} I(s') \frac{e^{-jkR}}{R} ds' \right\}. \qquad (307a)$$

Integrating the first term in Eq. 307a by parts, one may also write it as

$$E_{\parallel}(s) \approx \frac{-j}{4\pi\omega\epsilon}\left\{-\int_{-\infty}^{\infty} I(s')\,\frac{\partial^2}{\partial s\,\partial s'}\left(\frac{e^{-jkR}}{R}\right)ds' + k^2\int_{-\infty}^{\infty}\bar{a}_{s'}\cdot\bar{a}_s\, I(s')\,\frac{e^{-jkR}}{R}ds'\right\}. \quad (307b)$$

The above development is, of course, quite intimately related to the approach extensively used in recent years in the analysis of linear antennas (54). It should be emphasized that the theory considers the current to flow along a line coincident with the axis of the wire, but the fields are calculated and the boundary conditions satisfied on a line lying on the surface of the conductor.

The analysis can now be applied to the helix. The point of observation is defined by

$$x = (a+b)\cos\theta \quad (308)$$

$$y = (a+b)\sin\theta \quad (309)$$

$$z = s\sin\psi_o = \frac{p}{2\pi}\theta \quad (310)$$

whereas the line along which the current is assumed to flow is defined by Eqs. 271, 272, and 273. b is taken as the radius of the wire which is assumed to be circular in cross section, and b is considered to be much smaller than a, p, or λ. As a consequence, ψ_o may be considered equal to ψ. In Eq. 307, $\bar{a}_{s'}$ is $a_{\parallel}$ given by Eq. 275, and with the assumptions just given, a similar expression results for $\bar{a}_s$. It is found that to this approximation

$$\bar{a}_{s'}\cdot\bar{a}_s \approx \sin^2\psi + \cos^2\psi\cos(\theta-\theta'). \quad (311)$$

With R measured from the axis of the wire to the point of observation given by Eqs. 308, 309, and 310

$$R = \left[a^2\left(1+\frac{b}{a}\right)^2 + a^2 - 2a^2\left(1+\frac{b}{a}\right)\cos(\theta-\theta') + a^2\tan^2\psi\,(\theta-\theta')^2\right]^{1/2} \quad (312)$$

where $\psi \approx \psi_o$ is taken as a satisfactory approximation here also. In view of the symmetrical position of θ and θ' in Eq. 312 it is evident that $\partial/\partial s = -\partial/\partial s'$. Using this in Eq. 307a, integrating the first term by parts, and substituting Eq. 311 result in

$$E_{\parallel}^{e}(s) \approx \frac{-j}{4\pi\omega\epsilon}\int_{-\infty}^{\infty}\left\{\frac{\partial^2 I(s')}{\partial s'^2} + k^2\left[\sin^2\psi + \cos^2\psi\cos(\theta-\theta')\right]I(s')\right\}\frac{e^{-jkR}}{R}ds' \quad (313)$$

where the e superscript is affixed for obvious reasons. If I(s') is assumed to be of the form given by Eq. 270, Eq. 313 takes the form given in reference 6 and elsewhere (13, 52). Finally, if the procedure described in section III-A is used to evaluate Eq. 313, the result obtained is almost exactly like Eq. 290, with $r = (a+b) = a(1+\Delta)$ and $(2\pi/p)z = \theta$ there. This is to be expected in view of the relationship between the development leading to Eq. 290 and that given in this section. There is a slight difference

in the algebraic multiplier of the first term (the term in the brackets) but this is a coefficient of order $\Delta = b/a$ which is negligible. If $E_{||}^{e}(s)$ is now required to be zero on the assumption that the conductor has infinite conductivity, it is apparent from the discussion in section III-B that the free mode solutions are those considered in section II. Since $E_{||}$ is required to be zero only along a line on the surface, it seems clear that it will not be zero on a circular wire of radius b whose axis is the helix line, but rather on some conductor whose shape and cross sectional dimensions are slightly different.

D. The Gap Source

1. Application of the Source; the Free Modes

If the transverse dimensions of the helix wire are sufficiently small so that it can be considered to be a one-dimensional conductor, then the current function can be written in the form of a Fourier integral as

$$I(s) = \int_{-\infty}^{\infty} I(\beta)\, e^{-j\beta s}\, d\beta. \tag{314}$$

The component of electric field along the wire, $E_{||}(s)$, is taken to be

$$E_{||}(s) = \frac{E}{\pi} \int_{-\infty}^{\infty} \frac{\sin \frac{\beta \ell}{2}}{\beta} e^{-j\beta s}\, d\beta. \tag{315}$$

It is assumed, as before, that $E_{||}(s)$ is the same around the periphery of the wire at any point s. In this case $E_{||}(s)$ is zero everywhere except in a gap, or for $|s| < \ell/2$, where it has a constant magnitude. It is assumed further that the distribution described by Eq. 315 is maintained by an impressed electric field which is the negative of Eq. 315, and that this is the result of a voltage source placed in series with the helix wire at $s = 0$, or at $x = a, y = 0, z = 0$. In Eqs. 314 and 315 β is considered as a general complex variable, and the integration in Eq. 314 proceeds along the real axis with any necessary indentations which must be determined. The remarks of section I-G are pertinent here. If the conductor is assumed to be perfect, the current in the presence of the source may be determined by substituting Eqs. 314 and 315 in Eq. 313, or

$$\frac{E}{\pi} \int_{-\infty}^{\infty} \frac{\sin \frac{\beta \ell}{2}}{\beta} e^{-j\beta s}\, d\beta \approx \frac{-j}{4\pi\omega\epsilon} \int_{-\infty}^{\infty} \left\{ - \int_{-\infty}^{\infty} \beta^2 I(\beta) e^{-j\beta s'} + k^2 \left[\sin^2\psi + \cos^2\psi \cos(\theta - \theta') \right] \int_{-\infty}^{\infty} I(\beta) e^{-j\beta s'}\, d\beta \right\} \frac{e^{-jkR}}{R}\, ds'. \tag{316}$$

Interchanging the order of the integrations results in

$$\int_{-\infty}^{\infty}\left\{\frac{E}{\pi}\frac{\sin\frac{\beta\ell}{2}}{\beta}e^{-j\beta s}+j\frac{I(\beta)}{4\pi\omega\epsilon}\left[\int_{-\infty}^{\infty}\left(-\beta^2+k^2\left[\sin^2\psi\right.\right.\right.\right.$$

$$\left.\left.\left.\left.+\cos^2\psi\cos(\theta-\theta')\right]\right)e^{-j\beta s'}\times\frac{e^{-jkR}}{R}ds'\right]\right\}d\beta\approx 0. \qquad (317)$$

Equation 317 will be satisfied if the term in the braces is zero. Now the integral with respect to s' has already been evaluated since it is essentially the expression for $E_{11}^{e}(s)$ obtained from Eq. 313. Thus, solving Eq. 317 for $I(\beta)$, inserting this in Eq. 314, changing the variable to h which is related to β by Eq. 207, and using Eq. 310, one finally obtains

$$I(s)\approx -jV\omega\epsilon a^2\int_{-\infty}^{\infty}\frac{\dfrac{\sin\left[(h\sin\psi)\frac{\ell}{2}\right]}{(h\sin\psi)\frac{\ell}{2}}e^{-jhz}}{\sum_m\left\{\left[h^2a^2-k^2a^2+\dfrac{m^2}{\eta_m^2}k^2a^2\cot^2\psi\right]I_m(\eta_m)K_m\left[\eta_m(1+\Delta)\right]\right.}dh. \qquad (318)$$

$$\left.+k^2a^2\cot^2\psi\,I_m'(\eta_m)K_m'\left[\eta_m(1+\Delta)\right]\right\}$$

In Eq. 318, η_m is again the quantity defined by Eq. 146, and $\Delta = b/a$. h is now considered as a generalized complex variable, and the path of integration along the real axis must be properly indented around the singularities on that axis. $V = E\ell$ and is the voltage of the source. Equation 318 gives I(s) as a function of z, where z is related to s through Eq. 310. A multiplier, $1/(1+\Delta)$, of the term $(m^2/\eta_m^2)k^2a^2\cot^2\psi$ in the denominator of Eq. 318 has been placed equal to unity in accordance with the argument following Eq. 295. Equation 318 is reminiscent of the expressions encountered in section I-G except that here the denominator of the integrand is an infinite series. It is clear that the free modes correspond to the poles of the integrand of Eq. 318 or the zeros of the infinite series in the denominator. This is, of course, the usual determinantal equation which has already been discussed. It would appear from section III-B that one could substitute the approximate determinantal equation of the narrow tape helix for the denominator of the integrand in Eq. 318 with only little error.

In order to decide how the indentations around the singularities on the real axis must be made, the disposition of these singularities when the medium is slightly lossy is considered. Since the development leading to Eq. 138, which describes how the free mode zeros move off the real axis in terms of the group velocity, is still valid here, the location is readily ascertained. It is evident from Eqs. 318 and 146 that there are

an infinite number of branch points in the integrand of Eq. 318, as opposed to just two which occur in the simpler expressions derived in section I-G for the sheath system. Using the notation of that section and assuming that the medium is slightly lossy, one finds that the branch points are located where $\eta_m = 0$, or where

$$ha = \pm ka - m \cot \psi = \pm k_o a \sqrt{1 - j \frac{v_o \mu \sigma}{k_o}} - m \cot \psi \qquad (319)$$

with m taking on all integer values including zero. Figure 41 shows how these branch points are located in the ha plane. In addition to the branch point locations, the points at which the roots of the determinantal equation occur for $\psi = 10°$ as calculated for the narrow tape helix are shown. The manner in which these vary as ka varies is indicated in Figs. 41a through 41e which are only approximately to scale. These plots should be compared with Fig. 28. For a lossless medium the poles and branch points move into the real axis, and the contour of integration along the real axis is indented in an obvious fashion. Note that for $ka = \cot \psi/2$ the branch points lie in juxtaposition across the real axis.

The following discussion parallels a similar one in section I-G. Because of the presence of the e^{-jhz} factor in the integrand of Eq. 318, it vanishes on a circle of infinite radius in the third and fourth quadrants of the h or ha plane for $z > 0$. This assumes that the denominator of the integrand in Eq. 318 does not cause any convergence difficulties as $|h|$ becomes infinite. Such difficulty is encountered for $\psi = 90°$ as noted in section III-D-2 of this section, although examination of the denominator of the integrand in Eq. 318 (the approximate determinantal equation) by the use of the more convergent forms obtained by transformation indicates that for $\psi < 90°$ no trouble should be encountered. However, an explicit proof of this has not been constructed. Nevertheless, one can argue from physical considerations that the exact current representation would be convergent and that it would not be much different from Eq. 318 over most of the range of h. Thus, it seems quite proper to consider Eq. 318 as a good approximation for I(s) and to assume some convergence factor for large $|h|$ if necessary. With the deformation of the contour noted above, the integral in Eq. 318 becomes a sum of integrals around the poles of the integrand plus integrals along the branch cuts which are taken to extend downward from $+ka - m \cot \psi$ with $+\infty \geq m \geq -\infty$. For z very large the contributions from the branch cut integrations become small like $1/z$, whereas the contributions from the poles have a z variation like e^{-jhz} with h real. The reasons for calling the various waves inward and outward traveling waves should now be clear. Obviously, an argument similar to the above holds for $z < 0$ if the contour of integration is swept into the upper half plane.

The current associated with the various free mode waves can be obtained by evaluating the residues of the integrand at its poles. If it is assumed that ℓ is sufficiently small so that for any of the h roots

$$\frac{\sin\left[(h \sin\psi)\frac{\ell}{2}\right]}{\left[(h \sin\psi)\frac{\ell}{2}\right]}$$

can be considered equal to unity, and if the infinite series determinantal equation in the denominator of the integrand in Eq. 318 is called $f_1(ha)$, it is readily found that

$$I_{fm}(s) \underset{\substack{z >> 0 \\ (z << 0)}}{\approx} \mp 2\pi \, ka \sqrt{\frac{\epsilon}{\mu}} \, V \sum_{\substack{h \text{ roots} \\ \text{in} \\ \text{lower (upper)} \\ \text{half plane}}} \frac{e^{-jhz}}{\frac{df_1(ha)}{d(ha)}}. \tag{320}$$

The fm subscript refers to the fact that these are the free mode waves. While it does not seem possible to find a simple expression for $\left[df_1(ha)\right]/\left[d(ha)\right]$ (however, see reference 69), it should be noted that solving for the roots in a graphical manner leads immediately to a numerical value for $\left[df_1(ha)\right]/\left[d(ha)\right]$. It can be shown (68) that $\left[df_1(ha)\right]/\left[d(ha)\right]$ near the boundaries of the $|m| = 1$ region, in particular where $f_1(ha)$ equals zero, is extremely large so that the amplitudes of these waves, at least for small values of ka,

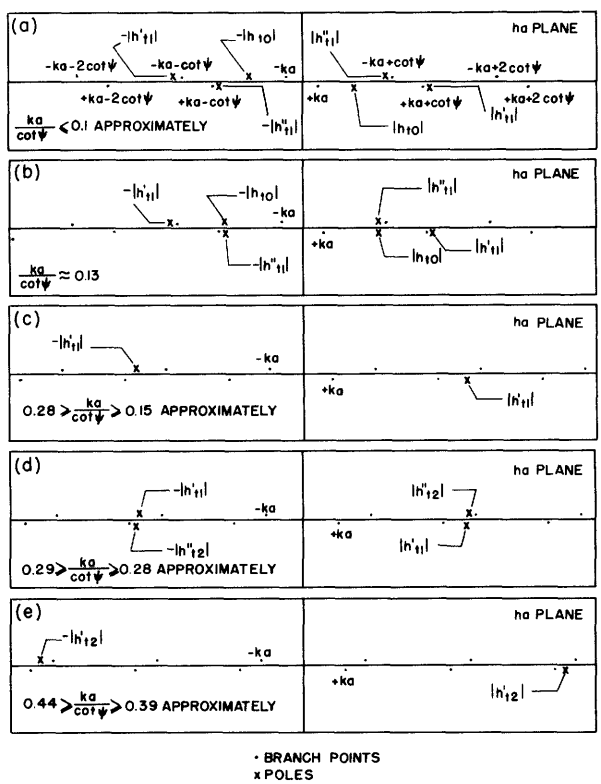

Fig. 41

The small wire helix, $\psi = 10°$.

are very small. This confirms the remarks made in sections II-G and II-I concerning these waves. If the amplitudes of the currents associated with the different free mode waves are calculated by the above procedure, the power flow and the various field components associated with these waves can be determined from formulas already given.

The input admittance of the infinite helix can be written

$$Y\left(s = \frac{\ell}{2} \text{ or } z = \frac{\ell}{2}\sin\psi\right) \approx -\frac{I\left(s = \frac{\ell}{2} \text{ or } z = \frac{\ell}{2}\sin\psi\right)}{V} \tag{321}$$

the minus sign occurring since the applied voltage is opposite to the induced voltage. The input admittance contains the contributions from the poles which are essentially real terms plus the contributions from the branch cuts which contain both real and imaginary parts. The equivalent circuit for the helix shown in Fig. 35 is an immediate consequence of Eqs. 318 and 321, and these equations form a rigorous basis for the remarks made in section II-I in connection with the equivalent circuit. The real impedances $R_{|h_{to}|}(ka)$, $R_{|h''_{t1}|}(ka)$, etc. are the characteristic impedances of the free mode waves. Such impedances can be defined in several ways: that is, on a voltage-current basis, on a power-current basis, or on a power-voltage basis (2). One has then

$$R_{|h_t|_{V,I}}(ka) = \frac{|V|}{|I|}, \qquad R_{|h_t|_{P_z,I}}(ka) = \frac{2P_z}{|I|^2}, \qquad R_{|h_t|_{P_z,V}}(ka) = \frac{|V|^2}{2P_z}. \tag{322}$$

If $|V|$ is taken as the amplitude of the source voltage, $|I|$ as the amplitude of the free mode current wave, and P_z as the total average real axial power flow, it is possible to calculate the $R_{|h_t|}(ka)$ values given by the first two equations in Eq. 322 for $\psi = 10°$ from available data. For $ka \lesssim 1.2$, $R_{|h_t|_{V,I}}(ka) \approx 2R_{|h_t|_{P_z,I}}(ka)$ for all the waves with an error of less than 20 percent even in the worst case. For $ka > 1.2$ no definite regularity was noted. To complete the solution for the input admittance one must perform the integration along the branch cuts. This is usually a quite difficult operation, and no attempt was made to carry it out here. It is to be expected from analogy with similar problems that the imaginary part resulting from such a calculation will depend to a considerable extent on the assumed shape of the wire, whereas the real part, as well as the free mode wave amplitudes resulting from the pole residues, will not be so dependent. Also, one would expect the imaginary and real parts of the resultant of the branch cut integrations to approach infinity and a finite limit, respectively, as the gap length approaches zero.

It has been assumed so far that the determinantal equation of the helix has only pure real h roots. Although it has not been possible to prove this for the exact case, as discussed in section II-D, it can be proved for the approximate cases. Taking the denominator of Eq. 318 as an example, one has

$$\sum_m \left\{ \left[h^2a^2 - k^2a^2 + \frac{m^2}{\eta_m^2} k^2a^2\cot^2\psi \right] I_m(\eta_m)K_m\left[\eta_m(1+\Delta)\right] \right.$$

$$\left. + k^2a^2\cot^2\psi\, I'_m(\eta_m)K'_m\left[\eta_m(1+\Delta)\right] \right\} = 0 \qquad (323)$$

where for reference

$$\eta_m = \left[m^2\cot^2\psi + 2mha\cot\psi + h^2a^2 - k^2a^2 \right]^{1/2}. \qquad (146)$$

From the fact that the complex Maxwell field equations are the Fourier transforms of the time dependent field equations, it is shown that the propagation constant for any free mode wave satisfies the relationship $\tilde{h}(\omega) = -h(-\omega)$, where the tilde, as usual, means complex conjugate (39). It should be emphasized now that only lossless systems are being considered so that $k^2 = \omega^2\mu\epsilon$ is pure real. Since the left side of Eq. 323 equals zero, this implies that its complex conjugate does also. Thus, taking the complex conjugate of Eq. 323, replacing $\tilde{h}(\omega)$ with $-h(-\omega)$, and then replacing $-h(-\omega)$ by $h'(\omega)$ result in an equation identical to Eq. 323 with $h'(\omega)$ in place of $h(\omega)$. Consequently, for every $h(\omega)$ root there is an identical $h'(\omega)$ root. But this requires that for such roots

$$h(\omega) = h'(\omega) = -h(-\omega) = \tilde{h}(\omega) \qquad (324)$$

from which it can be immediately concluded that Eq. 323 has roots only for real values of h, and not for complex or pure imaginary values. It should be clear that a similar proof applies to all the approximate determinantal equations given for the helix problem in this and the previous section.

The true significance of the realness of the h roots as well as the solution given by Eq. 318 should be emphasized. The point is that to the order of the approximations which have been made, the solution of the infinite helix source-present problem assumes a form quite similar to those available for more rigorously solvable open boundary problems. Among these are the infinite straight wire, the dielectric rod, the dielectric slab, the two wire line, the sheath helix (given here), and others (2, 39, 48). In common with these the lossless infinite helix supports purely propagating waves, or free modes, but none in which the propagation constant h is pure imaginary or complex. Radiation from an infinite driven helix is represented by a branch cut integration (really an infinite number of such integrations) or a continuum of exponential waves and not by discrete simple exponentially damped terms. Radiation from a finite helix occurs as a result of the end effects, as in finite linear antennas and dielectric rods, and the function of the free modes is to transport energy between the source and the ends (2, 39). This is not to say that the radiation properties of a finite helix cannot be determined approximately by the assumption of the existence of a simple outward traveling current wave.

Indeed, it has been found that the far-field radiation patterns of finite helices calculated on the basis of such an assumption are in good agreement with experimentally measured patterns, at least over restricted frequency regions (25, 27, 30). Nevertheless, as in the theory of linear antennas, the need for making assumptions about the current distribution on a finite helix should be considered only a temporary expedient until a better solution becomes available.

It is clear from the foregoing development (and from reference 52) that one can write down the integral equation for the current on a driven helix of finite length. The solution of this equation would provide a solution of the helical antenna problem which should prove of great interest and use (25). However, the occurrence of finite limits in the integral makes the problem considerably more difficult than the infinite helix problem.

After this report was written but before it came out in its present form, reference 69 became available in which essentially the same approach was used as is employed here for finding the form of the solution in the driven helix case.

2. Limiting Case of $\psi = 90°$; Effect of Loss in Wire

If $\psi = 90°$, that is cot $\psi = 0$, and $s = z$, the approximate expression for the current obtained from Eq. 318 becomes

$$I(z) \approx -jV\omega\epsilon a^2 \int_{-\infty}^{\infty} \frac{\frac{\sin \frac{h\ell}{2}}{\frac{h\ell}{2}}}{\eta_o^2 \sum_m I_m(\eta_o) K_m \left[\eta_o(1+\Delta)\right]} \, dh \tag{325}$$

where

$$\eta_o = \zeta a = \sqrt{h^2 a^2 - k^2 a^2}. \tag{197}$$

Since (3)

$$\sum_m I_m(\zeta a) K_m \left[\zeta a \left(1 + \frac{b}{a}\right)\right] = K_o(\zeta b) \tag{326}$$

from Eq. 325

$$I(z) \approx -jV\omega\epsilon b^2 \int_{-\infty}^{\infty} \frac{\frac{1}{\zeta b} \frac{\sin \frac{h\ell}{2}}{\frac{h\ell}{2}}}{\zeta b K_o(\zeta b)} e^{-jhz} \, dh. \tag{327}$$

Equation 327 gives an approximation for the current distribution on an infinite straight perfectly conducting circular cylindrical wire of radius b excited by a gap source centered at $z = 0$. From Eqs. 124 and 140 it is clear that the exact expression for the current in this circumstance is given by

$$I(z) = -jV\omega\epsilon b^2 \int_{-\infty}^{\infty} \frac{K_1(\zeta b)\,\dfrac{\sin\frac{h\ell}{2}}{\frac{h\ell}{2}}}{\zeta b K_o(\zeta b)}\, e^{-jhz}\, dh \qquad (328)$$

where it should be recalled that b here plays the role of a there. Equations 327 and 328 are identical except that $1/\zeta b$ appears in the numerator of the integrand of the approximate expression, whereas $K_1(\zeta b)$ appears in this position in the exact expression. Since $1/\zeta b$ is the dominant term in the expansion of $K_1(\zeta b)$, Eq. 327 should give a fair approximation to Eq. 328 if kb is small.

The integrand of Eq. 327 diverges for $|h|$ large, and some further approximations and assumptions are required before any comparisons can be made. No such comparisons are made here, and the only purpose of the above is to show that the approximate current expression agrees in a certain fashion with the exact expression in the limit of $\psi = 90°$. As a matter of fact, in reference 58, page 165, except for a change of notation and the use of $\ell = 0$ there, Eq. 327 appears as the solution for the driven infinite conductor problem. The matter of divergent integrals in such circumstances is discussed in reference 58, page 147. Incidentally, Eq. 328 is derived in section 10.16 of reference 2, and a solution valid for thin wires is given. (See also reference 67.)

So far in the analysis in this section it has been assumed that the wire is perfectly conducting. If the concept of surface or internal impedance is introduced, the effect of finite conductivity may be determined (1, 2, 58). It is necessary to assume that the current distribution in the wire is the same as that in a straight infinitely long circular wire of radius b. In this case the term $Z_i I(s)$ is added to the left side of Eq. 316 where Z_i is given below. Proceeding as before, one obtains in place of Eq. 318

$$I(s) \approx -jV\omega\epsilon a^2 \int_{-\infty}^{\infty} \frac{\dfrac{\sin\left[(h\sin\psi)\frac{\ell}{2}\right]}{(h\sin\psi)\frac{\ell}{2}}\, e^{-jhz}}{jZ_i\frac{2\pi\omega\epsilon a^2}{\sin\psi} + \sum_m \left\{\left[h^2a^2 - k^2a^2 + \frac{m^2}{\eta_m^2}k^2a^2\cot^2\psi\right] I_m(\eta_m)K_m\left[\eta_m(1+\Delta)\right] + k^2a^2\cot^2\psi\, I'_m(\eta_m)K'_m\left[\eta_m(1+\Delta)\right]\right\}} dh. \qquad (329)$$

The determinantal equation is modified in this case by the addition of the term $jZ_i(2\pi\omega\epsilon a^2/\sin\psi)$. With the usual assumption that the displacement current in the wire is negligible compared with the conduction current (1, 2, 58)

$$Z_i = \frac{1}{2\pi b}\left(j\frac{\omega\mu_t}{\sigma_t}\right)^{1/2}\frac{I_o\left[(j\omega\mu_t\sigma_t)^{1/2}\, b\right]}{I_1\left[(j\omega\mu_t\sigma_t)^{1/2}\, b\right]} \tag{330}$$

where μ_t and σ_t are the permeability and conductivity of the wire material. If the skin effect is relatively complete, an excellent approximation for Eq. 330 is

$$Z_i \approx \frac{1}{2\pi b}\left(j\frac{\omega\mu_t}{\sigma_t}\right)^{1/2}. \tag{331}$$

With a wire of finite conductivity the free mode propagation constants are no longer pure real but have a small imaginary part. It is probably simpler to use the usual approximation methods discussed in section II-I in order to determine the attenuation constant, rather than to attempt to solve the determinantal equation including loss. However, if the losses are small and if the lossless determinantal equation (call this $f_1(ha)$ as before) has been solved numerically or in some fashion so that $\left[df_1(ha)\right]/\left[d(ha)\right]$ is available, then by the usual first order perturbation assumption

$$(ha)_{loss} \approx \frac{-jZ_i\,\frac{2\pi\omega\epsilon a^2}{\sin\psi}}{\left[\frac{df_1(ha)}{d(ha)}\right]_{ha=h_t a}} + (h_t a) \tag{332}$$

where $h_t a$ is a solution of the lossless determinantal equation.

It will be recalled that for a lossless single wire helix immersed in an infinite homogeneous lossless medium no free mode or exponentially propagated wave occurs for $p > \lambda/2$. For a lossy wire with $p = \infty$, that is, an infinite straight wire, exponential propagation occurs although with a complex propagation constant (1, 59). However, if the wire is lossless in this case, $p = \infty$, true exponential propagation does not occur, and the variation of the current with distance is exponential as a first approximation only (2, 58). It is evident that single wire helices wound of lossless and lossy wires act in a somewhat different fashion for $p > \lambda/2$, although it would be expected that for $p < \lambda/2$ the difference is quite small. It appears that the forbidden region restriction must be modified somewhat for lossy wires, and an investigation of the determinantal equation with loss (the denominator of the integrand of Eq. 329) is required. No such investigation was attempted for this report, but this problem is worthy of further analysis.

Acknowledgment

The writer wishes to express his gratitude to Professor L. J. Chu for his many helpful suggestions in the supervision of this work. He would also like to thank Professor R. B. Adler for the time he spent in numerous discussions and Miss E. Pauline Leighton and Mrs. Barbara Levine for carrying through some rather tedious calculations.

Bibliography and References

1. J. A. Stratton: Electromagnetic Theory, McGraw-Hill, New York, 1941
2. S. A. Schelkunoff: Electromagnetic Waves, Van Nostrand, New York, 1943
3. G. N. Watson: A Treatise on the Theory of Bessel Functions, Second Edition, Macmillan, New York, 1948
4. H. B. Dwight: Tables of Integrals and Other Mathematical Data, Revised Edition, Macmillan, New York, 1947
5. L. Brillouin: Wave Propagation in Periodic Structures, McGraw-Hill, New York, 1946
6. H. C. Pocklington: Electrical Oscillations in Wires, Proc. Camb. Phil. Soc. 9, 324, 1897
7. F. Ollendorf: Die Grundlagen der Hochfrequenztechnik, Springer, Berlin, 79, 1926
8. J. R. Pierce: Theory of the Beam Type Traveling-Wave Tube, Proc. I. R. E. 35, 108, Feb. 1947
9. J. R. Pierce: Traveling-Wave Tubes, Van Nostrand, New York, 1950
10. L. J. Chu, D. J. Jackson: Field Theory of Traveling-Wave Tubes, Technical Report No. 38, Research Laboratory of Electronics, M.I.T. April 1947
11. C. Schulman, M. S. Heagy: Small Signal Analysis of Traveling-Wave Tube, R.C.A. Review, 8, No. 4, 593, Dec. 1947
12. L. Brillouin: Spiralled Coils as Waveguides, Harvard University, Cruft Laboratory Technical Report No. 10, March 1947
13. E. T. Kornhauser: Electromagnetic Wave Propagation in Helical Structures, D. Sc. Thesis, Harvard University, June 1949; also Cruft Laboratory Technical Report No. 88, Aug. 1949
14. R. Rudenberg: Electromagnetic Waves on Transformers, J.A.P. 12, 129, March 1941
15. P. Parzen: Propagation of Electromagnetic Waves Along Helical Wires, U. R. S. I. - I. R. E. Convention, Washington, D.C. Oct. 1947 (unpublished)
16. W. Sollfrey: Propagation Along a Helical Wire, Report TW-10 of the New York University Mathematics Research Group, June 1949
17. R. S. Phillips: The Electromagnetic Field Produced by a Helix, Report TW-11 of the New York University Mathematics Research Group, June 1949; Q.A.M. 8, 229, Oct. 1950
18. R. S. Phillips: A Helical Wave Guide I, Research Report 170-2 of the New York University Mathematics Research Group, Jan. 1947
19. R. S. Phillips, H. Malin: A Helical Wave Guide II, Research Report 170-3 of the New York University Mathematics Research Group, Aug. 1947
20. J. W. Nicholson, Resistance and Inductance of a Helical Conductor, Phil. Mag. 19, 77, 1910
21. J. P. Blewett, J. H. Rubel: Video Delay Lines, Proc. I. R. E. 35, 1580, Dec. 1947
22. C. C. Cutler: Experimental Determination of Helical Wave Properties, Proc. I. R. E. 36, 230, Feb. 1948
23. L. A. Harris, H. R. Johnson, A. Karp, L. D. Smullin: Some Measurements of Phase Velocity Along a Helix with Dielectric Supports, Technical Report No. 93, Research Laboratory of Electronics, M.I.T. Jan. 1949
24. A. E. Marston, M. D. Adcock: Radiation from Helices, Naval Research Laboratory Report No. R-3634, March 1950. Also, A. E. Marston: The Radiation Fields of Helical Antennas, Naval Research Laboratory Report No. R-3357, Sept. 1948

25. J. D. Kraus: Antennas, McGraw-Hill, New York, 1950

26. J. D. Kraus: Helical Beam Antenna, Electronics, 20, 109, April 1947

27. J. D. Kraus, J. C. Williamson: Characteristics of Helical Antennas Radiating in the Axial Mode, J.A.P. 19, 87, Jan. 1948

28. J. D. Kraus, O. J. Glasser: Measured Impedance of Helical Beam Antennas, J.A.P. 19, 193, Feb. 1948

29. J. D. Kraus: Helical Beam Antennas for Wide Band Application, Proc. I.R.E. 36, 1236, Oct. 1948

30. J. D. Kraus: The Helical Antenna, Proc. I.R.E. 37, 263, March 1949

31. C. K. Bagby: A Theoretical Investigation of Electromagnetic Wave Propagation on the Helical Beam Antenna, M. S. Thesis, Ohio State University, 1948 (unpublished)

32. J. A. Marsh: Current Distributions on Helical Antennas, Project Report No. 339-10, Ohio State University Research Foundation, a portion of a D. Sc. Thesis, Ohio State University, 1949

33. M. Aronoff: Measured Phase Velocity and Current Distribution Characteristics of Helical Antennas Radiating in the Beam Mode, M. S. Thesis, Ohio State University, 1948 (unpublished)

34. J. D. Kraus, T. E. Tice: The Influence of Conductor Size on the Properties of Helical Beam Antennas, Proc. I.R.E. 37, 1296, Nov. 1949

35. H. A. Wheeler: A Helical Antenna for Circular Polarization, Proc. I.R.E. 35, 1484, Dec. 1947

36. W. W. Hansen: On The Resonant Frequency of Closed Concentric Lines, J.A.P. 10, 38, Jan. 1939

37. J. C. Slater: The Design of Linear Accelerators, Technical Report No. 47, Research Laboratory of Electronics, M.I.T. Sept. 1947

38. J. C. Slater: Electromagnetic Waves in Iris Loaded Waveguides, Technical Report No. 48, Research Laboratory of Electronics, M.I.T. Sept. 1947

39. R. B. Adler: Properties of Guided Waves on Inhomogeneous Cylindrical Structures, Technical Report No. 102, Research Laboratory of Electronics, M.I.T. May, 1949

40. J. W. Nicholson: The Approximate Calculation of Bessel Functions of Imaginary Argument, Phil. Mag. 20, 938, Dec. 1910

41. H. Jeffreys, B. S. Jeffreys: Methods of Mathematical Physics, First Edition, Cambridge University Press, Cambridge, 1946

42. A. Fletcher, J. C. P. Miller, L. Rosenhead: An Index of Mathematical Tables, Scientific Computing Service, Ltd. London, 1946

43. F. L. Yost, J. A. Wheeler, G. Breit: Coulomb Wave Functions in Repulsive Fields, Phys. Rev. 49, 174, Jan. 1936

44. H. Bateman, R. C. Archibald: A Guide to Tables of Bessel Functions, M.T.A.C. I, No. 7, 205, July 1944

45. E. Jahnke, F. Emde: Tables of Functions, Dover Publications, New York, 1943

46. A. Gray, G. B. Mathews, T. M. MacRobert: A Treatise on Bessel Functions, Second Edition, Macmillan, Ltd. London, 1931

47. H. T. Davis: Tables of Higher Mathematical Functions, Vol. I and Vol. II, The Principia Press, Bloomington, Indiana, 1933

48. R. M. Whitmer: Fields in Nonmetallic Waveguides, Proc. I.R.E. 36, 1105, Sept. 1948

49. W. M. Elsasser: Attenuation in a Dielectric Circular Rod, J.A.P. 20, 1193, Dec. 1949

50. P. M. Morse, H. Feshbach: Methods of Theoretical Physics, Technology Press, Cambridge, Massachusetts, 1946

51. S. Kh. Kogan: The Propagation of Waves along an Endless Helix, (in Russian), C. R. Acad. Sci. U.R.S.S. June 1949, 66, No. 5, 867. Referred to in Wireless Engineer, XXVIII, Jan. 1951, p. A.3, Item 30

52. C. P. Hsu: Theory of Helical Waveguides and Helical Radiators, Harvard University, Cruft Laboratory Technical Report No. 95, Jan. 1950

53. C. J. Bouwkamp: On the Diffraction of Electromagnetic Waves by Small Circular Disks and Holes, Phillips Research Reports, 5, 401, Dec. 1950

54. J. Aharoni: Antennae, Oxford Press, London, 1946

55. W. Walkinshaw: Notes on "Wave Guides for Slow Waves," J.A.P. 20, 634, June 1949

56. S. Silver: Microwave Antenna Theory and Design, McGraw-Hill, New York, 1949

57. G. M. Roe: The Theory of Acoustic and Electromagnetic Wave Guides and Cavity Resonators, Ph. D. Thesis, University of Minnesota, March 1947 (unpublished)

58. E. D. Sunde: Earth Conduction Effects in Transmission Systems, Van Nostrand, New York, 1949

59. G. Goubau: Surface Waves and Their Application to Transmission Lines, J.A.P. 21, 1119, Nov. 1950

60. E. T. Kornhauser: Radiation Field of Helical Antennas with Sinusoidal Current, Harvard University, Cruft Laboratory Technical Report No. 115, Sept. 1950

61. W. Rotman: A Study of Single-Surface Corrugated Guides, Air Force Cambridge Research Laboratories, E5055, Feb. 1950

62. H. A. Haus: Attenuation of Noise in a Beam by Means of a Slow Waveguide Structure, M. S. Thesis, Rensselaer Polytechnic Institute, Jan. 1951 (unpublished)

63. E. M. T. Jones: A Negative Dispersion Helix Structure, Stanford University, Electronics Research Laboratory Technical Report No. 27, Aug. 1950

64. C. O. Lund: Broadband Transition from Coaxial Line to Helix, R.C.A. Review 11, 133, March 1950

65. R. S. Phillips, H. Malin: Investigation of the Exceptional Modes, $n = \pm 1, \pm 2$, Research Report 170-3 (Addendum), New York University Mathematics Research Group, June 1948

66. S. A. Schelkunoff: Concerning Hallén's Integral Equation for Cylindrical Antennas, Proc. I.R.E. 33, 872, Dec. 1945

67. E. Hallén: Properties of a Long Antenna, J.A.P. 19, 1140, Dec. 1948

68. S. Sensiper: Electromagnetic Wave Propagation on Helical Conductors, Sc.D. Thesis, Department of Electrical Engineering, M.I.T. May 1951

*69. S. Kh. Kogan: The Excitation of a Helical Conductor, (in Russian), C. R. Acad. Sci. U.R.S.S. Sept. 1950, 74, No. 3, 489-492. Referred to in Wireless Engineer, XXIX, Jan. 1952, No. 340, p. A.9, Item 112

*70. P. K. Tien: Helix Impedance of Traveling Wave Tubes, Stanford University, Electronics Research Laboratory Technical Report No. 50, June 1952

*71. E. Roubine: Study of Electromagnetic Waves Guided by Helical Circuits (in French), Annales des Telecommunications 7, 206, May 1952; 262, June 1952; 310, July-Aug. 1952

*Added in proof.